

**Development of Charge Manipulation Nanoelectrospray Ion Mobility-Mass  
Spectrometry Techniques for Multiprotein Complex Analysis**

**by**

**Russell E. Bornschein**

A dissertation submitted in partial fulfillment  
of the requirements for the degree of  
Doctor of Philosophy  
(Chemistry)  
in the University of Michigan  
2015

Doctoral Committee

Assistant Professor Brandon T. Ruololo, Chair  
Professor Kristina I. Håkansson  
Professor Robert T. Kennedy  
Associate Professor Georgios Skiniotis

© Russell E. Bornschein

---

All Rights Reserved

2015

## **Acknowledgments**

So many people have touched my life through the long journey of earning my Ph.D. I am at a very different place in my life now than I was five years ago, and I know I would not be here if it were not for all their help and support.

First and foremost I would like to thank my advisor, Dr. Brandon Ruotolo, for all of his support and help, both personally and professionally. You have been very patient and understanding through all the ups and downs of this project, and have been extremely understanding and accommodating while I have dealt with my work-life balance. I'd also like to thank the other members of my doctoral committee, Dr. Kristina Håkansson, Dr. Robert Kennedy, and Dr. Georgios Skiniotis. You have all been very supportive and insightful during meetings and discussions, and I thank you for pushing me to expand my view of how my research plays a role beyond the chemistry community and more broadly into the life science community.

The Ruotolo Group has contained an amazing group of people, and has always felt like the right place for me to conduct my research. I would like to thank all the group members, past and present, for creating a cooperative and fun work environment. Specifically, I would like to thank Dr. Suk-Joon Hyung for all his help teaching me how to conduct experiments in the lab; Dr. Yueyong Zhong for being a great friend, and fellow parent, it was an adventure being with you from the beginning to start the lab; Dr. Linjie Han for always being a model researcher, you helped create a standard by which all others should follow; Dr. Billy Samulak for being one of the nicest people I have ever known, you were always willing to drop what you were doing to

help someone in need; Dr. Richard Kerr for always being the person I could count on for a nerdy coffee break; Shuai Niu for help with modeling and understanding the computational data; Molly Soper and Jessica Rabuck-Gibbons, since you can't talk about one without talking about the other, I thank you both for always willing to listen to a problem and helping solve issues as they arise, and of course sharing gossip, solicited or otherwise; Joseph Eschweiler for being the programming powerhouse of the lab, thanks for all your help and contributions solving anything theoretical, and for making a darn good cup of coffee; Yuwei Tian, Alec Valenta, and Sugyan Dixit you are all just starting your careers, so you've brought a freshness to the lab that is a welcome reminder to how exciting the work can be, so thank you.

I would also like to thank the many people at Michigan who have been helpful and supportive outside of research and the lab. Particularly, Nancy Kerner for seeing something in me and encouraging me to follow a career path I had not thought to take, and help foster me through that transition. All the staff in the Chemistry business office, past and present, for your guidance in navigating graduate school. The staff at the Center for Research on Learning and Teaching and the staff at Rackham Graduate School for support and guidance throughout my tenure here at Michigan.

Finally, I would like to thank my friends and family. There are innumerable friends from both Denison University and here at the University of Michigan that have been encouraging and supportive, and to all of them I send my gratitude. Thank you to my parents for encouraging me to follow my interests, pushing me to excellence, and instilling the value of a great education. Thank you to my brother for sharing the graduate school experience, and for somehow always turning science into a question of ethics. Thank you to my in-laws for all your continued help and support. I'd like to thank my two daughters, Charlotte and Elizabeth, for making everyday

unpredictable, exciting, and a whole lot of fun. Lastly, but certainly not least, I would like to thank my wife, Amy; you have been beyond supportive and understanding. Your patience and love have gone farther than you could imagine, I'm so lucky to have you in my life and to have shared this experience with you. You are the best mother, wife, and friend anyone could ask for, and I love you.

## Table of Contents

Acknowledgments .....	ii
List of Figures.....	viii
List of Tables .....	xi
List of Appendices.....	xii
List of Abbreviations .....	xiii
Abstract.....	xvii
Chapter 1. Introduction .....	1
1.1 Mass Spectrometry in Structural Biology .....	3
1.1.1 Electrospray Ionization (ESI).....	5
1.1.2 Native Mass Spectrometry.....	8
1.2 Ion Mobility-Mass Spectrometry (IM-MS) .....	9
1.2.1 Quadrupole Mass Spectrometry .....	12
1.2.2 Traveling Wave (T-wave) Ion Mobility .....	13
1.2.3 Time-of-Flight (ToF) Mass Spectrometry .....	14
1.3 Protein Complex Subunit Analysis in Mass Spectrometry .....	17
1.3.1 Solution Disruption Strategies.....	17
1.3.2 Gas-Phase Complex Dissociation.....	18
1.4 Charge Manipulation Techniques .....	22
1.4.1 Solution Based Methods.....	22
1.4.2 Gas-Phase Methods .....	24

1.5 Modeling Protein Complex Structures with IM-MS Datasets .....	26
1.5.1 Molecular Dynamics: Simulated Annealing.....	27
1.5.2 Monte Carlo Simulations.....	28
1.6 Summary .....	28
1.7 References.....	30
Chapter 2. Ion Mobility-Mass Spectrometry Reveals Conformational Changes in Charge	
Reduced Multiprotein Complexes.....	38
2.1 Introduction.....	38
2.2 Experimental .....	42
2.3 Results and Discussion.....	45
2.4 Conclusions.....	53
2.5 Acknowledgments.....	55
2.6 References.....	55
Chapter 3. Ion Mobility-Mass Spectrometry Reveals Highly-Compact Intermediates in the	
Collision Induced Dissociation of Charge-reduced Protein Complexes .....	58
3.1 Introduction.....	58
3.2 Experimental .....	61
3.2.1 Sample Preparation.....	61
3.2.2 Instrumentation and Data Analysis.....	62
3.2.3 Molecular Modeling .....	62
3.3 Results and Discussion.....	63
3.4 Conclusions.....	72
3.5 Acknowledgments.....	76

3.6	References .....	76
Chapter 4. Ion Mobility-Mass Spectrometry Reveals General Trends in the Gas-phase Ejection		
	of Compact Subunits from Intact Protein Complexes .....	79
4.1	Introduction .....	79
4.2	Experimental .....	82
4.2.1	Sample Preparation.....	82
4.2.2	Instrumentation and Data Analysis.....	82
4.2.3	Corona Discharge Charge Reduction .....	83
4.3	Results and Discussion.....	84
4.3.1	CDP-nESI Optimization.....	84
4.3.2	Detecting the Dissociation of Compact Subunits.....	87
4.3.3	Alternative Dissociation Pathways.....	92
4.4	Conclusions .....	96
4.5	Acknowledgments.....	97
4.6	References .....	97
Chapter 5. Conclusions and Future Directions.....		
5.1	Conclusions.....	99
5.2	Future Directions.....	101
5.2.1	Alternative Charge Reducing Agents .....	102
5.2.2	Resigned Corona Discharge Probe .....	103
5.2.3	Gas-phase Supercharging .....	104
5.3	References.....	105
Appendices .....		107



## List of Figures

Figure 1-1	Common mass spectrometry (MS) technologies and their utility within the field of structural biology.....	4
Figure 1-2	Diagram depicting the operation and mechanics of electrospray ionization.....	6
Figure 1-3	Schematic diagram of the commercially available Waters Synapt G2 HDMS nanoelectrospray-quadrupole-ion mobility-time-of-flight mass spectrometer ...	11
Figure 1-4	Dissociation pathways for collision induced dissociation, surface induced dissociation, and electron transfer dissociation/electron capture dissociation ...	19
Figure 1-5	Charge reduction pathways for solution additive and gas-phase methodologies	23
Figure 2-1	A schematic diagram of the modified nanoelectrospray ion source for the Synapt G2 instrument .....	43
Figure 2-2	Plots of average avidin and alcohol dehydrogenase tetramer charge state against the concentration of DBU used in nebulized base solutions and as an additive in protein samples .....	46
Figure 2-3	Mass spectra and drift time verses m/z contour plots of avidin, alcohol dehydrogenase, and pyruvate kinase .....	48
Figure 2-4	Collision cross-section measurements verses charge state plots for avidin, alcohol dehydrogenase, and pyruvate kinase .....	51
Figure 3-1	Representative CIU fingerprints and comparison of CID and CIU threshold energies for aldolase .....	64

Figure 3-2	Representative CIU fingerprints and comparison of CID and CIU threshold energies for avidin .....	67
Figure 3-3	Plots of Monomer/tetramer CCS ratio versus monomer/tetramer charge state (CS) ratio for aldolase and avidin, and plot of avidin timers produced during CID .....	70
Figure 3-4	Proposed dissociation pathways for aldolase and avidin.....	75
Figure 4-1	Mass spectra for denatured cytochrome C under various charge reduction conditions.....	85
Figure 4-2	Mass spectra from $\beta$ -lactaglobulin, triosephosphate isomerase, serum amyloid P, and $\beta$ -galactosidase with and without corona discharge probe turned on.....	87
Figure 4-3	Representative data for $\beta$ -lactaglobulin used to determine the charge state where CID and CIU threshold energies converge and plots of all identified charge states from CID-CIU convergence screen .....	89
Figure 4-4	Monomer collision cross-sections for $\beta$ -lactaglobulin, triosephosphate isomerase, hemoglobin A, hemoglobin B, avidin, concanavalin A, serum amyloid P, and aldolase .....	91
Figure 4-5	Mass spectra produced from dissociation of $35^+$ and $47^+$ $\beta$ -galactosidase.....	93
Figure 4-6	Mass spectra produced from dissociation of $24^+$ and $33^+$ catalase.....	95
Figure 5-1	Structures and gas-phase basicities for HPP, DBN, TMG, and TEA.....	102
Figure 5-2	Cross-section of redesigned corona discharge probe with added Faraday cage and point-to-plane geometry positioned perpendicular to gas flow .....	104

Figure A-1	Mass spectra for concanavalin A under control conditions, under solution additive charge reduction conditions with DBU, and under gas-phase charge reduction conditions with DBU.....	107
Figure C-1	Aldolase collision induced unfolding fingerprints for measured native and charge reduced charge states .....	112
Figure C-2	Avidin collision induced unfolding fingerprints for measured native and charge reduced charge states.....	113
Figure D-1	Avidin mass spectra with and without corona discharge charge reduction.....	116
Figure D-2	Aldolase mass spectra with and without corona discharge charge reduction...	117
Figure D-3	Concanavalin A mass spectra with and without corona discharge charge reduction .....	118
Figure D-4	Alcohol dehydrogenase mass spectra with and without corona discharge charge reduction .....	119
Figure D-5	Pyruvate kinase mass spectra with and without corona discharge charge reduction .....	120
Figure D-6	Glutamate dehydrogenase mass spectra with and without corona discharge charge reduction .....	121
Figure D-7	Avidin CIU fingerprints generated from the 12+ ion with solution based charge reduction and corona discharge charge reduction .....	122

## List of Tables

Table C-1	Coarse grain avidin model structures generated during Monte Carlo search ..	114
Table D-1	Measured CCS values for each observed charge state of $\beta$ -Lac dimer, TPI, SAP, and $\beta$ -Gal under control and CDP charge reduction .....	123

## **List of Appendices**

Appendix A	Chapter 2 Supporting Information.....	107
Appendix B	Protocol for Nebulizing Sprayer Operation.....	109
Appendix C	Chapter 3 Supporting Information.....	112
Appendix D	Chapter 4 Supporting Information.....	115
Appendix E	Protocol for Corona Discharge Probe Operation.....	125

## List of Abbreviations

ADH	Alcohol dehydrogenase
AP	Affinity purification
$\beta$ -Gal	$\beta$ -galactosidase
$\beta$ -Lac	$\beta$ -lactoglobulin
BIRD	Blackbody infrared radioactive dissociation
CCS	Collision cross section
CEM	Chain ejection model
CID	Collision induced dissociation
CIU	Collision induced unfolding
ConA	Concanavalin A
CR	Charge reduction/reduced
CRM	Charge residue model
CS	Charge state
CSD	Charge state distribution
CXL	Chemical cross-linking
DBN	1,5-diazabicyclo[4.3.0]non-5-ene
DBU	1,8-diazabicyclo[5.4.0]undec-7-ene
DC	Direct current
DMA	Differential mobility analyzer
E	Electric field strength

ECD	Electron capture dissociation
EHSS	Exact hard-spheres scattering
EOF	Electroosmotic flow
ESI	Electrospray ionization
ETC	Electron transfer dissociation
FAIMS	High-field asymmetric waveform ion mobility spectrometry
GDH	Glutamate dehydrogenase
HDX	Hydrogen/deuterium exchange
Hgb	Hemoglobin
HPP	1,5,7-triazabicyclo[4.4.0]dec-5-ene
IEM	Ion evaporation model
IM	Ion mobility
IMS	Ion mobility spectrometry
K	Ion mobility
<i>m</i> -NBA	<i>m</i> -nitrobenzyl alcohol
<i>m/z</i>	Mass-to-charge ratio
MALDI	Matrix-assisted laser desorption ionization
MD	Molecular dynamics
MS	Mass spectrometry
MS/MS	Tandem mass spectrometry
nESI	Nanoelectrospray ionization
NMR	Nuclear magnetic resonance
OFP	Oxidative footprinting

PA	Projection approximation
PDB	Protein data bank
PK	Pyruvate kinase
R <sub>TW</sub>	Traveling wave resolution
Q	Quadrupole
RF	Radio frequency
SAP	Serum amyloid P
SID	Surface induced dissociation
SSNMR	Solid-state nuclear magnetic resonance
T	Temperature
TEA	Triethylamine
TEAA	Triethylammonium acetate
TEAB	Triethylammonium bicarbonate
TFA	Trifluoroacetic acid
TMG	1,1,3,3-tetramethyl guanidine
ToF	Time-of-flight
TPI	Triosephosphate isomerase
TRAP	Tryptophan-RNA binding attenuation protein
T-wave	Traveling wave
[WH]	Wave height
[WL]	Wave length
[WV]	Wave velocity
XRD	X-ray diffraction



z

charge

## **Abstract**

Macromoleclar protein complexes comprise a critical class of biomolecules unique in both their importance in biology and their relative impenetrability to detailed structural probes. Nanoelectrospray coupled to ion mobility-mass spectrometry (nESI-IM-MS) is an emerging tool for determining size and structure of protein complexes. However, its usefulness in such endeavors is largely dependent on the ability to accurately measure and correlate both intact assemblies and their protein building blocks in the gas phase to biologically-relevant structures in solution. Previous data have indicated that protein complex charge state has a demonstrated, yet currently unclear, influence on the dissociation pathways available to complexes upon collisional activation. Here, experiments designed to evaluate many different methods for ion charge state manipulation are described in the context of their potential applications in structural biology. In addition, the charge state-dependent mechanisms by which the building blocks of protein complexes are revealed via collisional activation in the gas phase are studied in detail, uncovering new intermediates and predicative correlations.

Following a comprehensive introductory chapter, Chapter 2 describes a detailed set of experiments aimed at evaluating the relative merits of different charge manipulation protocols for protein complex structure analysis. Gas-phase methods, such as ion-neutral chemistry performed in the source region of the instrument, are found to provide a superior ability to reduce protein charge without leading to unwanted protein unfolding. In Chapter 3, the dissociation pathways of two protein complexes that take near-identical product ion formation

pathways when high charge states are considered, are studied in detail revealing the role of previously-unknown compact states in their dissociation mechanisms upon charge state reduction. In Chapter 4, ion-ion chemistry is used to rapidly screen a relatively large number of charge-reduced protein complexes for charge states at which collision induced dissociation and unfolding energy thresholds converge, producing the first relationship capable of predicting the amount of charge reduction necessary to shift the dissociation mechanism of collisionally activated protein complexes generally toward the ejection of compact, native-like product ions. In Chapter 5, a final summary of this work is presented, along with a projected outlook of future endeavors in this area.

## Chapter 1: Introduction

In their native states proteins most often exist as noncovalently bound multiprotein complexes that are critical for carrying out a wide range of critical cellular processes.<sup>1</sup> Over the last several decades, tens of thousands of interactions between individual proteins have been identified,<sup>2,3</sup> however, the complete functional annotation of these complexes is still a major challenge.<sup>4</sup> One way of overcoming the challenges inherent in broadly annotating function to the growing list of putative protein assemblies currently available is to develop and rapidly deploy technologies capable of assessing the three-dimensional structures of the identified complexes.<sup>5</sup> Such efforts are currently underway,<sup>6</sup> and will undoubtedly lead to a more detailed understanding of protein structure, as well as next-generation therapies for human disease.<sup>7,8</sup>

A variety of technologies exist that are capable of probing the structure of protein complexes to produce high resolution, three-dimensional structure information. Two such technologies are X-ray diffraction (XRD)<sup>9</sup> and nuclear magnetic resonance (NMR) spectroscopy.<sup>10</sup> The former technique is often referred to as a “gold-standard” in structural biology, and is capable of generating structural data with resolutions less than two angstroms for assemblies as vast, and as complex as intact ribosomes.<sup>11,12</sup> However, the sample requirements for XRD typically necessitate a large amount of high-purity, mono-disperse protein to generate diffraction-grade crystals.<sup>13</sup> Meeting this requirement can be difficult, particularly if the sample is not easily over-expressed or is resistant to crystallization.<sup>4,6,14</sup> Alternatively, NMR can also produce high-resolution structures for protein-protein complexes within a limited size range,

directly from solution. Such experiments can reveal much of the dynamics and motion of protein assemblies in their native states,<sup>15</sup> especially in cases where dynamic nuclear polarization (DNP) experiments are performed, that enable NMR measurements to be carried out in the context of the cellular environment.<sup>16,17</sup> For most applications, however, high purity, high concentration protein samples are required to develop high-resolution structural data.<sup>18</sup> The many limitations of high-resolution structural biology tools necessitates the development and implementation of new probes of protein structure that can be deployed more-broadly in the context of the protein mixtures.

One such set of technologies is based upon mass spectrometry (MS), where analyte samples can be prepared at less than 10  $\mu$ M concentrations, sample consumption can be reduced to microliter levels, and data analysis can handle mixtures containing many interacting proteins and small molecules.<sup>19-21</sup> Alone MS and tandem MS (MS/MS) performed directly on intact protein complexes<sup>22,23</sup> can provide stoichiometry and connectivity information; coupling MS with other techniques such as ion mobility (IM),<sup>24-26</sup> chemical cross-linking (CXL),<sup>27-29</sup> affinity purification (AP),<sup>30,31</sup> hydrogen/deuterium exchange (HDX),<sup>32-35</sup> and oxidative footprinting (OFP),<sup>36,37</sup> the complete structural landscape of a protein assembly can be assessed. While it is important to note that many of these technologies are still under development and cannot individually provide the same detailed structures as XRD or NMR. By integrating structural MS data with protein modeling, the generation of detailed assembly structures, comparable to XRD or NMR, may be possible.<sup>38</sup> Importantly, a protein structure pipeline based on MS would not be limited to those relatively rare proteins that are available in large amounts, at high purities, that are amenable to tagging and devoid of any degree of polydispersity or structural plasticity.<sup>39</sup>

Instead, MS technologies as part of an integrative structural biology effort may enable the comprehensive structural characterization on a proteome scale.<sup>4,13,40</sup>

## **1.1 Mass Spectrometry in Structural Biology**

The structural information content from MS coupled technologies can be very diverse. As represented in Figure 1-1, the inner circle depicts the available MS technologies for studying the structure of multiprotein complexes, and the outer circle presents the structural information that can be determined from these types of analyses. HDX-MS and OFP-MS can both be used to measure protein-protein interface sizes between the multiprotein complex subunits as well as determine the folded and unfolded regions within the subunits on the residue level.<sup>41-44</sup> AP-MS and CXL-MS can be used to identify specific regions of connectivity between interacting subunits.<sup>45-49</sup> CXL-MS and IM-MS can both be used to measure the overall size of the multiprotein complex and distances between subunits, and can additionally be used to determine subcomplex topologies.<sup>50-54</sup> Alone IM-MS can be used to probe overall complex shape and determine angles between subunits.<sup>38,50,55,56</sup> IM-MS is unique among all these technologies in that it is the only method where intact, native-like protein structures are measured in the gas-phase, which provides unique challenges to its development and application in structural biology.<sup>55,57,58</sup>

All MS technologies in structural biology require the conversion of neutral, native-state proteins into gas-phase ions that carry useful protein structure information. While each of the many structural MS techniques described above have their own instrumentation and method requirements, since this work deals primarily with IM-MS of intact protein complexes, the following discussion focuses primarily upon the instrument requirements of such experiments. There are two well-known ionization methods that generate large multi-protein complex ions:

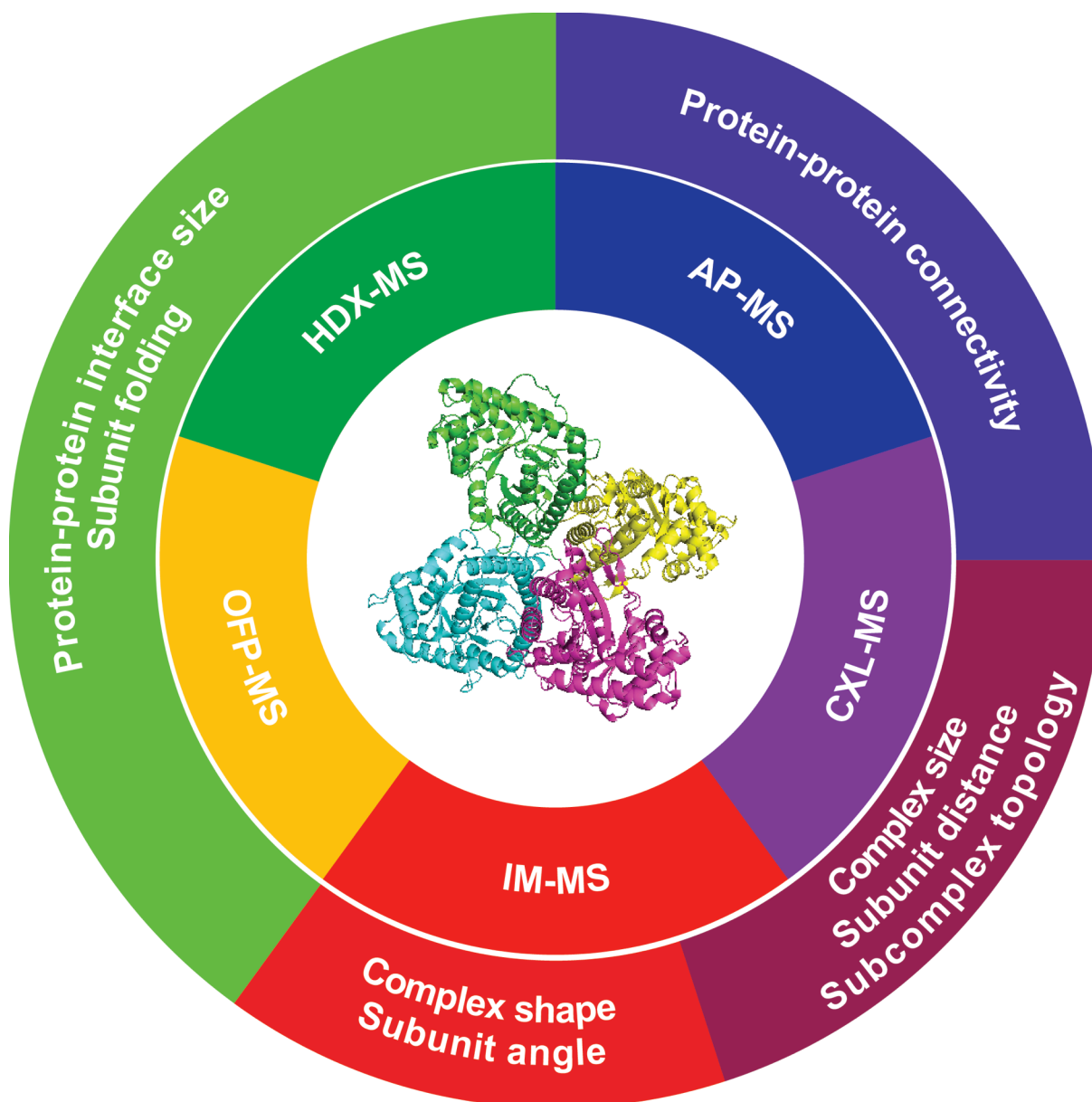


**Figure 1-1.** Common mass spectrometry (MS) coupled technologies and their utility within the field of structural biology. The inner circle lists the various methods: affinity purification (AP)-MS, chemical cross-linking (CXL)-MS, ion mobility (IM)-MS, oxidative footprinting (OFP)-MS, and hydrogen/deuterium exchange (HDX)-MS. The outer circle lists the various types of structural information that can be measured using the available technologies, where the color and placement of the outer circle regions correspond to the specific method used for measurements. For example, protein-protein connectivity information can be probed using either AP-MS or CXL-MS.

electrospray ionization (ESI)<sup>59-62</sup> and matrix-assisted laser desorption ionization (MALDI).<sup>63,64</sup>

While MALDI is capable of ionizing large analytes, the high concentrations of acid in traditional matrices are such that native-like conformations of multiprotein complexes are difficult to

maintain.<sup>39</sup> Furthermore, MALDI typically generates low charge state ions, which can make MS/MS experiments of large intact protein complex ions more difficult.<sup>65</sup> As a result, most MS experiments carried out on intact multiprotein complexes utilize ESI, since it has been observed to better enable the preservation of native-like conformations of protein complexes in the gas-phase.<sup>66,67</sup> The mechanics and mechanism of ESI, and the basics of native mass spectrometry will be discussed in greater detail in the following sections.

### **1.1.1 Nanoelectrospray Ionization (nESI)**

In 1989 the landscape of mass spectrometry changed forever when John Fenn and co-workers demonstrated that they could introduce large biomolecules into the gas-phase via electrospray ionization, eventually leading to Fenn earning part of the Nobel Prize in Chemistry in 2002.<sup>68</sup> Since then, ESI has evolved into a broadly-used analytical tool, enabling the ionization of molecules ranging from small metabolites to megadalton-scale protein complexes.<sup>69</sup> Furthermore, the scale of the technique has been reduced into what is known as nanoelectrospray ionization (nanoESI or nESI), which enables more efficient transport of ions from solution to the gas phase, while simultaneously reducing sample consumption and decreasing applied potentials.<sup>70</sup> The basic operating principles of nESI are simple; sample is delivered to the interface of the mass spectrometer through a tapered capillary tube coated with a conductive metal (typically gold or gold-palladium alloy) as depicted in Figure 1-2a, and a high electrical potential is applied (0.8-2.5 kV). Under these conditions a Taylor cone is formed at the tip of the tapered capillary and charged analyte droplets are formed, as shown in Figure 1-2b. Flow of the sample solution is maintained through electroosmotic flow (EOF). The charge droplets then undergo a series of successive solvent evaporation-droplet fission events, where droplet fission is



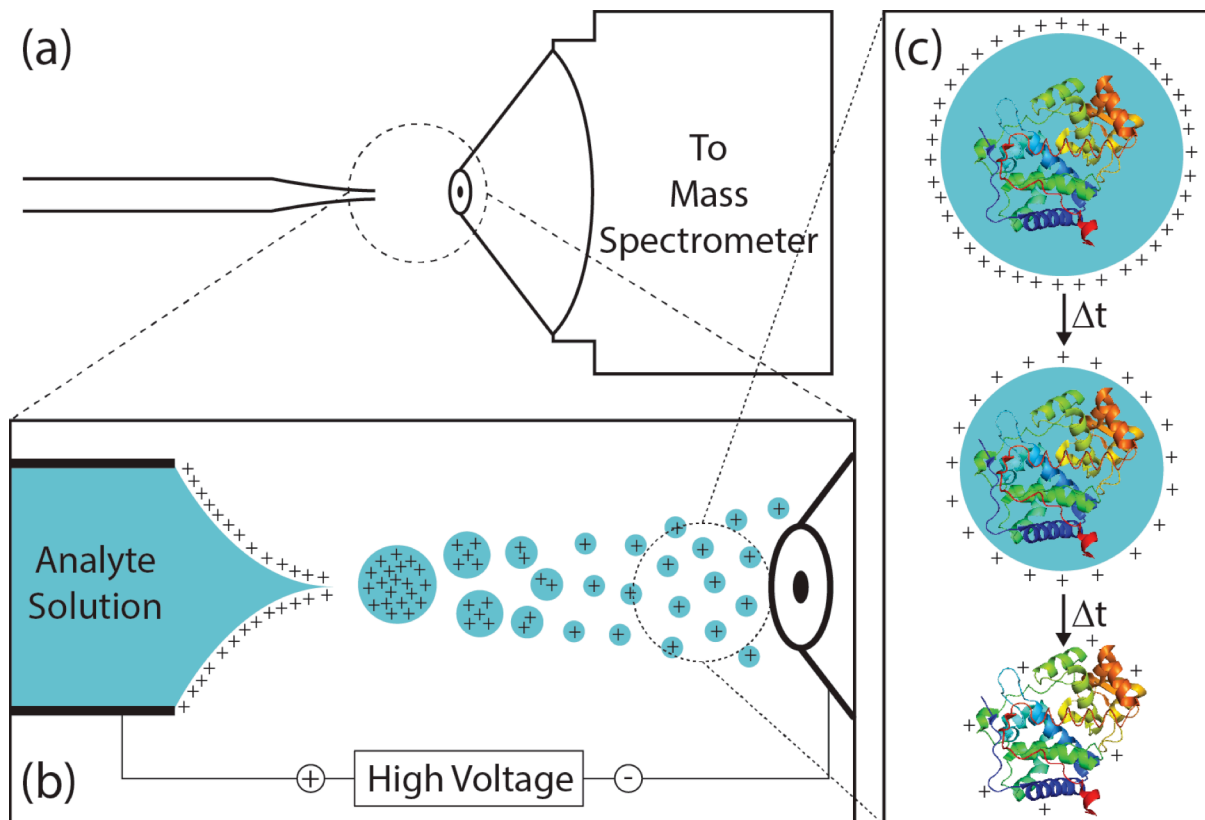


**Figure 1-2.** Diagram depicting the operation and mechanics of nano-electrospray ionization (nESI) where (a) shows the relative positioning of a tapered capillary needle containing an analyte solution near the entrance of a mass spectrometer. A blow up of the capillary tip and entrance (b) shows when a high voltage is applied relative to the capillary and entrance a Taylor cone forms and highly charged droplets are generated. These charge droplets undergo a series of solvent evaporation-droplet fission events until only charged analyte ions remain. As described by the charge residue model (CRM) during the final stage of ionization (c) a single analyte molecule exists in a highly charged droplet. As the droplet continues to evaporate and fission the surface charge decrease and moves closer to the surface of the analyte, as the last of the solvent evaporates the remaining surface charge is deposited onto the surface of the analyte producing a solvent-free gas-phase ion.

induced by the charge on the surface of the droplet when a limiting radius is reached, as governed by the Rayleigh equation:

$$z_R = \frac{8\pi}{e} (\gamma \epsilon_0 R^3)^{1/2} \quad (1.1)$$

Where  $z_R$  is the maximum charge attainable for a droplet of radius  $R$ ,  $e$  is the elementary charge,  $\gamma$  is the surface tension of the solvent, and  $\epsilon_0$  is the permittivity of the environment. When it is assumed that intact proteins are approximately spherical and have equal density, and are ionized

from standard nanoelectrospray conditions it has been shown that the charge state can be predicted by:

$$z_R = 0.078M^{1/2} \quad (1.2)$$

where M is the molecular mass of the protein.<sup>71</sup>

The final stage of ionization is still an active area of research. Currently there are many proposed models, with the two most prominent being the charge residue model (CRM)<sup>59,60</sup> and the ion evaporation model (IEM).<sup>72</sup> For the study of intact multiprotein complexes in the gas-phase the most widely accepted model for ion formation is CRM. As depicted in Figure 1-2c, during the final stages of ionization a single biomolecule is contained within a charged droplet, as evaporation and fission continues the droplet volume decreases until the residual droplet charge is deposited over the surface of the protein.<sup>59,60</sup> Alternatively, IEM suggests that instead of undergoing droplet fission in the later stages of ionization, analyte ions are produced directly from the larger charged droplets in an evaporation-like process.<sup>72</sup> Strong experimental evidence, however indicates that CRM is the dominant mechanism for large analytes, such as the multiprotein complexes studied here.<sup>71</sup>

Both CRM and IEM are mechanisms in which native-like protein conformations are preserved in the gas-phase, which accounts for experimental evidence validating equation 1.2.<sup>71</sup> However, ESI of proteins can adopt charge states distributions (CSDs) in great excess of the maximum CRM predicted charge.<sup>73</sup> Such experiments are performed in non-native solvent conditions (to be discussed in Section 1.1.2), which disrupts protein structure to cause unfolding in solution.<sup>65</sup> Because the protein exists in a different structure in solution a different model is used to describe the ESI process, the chain ejection model (CEM).<sup>74</sup> In CEM, large disordered polymer chains, such as unfolded proteins, exist in a charged droplet. Following desolvation of

the large, charged droplet, fission occurs in a fashion similar to IEM, where analyte ions are ejected directly from the charge droplet.<sup>73,74</sup> However, the long unfolded polymer chain cannot be ejected from the droplet on the same timescale as small analytes following IEM.<sup>73,74</sup> The longer timescale of the ion ejection allows for charge migration to occur. As a result, the droplet surface charge is depleted as charge migrates to the surface of the analyte as it is ejected.<sup>74</sup> Since the surface area of the unfolded analyte is must larger than the compact native-like form, the charge observed CSD is shifted to much higher charge states.<sup>74</sup>

### **1.1.2 Native Mass Spectrometry**

Many studies have shown that the solvent composition encountered by proteins prior to nESI plays a significant role in the ultimate gas-phase structures and mass-to-charge ratio ( $m/z$ ) observed from the resultant ions.<sup>65</sup> For example, when proteins are exposed to denaturing buffers or solvents prior to nESI, the gas-phase ions created acquire a relatively large amount of ionic charge when compared to those ionized under native-like conditions.<sup>65</sup> Typical solvent systems employed in such experiments include 50:50 water:methanol and water:acetonitrile mixtures, usually accompanied with a low percentage of acid. Such solution conditions disrupt the intra- and inter-molecular interactions within proteins and larger multiprotein complex systems.<sup>65</sup> If these same experiments are performed using proteins prepared in buffered, aqueous solutions at pH 7, protein fold and quaternary structure can be maintained, to a certain extent, upon gas-phase ion formation by nESI.<sup>55,66</sup> Ammonium acetate is typically added to maintain ionic strength and establish a weak buffer in such solutions, and is commonly utilized in such “native mass spectrometry” experiments.<sup>75-78</sup>

Until the early 1990s, protein ESI-MS research was limited to denaturing conditions described above. Work done separately by Henison<sup>79</sup> and Chait<sup>80</sup> demonstrated that protein-

ligand complexes could be observed by altering the electrospray conditions, specifically the pH.<sup>81</sup> The following year, Baca and Kent performed the first MS experiment of an intact protein-protein complex under similar solution conditions.<sup>75</sup> Quickly, other research groups began studying intact multiprotein complexes of increasingly higher and higher mass and complexity for the study of protein-protein interactions.<sup>76-78,82</sup> With the development of nESI, the field of native MS took another leap forward when Robison and co-workers demonstrated retention of protein-ligand complexes in the gas-phase, which were not observed under conventional ESI.<sup>83</sup> Work by Robinson and Heck has strived to push the field to study and characterize larger and more complex multiprotein complex systems. Complexes on the megadalton scale are now routinely studied,<sup>69,84,85</sup> as well as methods to monitor protein dynamics<sup>86</sup> and characterizing higher-order architecture.<sup>87</sup> Recently, the compact, native-like architecture of such protein ions have been examined by ion mobility spectrometry (see below) and gas-phase spectroscopy measurements, and have revealed strong correlations in the higher-order structure between solvent-free proteins and those found in solution, while noting differences in their local structure.<sup>55,56,66,88,89</sup>

## **1.2 Ion Mobility-Mass Spectrometry (IM-MS)**

Ion mobility (IM) separates ions based on their ability to traverse a chamber of inert neutrals under the influence of an electric field, resulting in longer transit times for ions larger in size or lower in charge and shorter transit times for those ions that are smaller in size or more highly charged.<sup>90</sup> Since many of the physical principles that dictate ion transport under such conditions are well understood, ion drift times can often be easily converted to collision cross-sections (CCS), precisely defined as a rotationally averaged ion-neutral interaction potential.<sup>91,92</sup> When combined with mass spectrometry (MS), the resulting multi-dimensional IM-MS technique can

provide a sensitive and efficient means of analyzing complex mixtures ranging from crude oil to cellular extracts.<sup>93-95</sup> Recently, applications of the IM-MS approach to challenges in structural biology and ligand screening have highlighted the ability of the technology to provide useful structure and stability information for protein samples difficult to analyze by other means.<sup>96-98</sup> Such experiments have concentrated on multiprotein targets, due to their central roles in many critical biological processes, and present a multi-dimensional dataset from which gas-phase data can be extracted in a manner that has been shown to correlate strongly with solution based measurements.<sup>19</sup>

While there are several different commercially available platforms for performing ion mobility spectrometry (IMS), all fall into one of two groups: drift tube and differential devices. In drift tube devices, an analyte ion packet is introduced into a high-pressure drift cell under an electric field. Here all ions experience the same electric field and the time to traverse the drift cell is measured for all analyte ions (analogous to time-of-flight mass spectrometry; see section 1.2.3). Differential devices behave similarly in that analyte ions are introduced into a high-pressure cell and experience an electric field; however, they are introduced continuously and not all ions are detected under the same electric field conditions. In this instrument configurations analytes are separated by different electric field conditions (analogous to quadrupole mass spectrometry; see section 1.2.1).

As mentioned above, only in the past decade or so has the utility of IMS been expanded to studying large multiprotein complex structures. Coupled together with MS, IM-MS separates ions in two orthogonal dimensions, providing complementary information on both analyte mass and size. Several commercial IM-MS instruments are available utilizing a variety of IMS and MS technologies. Here we use the commercially available Waters Synapt G2 HDMS, shown in

Figure 1-3, which is equipped with a nESI source, a high- $m/z$  quadrupole mass filter, a traveling wave (T-wave) ion mobility drift cell, and a time-of-flight mass spectrometer. The inset of Figure 1-3 demonstrates how a packet of ions is introduced into the drift cell containing neutral gas molecules and is pushed through by the electric field, ions are separated within the cell based on their charge and size due to differences in the number of collisions with the neutral gas molecules. The measured drift times can be converted to CCS values using celebrants with known CCS values following a standard protocol.<sup>91</sup>

In addition to measuring ion CCS, protein structure transitions in the gas-phase can also be measured by IM-MS using collision induced unfolding (CIU).<sup>96,99,100</sup> A general approach for CIU measurements relies first upon ion selection within a quadrupole mass filter, and subsequent activation of the ion population of interest via collisions with Argon. For compact, low charge

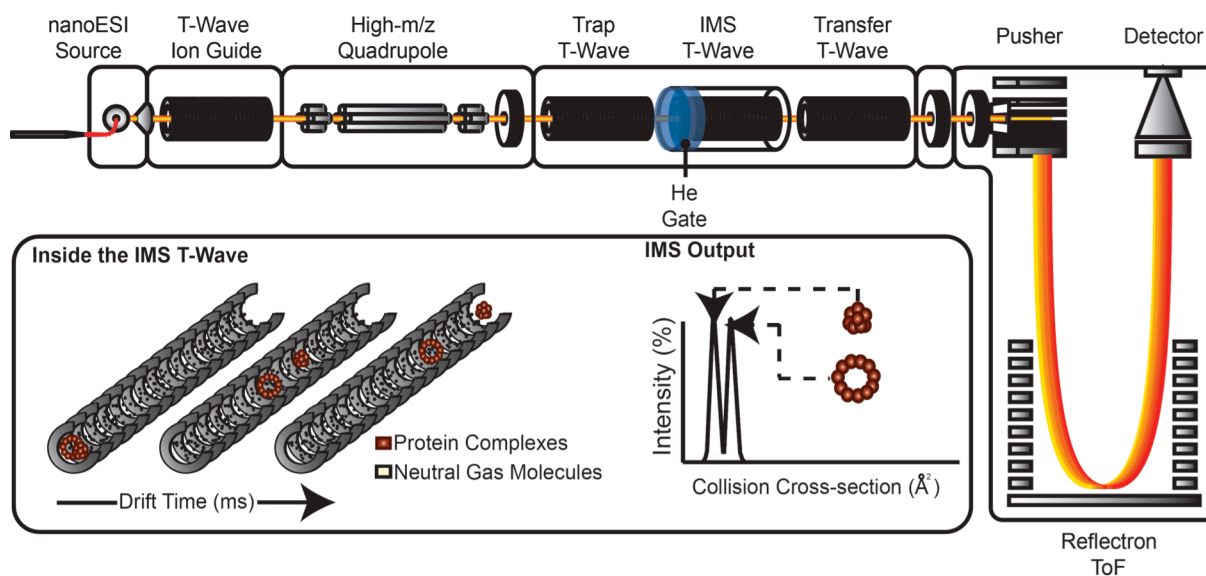


**Figure 1-3.** Schematic diagram of the commercially available Waters Synapt G2 HDMS nanoelectrospray-quadrupole-ion mobility-time-of-flight mass spectrometer. The instrument is equipped with an extended mass range quadrupole mass filter (32,000 Da) to allow for the analysis and selection of large analyte ions. The inset depicts how a packet of ions is introduced into the traveling wave ion mobility drift cell and is pushed through a field of inert neutrals by a series of low voltage waves formed by a time-varying electric field. Ions are separated based on their charge and size. The measured drift times can be converted to CCS values using calibrants of known CCS values.

state protein ions, this activation step induces protein unfolding.<sup>101</sup> In the case of similarly compact multiprotein complexes, most models suggest that one subunit within the assembly primarily unfolds.<sup>57,65</sup> In either case, multiple partially-folded intermediate states are observed which are unique to the gas-phase, stable on a millisecond time scale prior to dissociation, and reflective of the pre-existing tertiary structure of the unfolding protein.<sup>57</sup> In many cases, the appearance energy and CCS of these activated, intermediately unfolded conformers can be related back to protein-small molecule binding modes and stabilities using detailed comparisons and analysis.<sup>102,103</sup> The following sections introduces the various elements of the Synapt G2 instrument used throughout this thesis in the order in which they are encountered by ions transmitted from the nESI source (Figure 1-3).

### **1.2.1 Quadrupole Mass Spectrometry**

Quadrupole mass spectrometers consist of four parallel rods that are evenly, radially distributed about the center-axis of the instrument.<sup>104,105</sup> Opposing rods are electrically paired together, a combination of direct current (DC) and radio frequency (RF) voltages is applied to each rod-pair, where the DC voltage is the same for the two rod-pairs while the RF voltages oscillate at the same known frequency but are 180-degrees out of phase. At a specific combination of DC and RF potentials a quadrupolar field is created in which only a single  $m/z$  ion has a stable trajectory to reach the detector, all other ions have unstable trajectories and either collide with the quadrupole rods or are pumped away. Changing the quadrupolar field, by scanning over a range of DC and RF voltages, as a function of time enables the acquisition of a complete mass spectrum. A third mode of operation, in which the DC potential is zero (RF-only mode), allows the instrument to act as an ion guide, where a wide range of  $m/z$  ions are stable and can pass through the quadrupolar field. Since ions are continuously introduced into the quadrupole

analyzer, the technique is ideal for coupling with continuous ionization methods, such as nESI, and has been described in combination with both ion mobility<sup>106</sup> and time-of-flight<sup>107,108</sup> analyzers to create powerful tandem MS instrument platforms for applications in complex mixture analysis,<sup>109</sup> trace detection,<sup>110</sup> and structural biology.<sup>23</sup>

### **1.2.2 Traveling Wave (T-wave) Ion Mobility**

Many different IM-MS instrument platforms have been described in the literature<sup>24</sup>, including the Synapt HDMS system.<sup>111-113</sup> This particular platform uses a traveling wave (T-wave) ion guide to perform IM separation and was released as the first commercial IM-MS platform in 2006,<sup>111</sup> followed by a second generation platform (Synapt G2 HDMS) in 2009 (Figure 1-3).<sup>112,113</sup> T-wave IM uses low-voltage “waves” within a stacked-ring ion guide pressurized with inert neutrals to separate ions according to their size-to-charge ratio. Wave Height ([WH]), Wave Velocity ([WV]), and pressure in the IM separator are all key parameters for optimized performance.<sup>113</sup> Under high wave height and velocity conditions, with low pressure, T-wave instruments operate as ion guides, where there is no separation between differing ions due to the high energy barrier of the high wave height and few interactions with neutral gas molecule due to fast transit times at low pressure.<sup>111,114</sup> By lowering the wave height and velocity, while increasing pressure within the T-wave, ions of differing size-to-charge are separated due to the higher number of collision with neutral gas molecules due to slow transit times at higher pressure, and the possibility of rollover between consecutive electric field waves due to the decreased energy barrier associated with lower wave height.<sup>111,114</sup> The resolution of IMS data is characterized by several different factors including diffusion, space charge, initial pulse width, reaction chemistry, and conformational changes.<sup>113</sup> It is commonly assumed within the field that the total resolution



can be approximated by the effects due to diffusion alone.<sup>113,115</sup> Under such diffusion-limited conditions in T-wave instruments, resolution ( $R_{TW}$ ) can be defined by:

$$R_{TW} = \frac{1}{4} \left( \frac{2ze[\text{WH}][\text{WL}]KE}{[\text{WV}]kT \ln 2} \right)^{1/2} \quad (1.3)$$

where  $z$  is the ion charge,  $e$  is the electron charge,  $[\text{WL}]$  is the wave length,  $K$  is the ion mobility,  $E$  is the field strength,  $k$  is the Boltzmann constant, and  $T$  is the temperature in the T-wave ion guide.<sup>113,115</sup> From this equation, it is clear that resolution can be greatly influenced by multiple instrument parameters, making this methodology more advantageous over the traditional linear drift tube, which can only be influenced by a single instrumental variable, the electric field.<sup>113</sup> However, the T-wave resolution is limited by the capabilities of the instrument components (maximum/minimum achievable parameters), whereas the linear drift tube is theoretically limitless by increasing the length of the drift tube.<sup>48</sup>

The Synapt G2 was modified from the first generation instrument to enhance performance and resolution. Key differences between the first and second generation Synapt instruments include: 1) a longer IM separation region, 2) an ion guide pressurized with He gas between the trap and IM separation regions tuned to reduce activation upon ion injection, 3) increased pumping conductance in the ion trap and transfer regions enabling higher operating IM pressures (up to 4mTorr of N<sub>2</sub>), and 4) differential pairing of electrodes within the stacked ring ion guide that enables larger applied fields for IM separations (up to 90% of the field applied at the electrode surface). For all T-wave IM instruments, calibration with ions having known CCS is necessary to determine CCS values for unknown analytes.

### 1.2.3 Time-of-Flight (ToF) Mass Spectrometry

A basic time-of-flight (ToF) mass spectrometer is composed of three components: 1) an ion pusher, 2) a flight tube, and 3) a detector. In the pusher, ions are pulse injected into the flight

tube as a packet such that ions of equivalent charge in the packet are given equivalent kinetic energy, where ions of higher charge have higher kinetic energy. In the flight tube, ions separate due to differences in velocities since kinetic energy is directly proportional to both the mass and the velocity squared. Therefore, more massive, lower charged ions will traverse the flight tube at a slower velocity than less massive, higher charged ions, which have faster velocities. All ions must traverse the same distance in the flight tube to reach the detector. Since the ions have different velocities, the time each ion takes to reach the detector is recorded and is directly related to the  $m/z$  by:

$$t = \frac{d}{\sqrt{2U}} \sqrt{\frac{m}{z}} \quad (1.4)$$

where  $d$  is the fixed distance the ion travels through the drift tube and  $U$  is the electric potential applied in the pusher to give all like charged ions equivalent kinetic energy.

The physics of ion motion in the flight tube is well understood, where decreased peak resolution in the flight tube can be attributed to diffusion. The region that effects the peak resolution the most is in the pusher. In an idealized instrument, ions in the pusher would all have the same initial position, be stationary, and accelerate to the same kinetic energy in a single acceleration event before entering the flight tube at the same time. In a single acceleration, due to differences in initial position within the pusher region, ions of the same  $m/z$  will accelerate differently. Ions in the pusher initially positioned closer to the flight tube entrance will be accelerated for a shorter period of time before entering the field free flight tube, and will therefore have lower kinetic energies than those positioned further from the drift tube, assuming the ions have equivalent trajectories before acceleration. Additionally, ions of the same  $m/z$  and are at the same position within the pusher, but have different trajectories before acceleration, will leave the pusher at the same time, however, they will have different velocities. To account for

these differences in spatial position and trajectories, a dual-phase acceleration is known as delayed pulse excitation is performed.<sup>116</sup> Under this protocol, ions are allowed to separate in a field-free region before acceleration to allow of the same  $m/z$  but with different trajectories to separate in space. When the acceleration voltage is applied after a fixed delay time, the ions with higher initial velocities will be positioned closer to the flight tube entrance while ions with lower initial velocities will be positioned farther away. The ions closer to the entrance will accelerate for a shorter period of time and ultimately have a lower velocity in the flight tube than the ions which were farther from the entrance and experienced the acceleration voltage for a longer period. The delay time and the acceleration voltage can be tuned such that ions of a particular  $m/z$  will reach the detector at the same time. This process of space focusing is optimized for a single  $m/z$ , but also improves resolution for similar ions. To velocity focus a broader range of different  $m/z$  ions additional methods are implemented.

Most commercially available ToF instruments are equipped with one or more of a fourth element, a reflectron. When ions are ejected from the pusher into the flight tube, two ions with the same  $m/z$  theoretically have the same kinetic energy, and therefore the same velocity; due to differences in starting trajectories within the pusher, this is not the case. The purpose of the reflectron is to compensate for the different velocities of equivalent  $m/z$  ions.<sup>117</sup> To achieve this, the reflectron acts as an ion mirror, where a series of equally spaced ring or grid electrodes creates an electric field to redirect the ions, in a fashion similar to light on a mirror, toward the detector or a successive reflectron. Ions of greater velocity will penetrate the electric field more deeply and take a longer time to reach the detector, while ions with lower velocity will penetrate less deeply and more quickly reach the detector. Properly configured, the difference in flight distance caused by the reflectron will normalize equal  $m/z$  ions of different velocities to the same

flight time, and therefore produce higher resolution mass spectra.<sup>117</sup> As a consequence of the reflectron, ions travel a greater distance, allowing ions of similar  $m/z$  to become more temporally separated, and therefore, improve spectral resolution.<sup>117</sup>

### **1.3 Protein Complex Subunit Analysis in Mass Spectrometry**

In order to construct a model of a multiprotein complex it is essential to accurately measure the size of not just the intact complex, but also the individual subunits and subcomplexes that make up the intact system.<sup>38,118,119</sup> Such measurements define the detailed protein-protein connectivity and distances within the assembly, and act as constraints for computational simulations of model topology.<sup>38,50,118,120</sup> Such information is typically acquired in two generalized modes: solution disruption and gas-phase dissociation. The first strategy is characterized by altering solution conditions such that inter-molecular interactions are disrupted while intra-molecular interactions are preserved.<sup>97</sup> The latter strategy is characterized by introducing energy to the intact complex ions within the gas phase.<sup>121</sup>

#### **1.3.1 Solution Disruption Strategies**

Through the alteration of solution composition, protein-protein interfaces can be disrupted differentially based on their chemical compositions, stabilities, and structures.<sup>97</sup> For example, hydrophobic interactions are disrupted by the addition of organic solvents<sup>87,118,122,123</sup> while salt bridges are disrupted by increasing the ionic strength of the buffer.<sup>123,124</sup> While these approaches are currently our most effective means for generating native-like protein sub-complexes and subunits for IM-MS measurements,<sup>97</sup> care must be taken to retain the folds of individual proteins following disruption.<sup>50</sup> Indeed, the retention of protein tertiary and secondary structure following protein-complex disruption is not always possible due to the tight, domain-swapped architecture of some protein interfaces.<sup>125</sup> In addition, solution-phase protein disruption is both slow and

relatively poorly understood on a mechanistic level when compared with gas-phase methodologies (see below, Section 1.3.2),<sup>19</sup> although recent efforts have been made to perform rapid, comprehensive solution-phase disruption experiments for IM-MS.<sup>50</sup> As such, there is a strong motivation to develop gas-phase dissociation experiments that enable the generation of compact, “native-like” product ions.

### **1.3.2 Gas-Phase Complex Dissociation**

An alternative approach to generating subunits and subcomplexes of multiprotein complexes is through dissociation in the gas phase. Currently, there are several different commercially available dissociation techniques used within the field of structural biology: collision induced dissociation (CID), surface induced dissociation (SID), and electron transfer dissociation (ETD)/electron capture dissociation (ECD). Of the available techniques, the latter two add energy to precursor ions on the ps or fs timescales, which means that a single electron capture or surface collision event induces protein complex dissociation. CID, on the other hand, is a slower technique in which dissociation is induced over a series of energy transfer events between the background gas (typically Argon) and the precursor ion. These generalized differences between the technologies give rise to both different product ions and information content. Figure 1-4 demonstrates the dissociation pathways available across these different technologies as described currently in the literature.<sup>82,126-137</sup>

CID occurs when an ion is accelerated in an electric field and allowed to collide with neutral gas molecules at elevated kinetic energies.<sup>138</sup> The ion experiences multiple collisions, which convert its starting kinetic energy to rotational/vibrational internal energy on the microsecond timescale.<sup>138</sup> The collisional event that takes place during CID can be viewed in one of two frames of reference: the laboratory frame of reference and the center-of-mass frame of

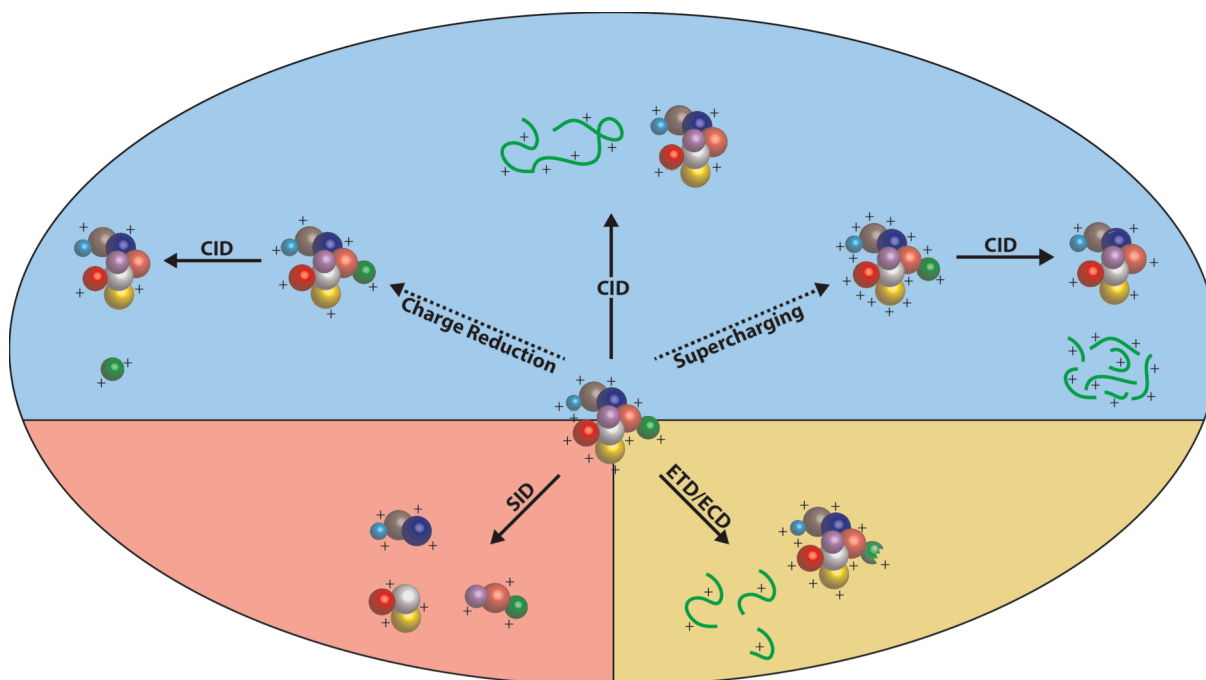


**Figure 1-4.** Dissociation pathways for collision induced dissociation (CID, blue), surface induced dissociation (SID, pink), and electron transfer dissociation/electron capture dissociation (ETD/ECD, yellow). The three different CID pathways are charge dependent, where the central pathway is most dominant for traditional charge states observed in native mass spectrometry and is characterized by the unfolding and dissociation of a single subunit, with that subunit carrying the majority of the charge from the precursor ion. When supercharged, the right pathway is observed, converting the unfolded subunit into peptide ions. The left pathway demonstrates dissociation from reduced charge states, where dissociation of a compact subunit is observed. The fast, high-energy collisions used in SID allow for the elimination of protein unfolding, producing compact, intact subcomplex ions. ETD/ECD proceeds to generate an unstable radical ion which undergoes backbone dissociation of a single subunit to generate peptide ions.

reference.<sup>139</sup> Under the lab frame of reference, the neutral gas-molecule is considered stationary, and therefore the kinetic energy of the collision can be simplified as the kinetic energy of the analyte ion, which is expressed as the product of the analyte charge state and the acceleration voltage. The CID dissociation pathway for protein complexes most commonly observed for native MS experiments is shown in the center of the blue region of Figure 1-4. Under these conditions, dissociation proceeds via an asymmetric charge partitioning pathway, where a single subunit from the complex dissociates from the remaining subcomplex while carrying a majority of the parent ions charge.<sup>82,126-129</sup> This phenomenon is observed across a wide range of proteins,

from the cytochrome *C* dimer where two distinct monomer CSDs are observed<sup>128</sup>, to the tetradecamer GroEL, which dissociates into monomer and tridecamer where the monomer carries up to 58.5% of the parent ions initial charge.<sup>140</sup> With the advent of IM-MS instruments capable of studying multiprotein complex ions in the gas-phase, we now know that subunit unfolding within a complex occurs, while the overall complex stoichiometry is maintained.<sup>57</sup> During this unfolding, charge likely migrates over the surface of the complex to maintain a uniform surface charge density over newly-formed unfolded gas-phase structures. Once sufficient unfolding within a single subunit has taken place, it dissociates and carries away a disproportionate amount of charge relative to its mass.<sup>57</sup> Since subunit unfolding plays a major role in this mechanism, the dissociation process is now often described as a symmetric charge partitioning process relative to the surface area available to the complex in the transition state.<sup>141</sup>

The asymmetric charge partitioning mechanism discussed above is not the only observed CID dissociation pathway for protein complex ions. Other pathways have been observed, often driven by an altered precursor ion charge state. For example, under supercharging, or charge amplification, conditions (right pathway of blue region in Figure 1-4), ions with amplified charge are accelerated to larger kinetic energies and thus undergo enhanced vibrational/rotational heating during CID.<sup>39</sup> Thus, primary monomeric product ions, likely produced by a mechanism similar to the asymmetric charge partitioning model described above, undergo further dissociation to generate peptide ions, which can be used to perform top-down type sequence analysis.<sup>131</sup> Alternatively, if the charge on precursor ions are reduced (left pathway of blue region in Figure 1-4), decreased Coulombic repulsion on the surface of the protein limits the extent of subunit unfolding. Although the CID of charge reduced protein complex ions has been shown to abrogate all subunit unfolding during collisional activation and lead to compact product ions,

general trends for this phenomenon are still unknown.<sup>130</sup> In addition, exceptions to the general trends presented in Figure 1-4 have been described in the literature,<sup>130,142-144</sup> highlighting the need for a more complete understanding of protein complex CID. Complete control over the protein complex CID mechanism, however, will undoubtedly lead to transformative structural biology methods that enable the rapid construction of multiprotein models.<sup>19,38,118</sup>

Relatively recently, protein complex dissociation in the gas-phase through SID and ETD/ECD has been demonstrated, and each of these methodologies offer orthogonal information content to the CID experiments described above. SID, like CID, occurs when the analyte is accelerated using an electric field to create an activating collision. However, in SID the collision event is a single collision with a stationary surface. As such, the timescale of ion activation is substantially shorter, significantly altering the resulting dissociation pathway and product ion populations produced. As depicted in the pink region of Figure 1-4 (lower left side), SID produces compact subcomplexes capable of producing useful topology information when coupled with IM-MS.<sup>132-135</sup>

ETD/ECD based product ions are formed in a rapid manor where excess energy comes from a captured, low-energy electron resulting in an electronic excitation event that produces product ion on the fs timescale, unlike CID which is coupled to rotational/vibrational activation on a much longer ms timescale.<sup>145</sup> As a result, the observed dissociation products from ETD and ECD are very different from slower methods. ETD and ECD both proceed after the generation of gas-phase radical ions generated through the reaction of the analyte with either an anion (in ETD)<sup>146,147</sup> or directly with an electron (in ECD), resulting in an excited radical.<sup>145,148</sup> For protein complexes, this excited state induces backbone dissociation of a single subunit to generate



peptide ions (as presented in the yellow, lower right region of Figure 1-4), which can be used in top-down sequencing efforts.<sup>136,137</sup>

## **1.4 Charge Manipulation Techniques**

As mentioned above, and shown in Figure 1-4, charge manipulation has been observed to dramatically alter the CID pathway of multiprotein complex ions.<sup>130,131</sup> For purposes of modeling protein complex topologies from IM-MS datasets, charge reduction represents a pathway to produce useful protein complex substructure information by enabling accurate size measurements of protein building blocks. However, in order to engage such alternative pathways, charge states must be altered from their native CSDs. To do this, two broad classes of approaches have been previously taken: use of solution additives that act to alter the ESI process in order to shift CSDs<sup>149-160</sup> or instruction of gas-phase reagents to react with protein ions in order to shift CSDs either during or post ionization.<sup>161-176</sup>

### **1.4.1 Solution Based Methods**

Both modification to aqueous buffer compounds<sup>134,135,153,160,177,178</sup> and the addition of specific bases<sup>155,179</sup> have been demonstrated as effective solution-phase approaches for reducing the resultant charge state of protein ions produced by nESI. Most alternative buffer options currently known act to shift protein charge states to lower values than those commonly encountered when using standard aqueous ammonium acetate buffer.<sup>153,155</sup> The buffers typically used are most often derived from ammonium acetate or ammonium bicarbonate buffers.<sup>152-154</sup> The most commonly used of these are triethylammonium acetate (TEAA) or triethylammonium bicarbonate (TEAB).<sup>134,135,160,177,178</sup> On the other hand, when solution additives are used to perform charge reduction they are usually strong gas-phase bases, and are selected to operate under the same principles as the alternative buffers described above.<sup>155,179</sup> Both protocols are

thought to operate under a shared mechanism that acts to reduce the final charge state observed for nESI produced ions.<sup>155</sup> As shown in Figure 1-5a, during the final stages of ionization, charge reducing species are hydrogen-bonded to protons at basic sites across the surface of the analyte protein. As desolvation continues, the protons are stripped from the surface of the protein as the basic species are ejected as charged species; this step is driven by the proton affinity of the basic site on the protein and the gas-phase basicity of the charge reducing species.

Unlike charge reduction, which is likely driven by a charge stripping mechanism that takes place during the later stages of nESI ionization, supercharging in nESI can also proceed by altering the physical properties of the droplet in order to influence the ionization mechanism.<sup>158</sup> Typically, this is done by adding agents that increase the surface tension of the solvent in order

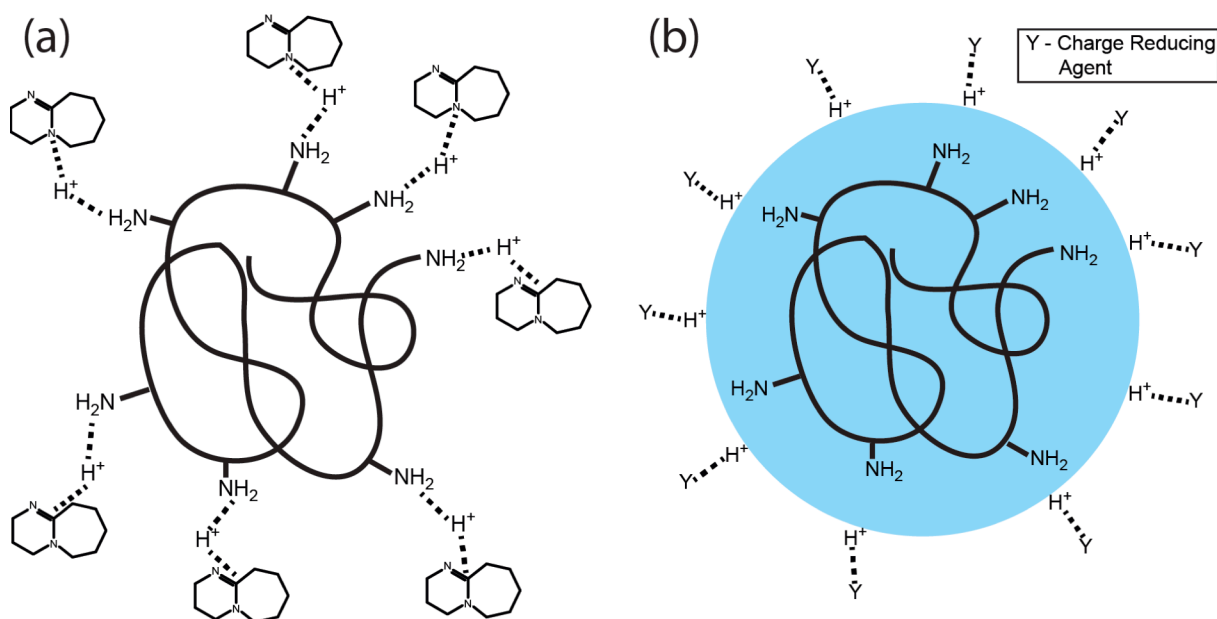


**Figure 1-5.** Charge reduction pathways for (a) solution additive and (b) gas-phase methodologies. In solution additive charge reduction, during the final stages of ionization charge reduction agents (here represented as DBU) are hydrogen-bonded to protons at basic sites across the surface of the protein. As desolvation continues, the protons are stripped from the surface of the protein as the basic species are ejected from the surface as ions. In gas-phase charge reduction, charge reducing agents (Y) can exist as both neutral or ionic species, and bond with protons on the surface of the droplet. Similar to solution charge reduction methods, surface charges are stripped based on proton affinity in ion-neutral reactions or are stripped/neutralized due to ion pairing or in ion-ion reactions.

to increase their charge density at the Rayleigh limit. An array of such supercharging reagents are available, with two of the most common being sulfolane and *m*-nitrobenzyl alcohol (*m*-NBA).<sup>150,151,156,157</sup> However, the mechanistic details of the charge amplification process are still an active area of research,<sup>157,160</sup> and there is strong evidence that such supercharging processes disrupt the structure of the proteins, making the current methods difficult to implement with IM-MS for analyzing multiprotein complex structures.<sup>159,160,180</sup>

#### **1.4.2 Gas-Phase Methods**

Like solution based charge manipulation methods, there are two different gas-phase approaches: ion-neutral reactions and ion-ion reactions. In such methods analyte ions react in the gas-phase with either counter ions or neutral reagents in an effort to either neutralize or strip protons from the protein, or to add protons when supercharging ions.<sup>163,175,181</sup> Additionally, there are two different protocols for introducing such gas-phase reactants to protein ions: charge manipulation can occur continuously in regions within or near the ESI source (such as the work done by Smith and co-workers),<sup>164-168</sup> or ion traps can be utilized to store analyte ions for subsequent reactions with neutrals or ionized species (such as the work done by McLuckey and co-workers).<sup>169,170,172,174</sup>

The earliest examples of gas-phase charge reduction used ion traps to store analyte ions and react them with a basic background gas (e.g. diethylamine) at pressures that ensured multiple collisions by reducing the mean free path of ions stored within the trap. Varying the trap times of the analyte affected the extent of charge reduction.<sup>161</sup> Similarly, ion-ion reactions can be performed in ion traps. For such experiments, analyte ions are typically stored, but rather than being exposed to relatively large numbers of neutrals reagents, ions of opposite polarity are generated from a secondary ion source and introduced into the trap using customized

waveforms.<sup>174</sup> The two ions are then allowed to react in the trap for controlled periods of time before mass analysis.<sup>169-174</sup> While there is evidence that compact native-like gas-phase conformations are retained during this process provided trapping times are short,<sup>182</sup> it is clear that increased trapping times are required to sufficiently reduce higher charge state ions, and with high mass analytes typically possessed of higher charge states, such extended trapping times are a concern for applications in structural biology.

Continuous methods for charge reduction are advantageous since they can generate charge reduced ions at a rapid rate due to the increased collision frequencies available between analyte and reagent, mitigating many of the potential issues that arise from extended trapping periods. However, as trapping times proved to be an important variable for controlling charge states in the experiments described above, gas-flow rates for the charge reducing species are equally important for controlling charge reduction in the nESI source.<sup>163,168,183</sup> Early work used a capillary mixing tee to combine analyte ions with either counter ions or neutral reagents.<sup>162,163</sup> In these experiments, charge reduction occurs after the generation of gas-phase analyte ions.<sup>162,163</sup> Alternative methods have been developed subsequently, where charge reduction occurs in the ion source prior to complete desolvation of the analyte nESI droplets.<sup>164-168</sup> Such early methods were dominated by ion-ion reactions where reagent ions are generated through either corona discharge<sup>166-168</sup> or from radioactive targets.<sup>164,165,168</sup> Recently, in source ion-neutral approaches have become more prevalent for reducing charge on nESI droplets.<sup>184-186</sup> Figure 1-5b shows the current model for such charge reduction reactions within the source region of the instrument. Here, charge reducing agents, neutrals or ions, interact with protons on the surface of the droplet. Similar to solution-phase charge reduction methods, surface charges are stripped based on proton affinity, or are neutralized through bound counter ion charge.

Recently, an ion-neutral supercharging approach has been developed for in source charge amplification of protein ions produced by nESI.<sup>175,176</sup> The method uses sheath gas seeded with acidic species to initiate proton transfer reactions that lead to highly charged protein ions independent of their starting solution condition. As there is strong evidence that links solution-phase supercharging reagents to protein unfolding, leading to altered gas-phase protein structures,<sup>160</sup> a gas-phase methodology potentially provides key advantages to retaining compact protein states by generating amplified protein charge states in the later stages of their formation. There is, however, evidence to support that even gas-phase methods for protein ion supercharging results in altered protein conformational states in the gas-phase,<sup>175</sup> necessitating further research and method development in order to apply such methods to challenging structural biology targets.

## **1.5 Modeling Protein Complex Structures with IM-MS Datasets**

The ultimate goal for IM-MS measurements in the context of structural biology is to generate three-dimensional models of multiprotein complexes, constrained by connectivity and size measurements acquired in the gas phase. The model generation process typically begins by constructing a starting state from available protein composition information, and inputting available constraints from IM-MS measurements to begin the refinement process. If high resolution structures are available, Monte Carlo simulations can be performed that simulate the IM experiment and estimate the CCS of protein conformers for direct comparison with experimental data.<sup>187</sup> To generate accurate depictions of small gas-phase protein structures and peptides, simulated annealing must be carried out to relax X-ray and NMR structures to their lowest-energy gas-phase conformer for comparison with IM data.<sup>188</sup> Multiple algorithms are available for comparing experimental CCS data with CCS estimates derived from model

structures.<sup>189-194</sup> These include various projection approximations,<sup>189,190</sup> the exact hard-sphere scattering method,<sup>191</sup> the trajectory method,<sup>192</sup> the projection superposition approximation,<sup>193</sup> and detailed calculations of polyatomic momentum transfer.<sup>194</sup> To provide accurate models, all methods other than projection approximations require detailed simulations of gas-phase structure, and are thus not typically suitable for work with large multiprotein complexes,<sup>19</sup> relegating most IM-MS models of such systems to coarse-grained representations.<sup>19,38,118</sup> Coarse-grained structures of multiprotein complexes can be generated directly from IM-MS datasets by measuring CCS values for monomers, subcomplexes and intact assemblies, and using all of this information to constrain a subunit-level model of the assembly under investigation.<sup>38,120</sup> Typically, protein-protein distances and connectivities are input into a Monte Carlo-guided random walk that searches protein topology space for those solutions that best satisfy the IM-MS data.<sup>120</sup> The output of such simulations typically take the form of clusters of models, with the confidence interval of the final model largely defined by the number of experimental constraints and the number of interacting proteins within the assembly studied.

### **1.5.1 Molecular Dynamics: Simulated Annealing**

When all-atom structures are available for subunits of multiprotein complexes, simulated annealing can be used to probe the structural landscape of the protein in the gas phase to generate models of its low energy structures *in vacuo*.<sup>188,195</sup> In simulated annealing, all-atom structures are subjected to a series of gradual temperature ramps, where raising the temperature increases the energy of the system in order to disorder the structure.<sup>196</sup> As the temperature is decreased the system refolds to form alternative structures. Each temperature increase is followed by a decrease in an effort to move the protein structure from local minima on the potential energy surface, eventually funneling toward its lowest energy configuration.<sup>195</sup> All of the structure

produced can be evaluated in comparison to CCS measurements as described above. Models found in good agreement are identified as candidate gas-phase structures and can be used to guide downstream experiments.<sup>120</sup> Due to the many challenges associated with finding low energy structures of large protein chains and multiprotein complexes, such simulated annealing approaches are typically limited to peptides and proteins less than 12 kDa. For larger systems, the details of gas-phase structure are ignored to produce coarse-grained models through the Monte Carlo simulations discussed below.<sup>38</sup>

### **1.5.2 Monte Carlo Simulations**

In order to generate coarse-grain structures of multiprotein complex systems, subunits are typically represented as spheres, where the size of the sphere correlates to the measured CCS from IM-MS measurements. These spheres are used to build subcomplexes, and ultimately the full multiprotein complex, by searching the conformational space between two subunits, a subunit and subcomplex, or two subcomplexes by altering protein distances, angles, and positions based on experimental CCS constraints. The best subcomplex model is selected and treated as constant for searching the conformational space of the next measured species.<sup>118</sup> Such coarse-grain models can be integrated with X-ray structures of subunits, homology models, or structures generated from simulated annealing to build all-atom, or partially refined, models.<sup>38</sup>

### **1.6 Summary**

Classical tools for determining the high-resolution structures of multiprotein complexes are limited in terms of their ability to deal with samples comprised of mixtures, where the target protein is present at low levels, or possesses flexible or polydisperse regions. IM-MS offers the ability to overcome many of these challenges, but the generation of sufficient data to provide constraints for the final models can be a challenge. For example, gas-phase measurements of

intact complexes, subunits, and subcomplexes are all needed to generate complete structures, and must correlate well with native, biologically relevant structures found in solution in order to provide relevant models. While strong correlations have been discovered that link solution and gas-phase protein structure, IM-MS is currently bottlenecked in its ability to generate and study native-like subunits and subcomplexes from intact assemblies.

CID of protein complexes provides a promising experimental route to the information needed to build models of multiprotein complexes using IM-MS, but a more detailed understanding of the CID mechanism at work for protein complex ion precursors is necessary in order to effectively use such data. Evidence of CID from low charge state parent ions suggests that compact, native-like structures can be retained in the gas phase; however, this dissociation pathway is not completely understood. In order to study this pathway, charge reduction must be able to effectively generate reduced charge states while simultaneously retaining native-like conformations in the gas-phase. Such charge reduction can be performed in solution or in the gas-phase. Solution based methods for charge reduction, while proven effective, show evidence of altered protein structures due to extended interactions with charge reducing agents. Gas-phase methods for charge reduction are advantageous in that analyte interactions with charge reducing agents are shorter and less likely to perturb native-like structures. However, few detailed studies have critically evaluated the information content of such ions for structural biology.

In Chapter 2, a newly designed source for performing gas-phase ion-neutral charge reduction is tested and evaluated against a solution additive approach in order to develop a method for producing low charge state gas-phase ions with retained native-like conformations.

**(Published, Bornschein, R.E.; Hyung, S.-J.; Ruotolo, B.T. Ion Mobility-Mass Spectrometry**



**Reveals Conformational Changes in Charge Reduced Multiprotein Complexes, *Journal of the American Society for Mass Spectrometry* 2011, 22, 1690-1698.)**

In Chapter 3, two homotetramers, avidin (64 kDa) and aldolase (157 kDa), are exhaustively screened for CID and CIU thresholds across all traditional, native MS charge states down to charge states that are ~37% charge reduced relative to the highest observed charge state. Two distinct dissociation pathways are observed at low charge states, both of which produce product ions from compact tetramer conformations. Modeling reveals previously unknown, large-scale structural rearrangements that occur on the sub-millisecond timescale.

In Chapter 4, a range of multiprotein complexes with varying mass, complex topology, and stoichiometry are evaluated using gas-phase ion-ion charge reduction to identify charge states where CID is observed prior to CIU. These data are then used to predict candidate charge states to select as CID precursors broadly, which can be used to extract compact subunit information for multiprotein complex topology construction efforts.

## 1.7 References

- (1) Alberts, B. *Cell*, 92, 291.
- (2) Aebersold, R.; Goodlett, D. R. *Chem. Rev.* **2001**, 101, 269.
- (3) Mann, M.; Hendrickson, R. C.; Pandey, A. *Annu. Rev. Biochem.* **2001**, 70, 437.
- (4) Robinson, C. V.; Sali, A.; Baumeister, W. *Nature* **2007**, 450, 973.
- (5) Alber, F.; Kim, M. F.; Sali, A. *Structure* **2005**, 13, 435.
- (6) Sali, A.; Glaeser, R.; Earnest, T.; Baumeister, W. *Nature* **2003**, 422, 216.
- (7) Liu, Y.; Gray, N. S. *Nat Chem Biol* **2006**, 2, 358.
- (8) Thaimattam, R.; Banerjee, R.; Miglani, R.; Iqbal, J. *Curr. Pharm. Design* **2007**, 13, 2751.
- (9) Hull, A. W. *J. Am. Chem. Soc.* **1919**, 41, 1168.
- (10) Rabi, I.; Zacharias, J.; Millman, S.; Kusch, P. *Physical Review* **1938**, 53, 318.
- (11) Wimberly, B. T.; Brodersen, D. E.; Clemons, W. M.; Morgan-Warren, R. J.; Carter, A. P.; Vonrhein, C.; Hartsch, T.; Ramakrishnan, V. *Nature* **2000**, 407, 327.
- (12) Ban, N.; Nissen, P.; Hansen, J.; Moore, P. B.; Steitz, T. A. *Science* **2000**, 289, 905.
- (13) Steven, A. C.; Baumeister, W. *Journal of Structural Biology* **2008**, 163, 186.
- (14) von Heijne, G. *Nat Rev Mol Cell Biol* **2006**, 7, 909.

- (15) Palmer III, A. G. *Annual Review of Biophysics and Biomolecular Structure* **2001**, *30*, 129.
- (16) Bayro, M. J.; Debelouchina, G. T.; Eddy, M. T.; Birkett, N. R.; MacPhee, C. E.; Rosay, M.; Maas, W. E.; Dobson, C. M.; Griffin, R. G. *J. Am. Chem. Soc.* **2011**, *133*, 13967.
- (17) Jacso, T.; Franks, W. T.; Rose, H.; Fink, U.; Broecker, J.; Keller, S.; Oschkinat, H.; Reif, B. *Angewandte Chemie* **2012**, *124*, 447.
- (18) Loo, J. A. *Mass Spectrom. Rev.* **1997**, *16*, 1.
- (19) Benesch, J. L. P.; Ruotolo, B. T. *Current Opinion in Structural Biology* **2011**, *21*, 641.
- (20) Heck, A. J. R. *Nat. Methods* **2008**, *5*, 927.
- (21) Berggård, T.; Linse, S.; James, P. *PROTEOMICS* **2007**, *7*, 2833.
- (22) Aquilina, J. A.; Benesch, J. L. P.; Bateman, O. A.; Slingsby, C.; Robinson, C. V. *Proc. Natl. Acad. Sci. U. S. A.* **2003**, *100*, 10611.
- (23) Benesch, J. L. P.; Aquilina, J. A.; Ruotolo, B. T.; Sobott, F.; Robinson, C. V. *Chem. Biol.* **2006**, *13*, 597.
- (24) Kanu, A. B.; Dwivedi, P.; Tam, M.; Matz, L.; Hill, H. H. *J. Mass Spectrom.* **2008**, *43*, 1.
- (25) Uetrecht, C.; Rose, R. J.; van Duijn, E.; Lorenzen, K.; Heck, A. J. R. *Chem. Soc. Rev.* **2010**, *39*, 1633.
- (26) Bohrer, B. C.; Merenbloom, S. I.; Koeniger, S. L.; Hilderbrand, A. E.; Clemmer, D. E. *Annual Review of Analytical Chemistry* **2008**, *1*, 293.
- (27) Jin Lee, Y. *Molecular BioSystems* **2008**, *4*, 816.
- (28) Leitner, A.; Walzthoeni, T.; Kahraman, A.; Herzog, F.; Rinner, O.; Beck, M.; Aebersold, R. *Mol. Cell. Proteomics* **2010**, *9*, 1634.
- (29) Petrotchenko, E. V.; Borchers, C. H. *Mass Spectrom. Rev.* **2010**, *29*, 862.
- (30) Gingras, A.-C.; Gstaiger, M.; Raught, B.; Aebersold, R. *Nat Rev Mol Cell Biol* **2007**, *8*, 645.
- (31) Yates, J. R.; Ruse, C. I.; Nakorchevsky, A. *Annual Review of Biomedical Engineering* **2009**, *11*, 49.
- (32) Englander, S. W. *J. Am. Soc. Mass Spectrom.* **2006**, *17*, 1481.
- (33) Engen, J. R. *Anal. Chem.* **2009**, *81*, 7870.
- (34) Kaltashov, I. A.; Bobst, C. E.; Abzalimov, R. R. *Anal. Chem.* **2009**, *81*, 7892.
- (35) Konermann, L.; Pan, J.; Liu, Y.-H. *Chem. Soc. Rev.* **2011**, *40*, 1224.
- (36) Konermann, L.; Stocks, B. B.; Pan, Y.; Tong, X. *Mass Spectrom. Rev.* **2010**, *29*, 651.
- (37) Kiselar, J. G.; Chance, M. R. *J. Mass Spectrom.* **2010**, *45*, 1373.
- (38) Politis, A.; Park, A. Y.; Hyung, S. J.; Barsky, D.; Ruotolo, B. T.; Robinson, C. V. *PLoS One* **2010**, *5*.
- (39) Benesch, J. L. P.; Ruotolo, B. T.; Simmons, D. A.; Robinson, C. V. *Chem. Rev.* **2007**, *107*, 3544.
- (40) Alber, F.; Dokudovskaya, S.; Veenhoff, L. M.; Zhang, W.; Kipper, J.; Devos, D.; Suprpto, A.; Karni-Schmidt, O.; Williams, R.; Chait, B. T.; Rout, M. P.; Sali, A. *Nature* **2007**, *450*, 683.
- (41) Pan, J.; Han, J.; Borchers, C. H.; Konermann, L. *Anal. Chem.* **2010**, *82*, 8591.
- (42) Pan, J.; Han, J.; Borchers, C. H.; Konermann, L. *J. Am. Chem. Soc.* **2009**, *131*, 12801.

- (43) Morgan, C. R.; Hebling, C. M.; Rand, K. D.; Stafford, D. W.; Jorgenson, J. W.; Engen, J. R. *Mol. Cell. Proteomics* **2011**, *10*.
- (44) Stocks, B. B.; Rezvanpour, A.; Shaw, G. S.; Konermann, L. *J. Mol. Bio.* **2011**, *409*, 669.
- (45) Sharon, M.; Taverner, T.; Ambroggio, X. I.; Deshaies, R. J.; Robinson, C. V. *PLoS Biol* **2006**, *4*, 1314.
- (46) Gavin, A.-C.; Aloy, P.; Grandi, P.; Krause, R.; Boesche, M.; Marzioch, M.; Rau, C.; Jensen, L. J.; Bastuck, S.; Dumpelfeld, B.; Edlmann, A.; Heurtier, M.-A.; Hoffman, V.; Hoefert, C.; Klein, K.; Hudak, M.; Michon, A.-M.; Schelder, M.; Schirle, M.; Remor, M.; Rudi, T.; Hooper, S.; Bauer, A.; Bouwmeester, T.; Casari, G.; Drewes, G.; Neubauer, G.; Rick, J. M.; Kuster, B.; Bork, P.; Russell, R. B.; Superti-Furga, G. *Nature* **2006**, *440*, 631.
- (47) Gavin, A.-C.; Bosche, M.; Krause, R.; Grandi, P.; Marzioch, M.; Bauer, A.; Schultz, J.; Rick, J. M.; Michon, A.-M.; Cruciat, C.-M.; Remor, M.; Hofert, C.; Schelder, M.; Brajenovic, M.; Ruffner, H.; Merino, A.; Klein, K.; Hudak, M.; Dickson, D.; Rudi, T.; Gnau, V.; Bauch, A.; Bastuck, S.; Huhse, B.; Leutwein, C.; Heurtier, M.-A.; Copley, R. R.; Edlmann, A.; Querfurth, E.; Rybin, V.; Drewes, G.; Raida, M.; Bouwmeester, T.; Bork, P.; Seraphin, B.; Kuster, B.; Neubauer, G.; Superti-Furga, G. *Nature* **2002**, *415*, 141.
- (48) Krogan, N. J.; Cagney, G.; Yu, H.; Zhong, G.; Guo, X.; Ignatchenko, A.; Li, J.; Pu, S.; Datta, N.; Tikuisis, A. P.; Punna, T.; Peregrín-Alvarez, J. M.; Shales, M.; Zhang, X.; Davey, M.; Robinson, M. D.; Paccanaro, A.; Bray, J. E.; Sheung, A.; Beattie, B.; Richards, D. P.; Canadien, V.; Lalev, A.; Mena, F.; Wong, P.; Starostine, A.; Canete, M. M.; Vlasblom, J.; Wu, S.; Orsi, C.; Collins, S. R.; Chandran, S.; Haw, R.; Rilstone, J. J.; Gandi, K.; Thompson, N. J.; Musso, G.; St Onge, P.; Ghanny, S.; Lam, M. H. Y.; Butland, G.; Altaf-Ul, A. M.; Kanaya, S.; Shilatifard, A.; O'Shea, E.; Weissman, J. S.; Ingles, C. J.; Hughes, T. R.; Parkinson, J.; Gerstein, M.; Wodak, S. J.; Emili, A.; Greenblatt, J. F. *Nature* **2006**, *440*, 637.
- (49) Vasilescu, J.; Guo, X.; Kast, J. *PROTEOMICS* **2004**, *4*, 3845.
- (50) Zhong, Y.; Feng, J.; Ruotolo, B. T. *Anal. Chem.* **2013**, *85*, 11360.
- (51) Jaya, N.; Garcia, V.; Vierling, E. *Proc. Natl. Acad. Sci. U. S. A.* **2009**, *106*, 15604.
- (52) Andréasson, C.; Fiaux, J.; Rampelt, H.; Druffel-Augustin, S.; Bukau, B. *Proc. Natl. Acad. Sci. U. S. A.* **2008**, *105*, 16519.
- (53) Scaloni, A.; Miraglia, N.; Orrù, S.; Amodeo, P.; Motta, A.; Marino, G.; Pucci, P. *J. Mol. Bio.* **1998**, *277*, 945.
- (54) Schulz, D. M.; Ihling, C.; Clore, G. M.; Sinz, A. *Biochemistry* **2004**, *43*, 4703.
- (55) Ruotolo, B. T.; Giles, K.; Campuzano, I.; Sandercock, A. M.; Bateman, R. H.; Robinson, C. V. *Science* **2005**, *310*, 1658.
- (56) Loo, J. A.; Berhane, B.; Kaddis, C. S.; Wooding, K. M.; Xie, Y. M.; Kaufman, S. L.; Chernushevich, I. V. *J. Am. Soc. Mass Spectrom.* **2005**, *16*, 998.
- (57) Ruotolo, B. T.; Hyung, S.-J.; Robinson, P. M.; Giles, K.; Bateman, R. H.; Robinson, C. V. *Angew. Chem. Int. Ed.* **2007**, *46*, 8001.
- (58) Hall, Z.; Politis, A.; Bush, M. F.; Smith, L. J.; Robinson, C. V. *J. Am. Chem. Soc.* **2012**, *134*, 3429.
- (59) Dole, M.; Mack, L. L.; Hines, R. L.; Mobley, R. C.; Ferguson, L. D.; Alice, M. B. *The Journal of Chemical Physics* **1968**, *49*, 2240.
- (60) Mack, L. L.; Kralik, P.; Rheude, A.; Dole, M. *The Journal of Chemical Physics* **1970**, *52*, 4977.
- (61) Yamashita, M.; Fenn, J. B. *J. Phys. Chem.* **1984**, *88*, 4451.

- (62) Aleksandrov, M.; Gall, L.; Krasnov, N.; Nikolayev, V.; Pavlenko, V.; Shkurov, V. *Dokl. Akad. Nauk SSR, (Moscow)* **1984**, 277, 379.
- (63) Karas, M.; Hillenkamp, F. *Anal. Chem.* **1988**, 60, 2299.
- (64) Tanaka, K.; Waki, H.; Ido, Y.; Akita, S.; Yoshida, Y.; Yoshida, T.; Matsuo, T. *Rapid Commun. Mass Spectrom.* **1988**, 2, 151.
- (65) Heck, A. J. R.; van den Heuvel, R. H. H. *Mass Spectrom. Rev.* **2004**, 23, 368.
- (66) Ruotolo, B. T.; Robinson, C. V. *Curr. Opin. Chem. Biol.* **2006**, 10, 402.
- (67) Wyttenbach, T.; Bowers, M. T. *Annu. Rev. Phys. Chem.* **2007**, 58, 511.
- (68) Fenn, J.; Mann, M.; Meng, C.; Wong, S.; Whitehouse, C. *Science* **1989**, 246, 64.
- (69) Snijder, J.; Rose, R. J.; Veesler, D.; Johnson, J. E.; Heck, A. J. R. *Angew. Chem. Int. Ed.* **2013**, 52, 4020.
- (70) Wilm, M.; Mann, M. *Anal. Chem.* **1996**, 68, 1.
- (71) de la Mora, J. F. *Analytica Chimica Acta* **2000**, 406, 93.
- (72) Iribarne, J. V.; Thomson, B. A. *The Journal of Chemical Physics* **1976**, 64, 2287.
- (73) Ahadi, E.; Konermann, L. *J. Phys. Chem. B* **2012**, 116, 104.
- (74) Konermann, L.; Ahadi, E.; Rodriguez, A. D.; Vahidi, S. *Anal. Chem.* **2012**, 85, 2.
- (75) Baca, M.; Kent, S. B. H. *J. Am. Chem. Soc.* **1992**, 114, 3992.
- (76) Huang, E.; Pramanik, B.; Tsarbopoulos, A.; Reichert, P.; Ganguly, A.; Trotta, P.; Nagabhushan, T.; Covey, T. *J. Am. Soc. Mass Spectrom.* **1993**, 4, 624.
- (77) Light-Wahl, K. J.; Winger, B. E.; Smith, R. D. *J. Am. Chem. Soc.* **1993**, 115, 5869.
- (78) Light-Wahl, K. J.; Schwartz, B. L.; Smith, R. D. *J. Am. Chem. Soc.* **1994**, 116, 5271.
- (79) Ganem, B.; Li, Y. T.; Henion, J. D. *J. Am. Chem. Soc.* **1991**, 113, 7818.
- (80) Katta, V.; Chait, B. T. *J. Am. Chem. Soc.* **1991**, 113, 8534.
- (81) Chowdhury, S. K.; Katta, V.; Chait, B. T. *J. Am. Chem. Soc.* **1990**, 112, 9012.
- (82) Schwartz, B.; Light-Wahl, K.; Smith, R. *J. Am. Soc. Mass Spectrom.* **1994**, 5, 201.
- (83) Robinson, C. V.; Chung, E. W.; Kragelund, B. B.; Knudsen, J.; Aplin, R. T.; Poulsen, F. M.; Dobson, C. M. *J. Am. Chem. Soc.* **1996**, 118, 8646.
- (84) Tito, M. A.; Tars, K.; Valegard, K.; Hajdu, J.; Robinson, C. V. *J. Am. Chem. Soc.* **2000**, 122, 3550.
- (85) Rostom, A. A.; Fucini, P.; Benjamin, D. R.; Juenemann, R.; Nierhaus, K. H.; Hartl, F. U.; Dobson, C. M.; Robinson, C. V. *Proc. Natl. Acad. Sci. U. S. A.* **2000**, 97, 5185.
- (86) Sobott, F.; Benesch, J. L. P.; Vierling, E.; Robinson, C. V. *Journal of Biological Chemistry* **2002**, 277, 38921.
- (87) Hernández, H.; Dziembowski, A.; Taverner, T.; Séraphin, B.; Robinson, C. V. *EMBO reports* **2006**, 7, 605.
- (88) de Vries, M. S.; Hobza, P. *Annu. Rev. Phys. Chem.* **2007**, 58, 585.
- (89) Bernstein, S. L.; Wyttenbach, T.; Baumketner, A.; Shea, J.-E.; Bitan, G.; Teplow, D. B.; Bowers, M. T. *J. Am. Chem. Soc.* **2005**, 127, 2075.
- (90) Mason, E. A.; McDaniel, E. W. *Transport Properties of Ions in Gases*; Wiley-VCH Verlag GmbH & Co. KGaA: Weinheim, Germany, 1988.
- (91) Ruotolo, B. T.; Benesch, J. L. P.; Sandercock, A. M.; Hyung, S. J.; Robinson, C. V. *Nat. Protoc.* **2008**, 3, 1139.
- (92) Smith, D. P.; Knapman, T. W.; Campuzano, I.; Malham, R. W.; Berryman, J. T.; Radford, S. E.; Ashcroft, A. E. *Eur. J. Mass Spectrom.* **2009**, 15, 113.

- (93) Clemmer, D. E.; Jarrold, M. F. *J. Mass Spectrom.* **1997**, *32*, 577.
- (94) Valentine, S. J.; Liu, X.; Plasencia, M. D.; Hilderbrand, A. E.; Kurulugama, R. T.; Koeniger, S. L.; Clemmer, D. E. *Expert Rev. Proteomics* **2005**, *2*, 553.
- (95) Fernandez-Lima, F. A.; Becker, C.; McKenna, A. M.; Rodgers, R. P.; Marshall, A. G.; Russell, D. H. *Anal. Chem.* **2009**, *81*, 9941.
- (96) Hyung, S. J.; Robinson, C. V.; Ruotolo, B. T. *Chem. Biol.* **2009**, *16*, 382.
- (97) Zhong, Y.; Hyung, S.-J.; Ruotolo, B. T. *Expert Rev. Proteomics* **2012**, *9*, 47.
- (98) Freeke, J.; Bush, M. F.; Robinson, C. V.; Ruotolo, B. T. *Chem. Phys. Lett.* **2012**, *524*, 1.
- (99) Han, L.; Hyung, S.-J.; Mayers, J. J. S.; Ruotolo, B. T. *J. Am. Chem. Soc.* **2011**, *133*, 11358.
- (100) Han, L.; Hyung, S.-J.; Ruotolo, B. T. *Angew. Chem. Int. Ed.* **2012**, *51*, 5692.
- (101) Shelimov, K. B.; Clemmer, D. E.; Hudgins, R. R.; Jarrold, M. F. *J. Am. Chem. Soc.* **1997**, *119*, 2240.
- (102) Han, L.; Hyung, S.-J.; Ruotolo, B. T. *Faraday Discussions* **2013**, *160*, 371.
- (103) Han, L.; Ruotolo, B. *Int. J. Ion Mobil. Spec.* **2013**, *16*, 41.
- (104) Paul, W.; Steinwedel, H. *Z. Naturforsch* **1953**, *8a*, 448.
- (105) Finnigan, R. E. *Anal. Chem.* **1994**, *66*, 969A.
- (106) Lawrence, A. H.; Barbour, R. J.; Sutcliffe, R. *Anal. Chem.* **1991**, *63*, 1217.
- (107) Morris, H. R.; Paxton, T.; Dell, A.; Langhorne, J.; Berg, M.; Bordoli, R. S.; Hoyes, J.; Bateman, R. H. *Rapid Commun. Mass Spectrom.* **1996**, *10*, 889.
- (108) Shevchenko, A.; Chernushevich, I.; Ens, W.; Standing, K. G.; Thomson, B.; Wilm, M.; Mann, M. *Rapid Commun. Mass Spectrom.* **1997**, *11*, 1015.
- (109) Hayter, J. R.; Robertson, D. H. L.; Gaskell, S. J.; Beynon, R. J. *Mol. Cell. Proteomics* **2003**, *2*, 85.
- (110) Jin, H.; Kumar, A. P.; Paik, D.-H.; Ha, K.-C.; Yoo, Y.-J.; Lee, Y.-I. *Microchemical Journal* **2010**, *94*, 139.
- (111) Pringle, S. D.; Giles, K.; Wildgoose, J. L.; Williams, J. P.; Slade, S. E.; Thalassinou, K.; Bateman, R. H.; Bowers, M. T.; Scrivens, J. H. *Int. J. Mass Spectrom.* **2007**, *261*, 1.
- (112) Giles, K.; Williams, J. P.; Campuzano, I. *Rapid Commun. Mass Spectrom.* **2011**, *25*, 1559.
- (113) Zhong, Y.; Hyung, S.-J.; Ruotolo, B. T. *Analyst* **2011**, *136*, 3534.
- (114) Giles, K.; Pringle, S. D.; Worthington, K. R.; Little, D.; Wildgoose, J. L.; Bateman, R. H. *Rapid Commun. Mass Spectrom.* **2004**, *18*, 2401.
- (115) Shvartsburg, A. A.; Smith, R. D. *Anal. Chem.* **2008**, *80*, 9689.
- (116) Wiley, W. C.; McLaren, I. H. *Rev. Sci. Instr.* **1955**, *26*, 1150.
- (117) Mamyurin, B. A.; Karataev, V. I.; Shmikk, D. V.; Zagulin, V. A. *JETP* **1973**, *37*, 45.
- (118) Pukala, T. L.; Ruotolo, B. T.; Zhou, M.; Politis, A.; Stefanescu, R.; Leary, J. A.; Robinson, C. V. *Structure* **2009**, *17*, 1235.
- (119) Taverner, T.; Hernandez, H.; Sharon, M.; Ruotolo, B. T.; Matak-Vinkovic, D.; Devos, D.; Russell, R. B.; Robinson, C. V. *Accounts Chem. Res.* **2008**, *41*, 617.
- (120) Hall, Z.; Politis, A.; Robinson, Carol V. *Structure* **2012**, *20*, 1596.
- (121) Hyung, S.-J.; Ruotolo, B. T. *PROTEOMICS* **2012**, *12*, 1547.

- (122) Leary, J.; Schenauer, M.; Stefanescu, R.; Andaya, A.; Ruotolo, B.; Robinson, C.; Thalassinou, K.; Scrivens, J.; Sokabe, M.; Hershey, J. *J. Am. Soc. Mass Spectrom.* **2009**, *20*, 1699.
- (123) Levy, E. D.; Erba, E. B.; Robinson, C. V.; Teichmann, S. A. *Nature* **2008**, *453*, 1262.
- (124) Zhou, M.; Sandercock, A. M.; Fraser, C. S.; Ridlova, G.; Stephens, E.; Schenauer, M. R.; Yokoi-Fong, T.; Barsky, D.; Leary, J. A.; Hershey, J. W.; Doudna, J. A.; Robinson, C. V. *Proc. Natl. Acad. Sci. U. S. A.* **2008**, *105*, 18139.
- (125) Nooren, I. M. A.; Thornton, J. M. *The EMBO Journal* **2003**, *22*, 3486.
- (126) Schwartz, B. L.; Bruce, J. E.; Anderson, G. A.; Hofstadler, S. A.; Rockwood, A. L.; Smith, R. D.; Chilkoti, A.; Stayton, P. S. *J. Am. Soc. Mass Spectrom.* **1995**, *6*, 459.
- (127) Felitsyn, N.; Kitova, E. N.; Klassen, J. S. *Anal. Chem.* **2001**, *73*, 4647.
- (128) Jurchen, J. C.; Williams, E. R. *J. Am. Chem. Soc.* **2003**, *125*, 2817.
- (129) Jurchen, J. C.; Garcia, D. E.; Williams, E. R. *J. Am. Soc. Mass Spectrom.* **2004**, *15*, 1408.
- (130) Pagel, K.; Hyung, S. J.; Ruotolo, B. T.; Robinson, C. V. *Anal. Chem.* **2010**, *82*, 5363.
- (131) Benesch, J. L. P.; Ruotolo, B. T.; Sobott, F.; Wildgoose, J.; Gilbert, A.; Bateman, R.; Robinson, C. V. *Anal. Chem.* **2009**, *81*, 1270.
- (132) Zhou, M.; Dagan, S.; Wysocki, V. H. *Angew. Chem. Int. Ed.* **2012**, *51*, 4336.
- (133) Zhou, M.; Huang, C.; Wysocki, V. H. *Anal. Chem.* **2012**, *84*, 6016.
- (134) Zhou, M.; Dagan, S.; Wysocki, V. H. *Analyst* **2013**, *138*, 1353.
- (135) Zhou, M.; Jones, C. M.; Wysocki, V. H. *Anal. Chem.* **2013**, *85*, 8262.
- (136) Horn, D. M.; Zubarev, R. A.; McLafferty, F. W. *Proc. Natl. Acad. Sci. U. S. A.* **2000**, *97*, 10313.
- (137) Ge, Y.; Lawhorn, B. G.; ElNaggar, M.; Strauss, E.; Park, J.-H.; Begley, T. P.; McLafferty, F. W. *J. Am. Chem. Soc.* **2002**, *124*, 672.
- (138) Mayer, P. M.; Poon, C. *Mass Spectrom. Rev.* **2009**, *28*, 608.
- (139) McLuckey, S. A. *J. Am. Soc. Mass Spectrom.* **1992**, *3*, 599.
- (140) Sobott, F.; Robinson, C. V. *Int. J. Mass Spectrom.* **2004**, *236*, 25.
- (141) Wanasundara, S.; Thachuk, M. *J. Am. Soc. Mass Spectrom.* **2007**, *18*, 2242.
- (142) Erba, E. B.; Ruotolo, B. T.; Barsky, D.; Robinson, C. V. *Anal. Chem.* **2010**, *82*, 9702.
- (143) Aquilina, J. A. *Proteins: Structure, Function, and Bioinformatics* **2009**, *75*, 478.
- (144) van den Heuvel, R. H. H.; van Duijn, E.; Mazon, H.; Synowsky, S. A.; Lorenzen, K.; Versluis, C.; Brouns, S. J. J.; Langridge, D.; van der Oost, J.; Hoyes, J.; Heck, A. J. R. *Anal. Chem.* **2006**, *78*, 7473.
- (145) Zubarev, R. A.; Kelleher, N. L.; McLafferty, F. W. *J. Am. Chem. Soc.* **1998**, *120*, 3265.
- (146) Syka, J. E. P.; Coon, J. J.; Schroeder, M. J.; Shabanowitz, J.; Hunt, D. F. *Proc. Natl. Acad. Sci. U. S. A.* **2004**, *101*, 9528.
- (147) Mikesch, L. M.; Ueberheide, B.; Chi, A.; Coon, J. J.; Syka, J. E. P.; Shabanowitz, J.; Hunt, D. F. *Biochimica et Biophysica Acta (BBA) - Proteins and Proteomics* **2006**, *1764*, 1811.
- (148) McLafferty, F.; Horn, D.; Breuker, K.; Ge, Y.; Lewis, M.; Cerda, B.; Zubarev, R.; Carpenter, B. *J. Am. Soc. Mass Spectrom.* **2001**, *12*, 245.

- (149) Muddiman, D. C.; Cheng, X.; Udseth, H. R.; Smith, R. D. *J. Am. Soc. Mass Spectrom.* **1996**, *7*, 697.
- (150) Iavarone, A. T.; Jurchen, J. C.; Williams, E. R. *Anal. Chem.* **2001**, *73*, 1455.
- (151) Iavarone, A. T.; Williams, E. R. *Int. J. Mass Spectrom.* **2002**, *219*, 63.
- (152) Lemaire, D.; Marie, G.; Serani, L.; Lapr evote, O. *Anal. Chem.* **2001**, *73*, 1699.
- (153) Verkerk, U. H.; Peschke, M.; Kebarle, P. *J. Mass Spectrom.* **2003**, *38*, 618.
- (154) Hautreux, M.; Hue, N.; Du Fou de Kerdaniel, A.; Zahir, A.; Malec, V.; Lapr evote, O. *Int. J. Mass Spectrom.* **2004**, *231*, 131.
- (155) Catalina, M. I.; van den Heuvel, R. H. H.; van Duijn, E.; Heck, A. J. R. *Chem.-Eur. J.* **2005**, *11*, 960.
- (156) Lomeli, S.; Yin, S.; Ogorzalek Loo, R.; Loo, J. *J. Am. Soc. Mass Spectrom.* **2009**, *20*, 593.
- (157) Lomeli, S.; Peng, I.; Yin, S.; Ogorzalek Loo, R.; Loo, J. *J. Am. Soc. Mass Spectrom.* **2010**, *21*, 127.
- (158) Sterling, H. J.; Williams, E. R. *J. Am. Soc. Mass Spectrom.* **2009**, *20*, 1933.
- (159) Sterling, H.; Daly, M.; Feld, G.; Thoren, K.; Kintzer, A.; Krantz, B.; Williams, E. *J. Am. Soc. Mass Spectrom.* **2010**, *21*, 1762.
- (160) Hogan, C. J., Jr.; Ogorzalek Loo, R. R.; Loo, J. A.; Mora, J. F. d. l. *Phys. Chem. Chem. Phys.* **2010**, *12*, 13476.
- (161) McLuckey, S. A.; Van Berkel, G. J.; Glish, G. L. *J. Am. Chem. Soc.* **1990**, *112*, 5668.
- (162) Loo, R. R. O.; Udseth, H. R.; Smith, R. D. *J. Am. Soc. Mass Spectrom.* **1992**, *3*, 695.
- (163) Loo, R. R. O.; Smith, R. *J. Am. Soc. Mass Spectrom.* **1994**, *5*, 207.
- (164) Scalf, M.; Westphall, M. S.; Krause, J.; Kaufman, S. L.; Smith, L. M. *Science* **1999**, *283*, 194.
- (165) Scalf, M.; Westphall, M. S.; Smith, L. M. *Anal. Chem.* **2000**, *72*, 52.
- (166) Ebeling, D. D.; Westphall, M. S.; Scalf, M.; Smith, L. M. *Anal. Chem.* **2000**, *72*, 5158.
- (167) Ebeling, D. D.; Westphall, M. S.; Scalf, M.; Smith, L. M. *Rapid Commun. Mass Spectrom.* **2001**, *15*, 401.
- (168) Frey, B. L.; Lin, Y.; Westphall, M. S.; Smith, L. M. *J. Am. Soc. Mass Spectrom.* **2005**, *16*, 1876.
- (169) Stephenson, J. L., Jr.; Van Berkel, G. J.; McLuckey, S. A. *J. Am. Soc. Mass Spectrom.* **1997**, *8*, 637.
- (170) Badman, E. R.; Chrisman, P. A.; McLuckey, S. A. *Anal. Chem.* **2002**, *74*, 6237.
- (171) Wu, J.; McLuckey, S. A. *Int. J. Mass Spectrom.* **2003**, *228*, 577.
- (172) Xia, Y.; Liang, X.; McLuckey, S. A. *J. Am. Soc. Mass Spectrom.* **2005**, *16*, 1750.
- (173) Zhao, Q.; Soyk, M. W.; Schieffer, G. M.; Fuhrer, K.; Gonin, M. M.; Houk, R. S.; Badman, E. R. *J. Am. Soc. Mass Spectrom.* **2009**, *20*, 1549.
- (174) Emory, J. F.; Hassell, K. H.; Londry, F. A.; McLuckey, S. A. *Rapid Commun. Mass Spectrom.* **2009**, *23*, 409.
- (175) Kharlamova, A.; Prentice, B. M.; Huang, T. Y.; McLuckey, S. A. *Anal. Chem.* **2010**, *82*, 7422.
- (176) Kharlamova, A.; Prentice, B. M.; Huang, T.-y.; McLuckey, S. A. *Int. J. Mass Spectrom.* **2011**, *300*, 158.

- (177) Hogan, C. J.; Carroll, J. A.; Rohrs, H. W.; Biswas, P.; Gross, M. L. *J. Am. Chem. Soc.* **2008**, *130*, 6926.
- (178) Hogan, C. J., Jr.; Carroll, J. A.; Rohrs, H. W.; Biswas, P.; Gross, M. L. *Anal. Chem.* **2009**, *81*, 369.
- (179) Bagal, D.; Zhang, H.; Schnier, P. D. *Anal. Chem.* **2008**, *80*, 2408.
- (180) Sterling, H.; Kintzer, A.; Feld, G.; Cassou, C.; Krantz, B.; Williams, E. *J. Am. Soc. Mass Spectrom.* **2012**, *23*, 191.
- (181) McLuckey, S. A.; Stephenson, J. L. *Mass Spectrom. Rev.* **1998**, *17*, 369.
- (182) Zhao, Q.; Schieffer, G. M.; Soyk, M. W.; Anderson, T. J.; Houk, R. S.; Badman, E. R. *J. Am. Soc. Mass Spectrom.* **2010**, *21*, 1208.
- (183) Loo, R. R. O.; Smith, R. D. *J. Mass Spectrom.* **1995**, *30*, 339.
- (184) Bornschein, R. E.; Hyung, S.-J.; Ruotolo, B. T. *J. Am. Soc. Mass Spectrom.* **2011**, *22*, 1690.
- (185) Hopper, J. T. S.; Sokratous, K.; Oldham, N. J. *Analytical Biochemistry* **2012**, *421*, 788.
- (186) Kharlamova, A.; DeMuth, J.; McLuckey, S. *J. Am. Soc. Mass Spectrom.* **2012**, *23*, 88.
- (187) Giles, K.; Wildgoose, J. L.; Langridge, D. J.; Campuzano, I. *Int. J. Mass Spectrom.* **2010**, *298*, 10.
- (188) Soper, M. T.; DeToma, A. S.; Hyung, S.-J.; Lim, M. H.; Ruotolo, B. T. *Phys. Chem. Chem. Phys.* **2013**, *15*, 8952.
- (189) Mack, E. *J. Am. Chem. Soc.* **1925**, *47*, 2468.
- (190) von Helden, G.; Hsu, M. T.; Gotts, N.; Bowers, M. T. *J. Phys. Chem.* **1993**, *97*, 8182.
- (191) Shvartsburg, A. A.; Jarrold, M. F. *Chem. Phys. Lett.* **1996**, *261*, 86.
- (192) Mesleh, M. F.; Hunter, J. M.; Shvartsburg, A. A.; Schatz, G. C.; Jarrold, M. F. *J. Phys. Chem.* **1996**, *100*, 16082.
- (193) Bleiholder, C.; Wyttenbach, T.; Bowers, M. T. *Int. J. Mass Spectrom.* **2011**, *308*, 1.
- (194) Siems, W. F.; Viehland, L. A.; Hill, H. H. *Anal. Chem.* **2012**, *84*, 9782.
- (195) Sakae, Y.; Hiroyasu, T.; Miki, M.; Okamoto, Y. *Journal of Computational Chemistry* **2011**, *32*, 1353.
- (196) Kirkpatrick, S.; Gelatt, C. D.; Vecchi, M. P. *Science* **1983**, *220*, 671.



## Chapter 2. Ion Mobility-Mass Spectrometry Reveals Conformational Changes in Charge Reduced Multiprotein Complexes

**Bornschein RE**, Hyung S-J, Ruotolo BT, Ion Mobility-Mass Spectrometry Reveals Conformational Changes in Charge Reduced Multiprotein Complexes, *Journal of the American Society for Mass Spectrometry* (2011) 22: 1690-1698.

### 2.1 Introduction

Over the last twenty years, the interconnected nature of life processes has been revealed through the development of analytical approaches that are able to capture and characterize the complexity of interacting proteins and other biomolecules. Because virtually all cellular processes are interconnected, protein assemblies consisting of multiple components have critical significance in health and medicine. Mass spectrometry (MS) has been a key tool in assessing such complex biological systems.<sup>1,2</sup> These experiments have been conducted using both “bottom-up” methods, where interacting partners are detected either by defining the composition of fractions derived from affinity capture or by chemical crosslinking,<sup>3,4</sup> and “top-down” approaches, where the interaction network is observed intact by MS.<sup>5,6</sup> Both types of datasets have been instrumental in defining contact diagrams for protein interaction networks, and can often provide limited information on the three-dimensional structure of such assemblies.<sup>7,8</sup>

The incorporation of ion mobility (IM) separation into such MS experiments is an important emerging approach for the structural characterization of biomolecules and their higher-order complexes.<sup>9-11</sup> Following on from early results indicating that the topology and quaternary organization of multiprotein complexes can be assessed and related to structures determined

using X-ray crystallography and nuclear magnetic resonance spectroscopy,<sup>12,13</sup> the applications of IM-MS to protein assemblies have increased dramatically. Recent examples include studies aimed at assessing binding events within protein cavities,<sup>14</sup> refining protein interaction networks,<sup>15,16</sup> characterizing multiprotein complexes bound to small molecules,<sup>17</sup> and assessing the relative stability of membrane protein complexes.<sup>18</sup> In all of these reports, IM provided a critical structural assessment of a multiprotein complex system found difficult or impossible to characterize using other structural biology technologies.

In multiple studies, the influence of protein complex ion charge state is often highlighted as a key factor in altering the information content of IM-MS and tandem MS measurements.<sup>13,14</sup> For example, the collision induced dissociation (CID) process for natively-charged multiprotein complexes produced by nano-electrospray ionization (nESI) often results in an effective charge reduction step, where the stripped protein complexes that have lost a monomeric unit also lose a large portion of the charge originally carried by precursor ions.<sup>5,19</sup> This effect has been used to great advantage to characterize polydisperse protein complexes for which the primary ion mass spectrum is difficult to interpret due to spectral overlap.<sup>20</sup> Further, several datasets have highlighted the influence of precursor ion charge state on both the structure and type of product ions produced from multiprotein complex CID. Recent data have highlighted the ability of ion charge state to alter the apparent mechanism of dissociation, where precursor ions of lower charge tend to eject compact (rather than the typically unfolded) monomers.<sup>21</sup> Additional datasets have indicated similar effects for charge amplified protein complexes in specialized cases.<sup>22,23</sup> In datasets where extremely low or high charge states are achieved through altering either solvent composition or nESI emitter position, covalent bonds rather than non-covalent protein-protein interactions can be broken to produce sequence informative fragment ions.<sup>21,22</sup>

A further set of charge-related effects observed for multiprotein complex ions center on datasets that demonstrate the apparent reliance of gas-phase structure upon ion charge state. In most cases, protein ions display a distribution of charge states when produced through nESI, and IM and MS measurements indicate that ions having the lowest ionic charge are the most ‘native-like’,<sup>11,13,24</sup> in that ions of low charge state are, in general, resemble X-ray and nuclear magnetic resonance (NMR) datasets the best in terms of rotationally-averaged sizes<sup>25-27</sup> and are the most useful data points when constraining topological models of multiprotein complexes from IM-MS data.<sup>16</sup> For example, in early experiments involving tryptophan-RNA binding attenuation protein (TRAP) 11-mer ions, higher charge states were observed to be more compact relative to ions having lower charge.<sup>13</sup> The charge state dependent nature of protein complex structure has also been observed in other datasets, including a large database of high-precision collision cross-section measurements, in which both increases and decreases in ion size as a function of charge state are observed<sup>28</sup>. Although all of these reports end with similar conclusions regarding the influence of charge on gas-phase protein structure, the mechanistic details that lead to this apparent charge-state dependant behavior have yet to be completely elucidated.

There are multiple methods and protocols available for manipulating the charge state of ions produced by nESI.<sup>29-39</sup> In general, charge manipulation is achieved using three strategies: solution additives, ion-neutral chemistries, and ion-ion chemistries. Methods that utilize solution additives are among the simplest approaches to implement experimentally,<sup>31</sup> but have distinct disadvantages for the analysis of multiprotein complexes where the stability of the assembly may be altered significantly through only small changes in solution composition, pH, or ionic strength.<sup>40</sup> Ion-ion chemistries allow for fine control and high efficiency in manipulating the charge states of biomolecules, but require either modified ion sources or specialized ion trap

approaches for successful charge reduction or amplification.<sup>36,39</sup> Approaches centering upon ion-neutral chemistries are inherently less efficient than those described above,<sup>30</sup> but combine some of the simplified aspects of solution additive approaches with the fine control of ion-ion approaches for the generation of charge-modulated biomolecular ions. Critically, there is little data currently that describes the relative influence of these different charge modulation strategies on the gas-phase structures of biomolecular ions, with the majority of data focused on monomeric proteins.<sup>29,41-46</sup> Multiprotein complexes have been charge-modulated using primarily solution additive-type strategies,<sup>31</sup> but the influences of such approaches on the quaternary structure of multiprotein complexes in the absence of bulk solvent is poorly understood.

In this report, we compare charge reduction methods based on solution-additives to that based on gas-phase ion-neutral reaction chemistry by assessing and comparing the structures of the ions generated in terms of their collision cross-sections as a function of charge state. We find that while both approaches achieve similar amounts of charge reduction, ranging from 2.1-27% efficiency, the solution based-additive approach studied here requires significant levels of collisional activation in order to shed positive ions and generate charge reduced protein complex ions. Therefore, the ions produced by the solution-additive based method produce larger ions having undergone conformational rearrangements and unfolding.<sup>47</sup> Conversely, the gas-phase ion-neutral approach universally produces compact, native-like ions. Critically, charge reduction carried out by ion-neutral chemistry in the gas-phase can impart similar charge reduction effectiveness when compared to analogous solution-phase approaches, without the need to introduce solution additives that may act to disrupt the oligomeric state or structure of ions prior to nESI analysis. Thus, we demonstrate that charging on multiprotein complexes by ESI can be modulated by the gas-phase ion-neutral chemistry methods described herein, and can be further

applied to CID to improve the utility of IM-MS as a tool for characterizing structure of biomolecules.

## 2.2 Experimental

The protein complexes studied here, avidin (*chicken egg white*), alcohol dehydrogenase (*yeast*, ADH), and pyruvate kinase (*rabbit muscle*, PK), were purchased from Sigma-Aldrich (St. Louis, MO) as well as ammonium acetate and the charge reducing bases triethylamine (TEA), 1,5-diazabicyclo[4.3.0]non-5-ene (DBN), and 1,8-diazabicyclo[5.4.0]undec-7-ene (DBU). Protein stock samples prepared to 100 or 50  $\mu\text{M}$  in 100 mM ammonium acetate (pH 6.9) were buffer exchanged into 100 mM ammonium acetate using Micro Bio-Spin 6 columns (Bio-Rad, Hercules, CA) and diluted to a final concentration of 10  $\mu\text{M}$  with 100mM ammonium acetate. Protein samples prepared with solution additives contained charge reducing agents at concentrations of 5-20 mM. For the study of gas-phase ion-neutral reactions, aqueous solutions of the charge reducing agents TEA, DBN, and DBU were prepared to 1.4 M, 1.7 M and 0.7-2.0 M concentrations, respectively. Bases were chosen based on their common use in previous experiments involving multiprotein complexes both in our lab and others.<sup>31</sup>

Ion mobility-mass spectrometry experiments were performed on a quadrupole-ion mobility-time-of-flight mass spectrometer (Q-IM-ToF MS) purchased from Waters (Synapt G2 HDMS, Manchester, UK). While earlier versions of the Synapt instrument platform utilizing a nano-electrospray ionization (nESI) source were also fitted with a reference emitter that included a nebulizing sheath flow, the reference sprayer provided by the manufacturer for the nESI source on the Synapt G2 does not. Figure 2-1 shows a schematic diagram of the modified nESI ion source, where the nESI reference sprayer is replaced with a simple nebulizer which acts to introduce neutral base molecules into the source near the sampling cone, perpendicular to the

analyte spray, allowing ion-neutral chemistry to occur before protein ions enter the sampling orifice. The device was designed to introduce base into the source through a stainless steel capillary; the capillary passes through a hollow chamber within the sprayer, which directs to sheath gas flow. The sprayer tip then focuses the sheath gas to pass directly over the capillary tip in order to nebulize the base molecules. The sheath gas used is nitrogen and base flow rates range from 10-25 mL/hr with the gas pressure optimized for continuous nebulized droplet formation ranging from 20-35 psi. A typical nebulizer flow rate used in these studies is 10

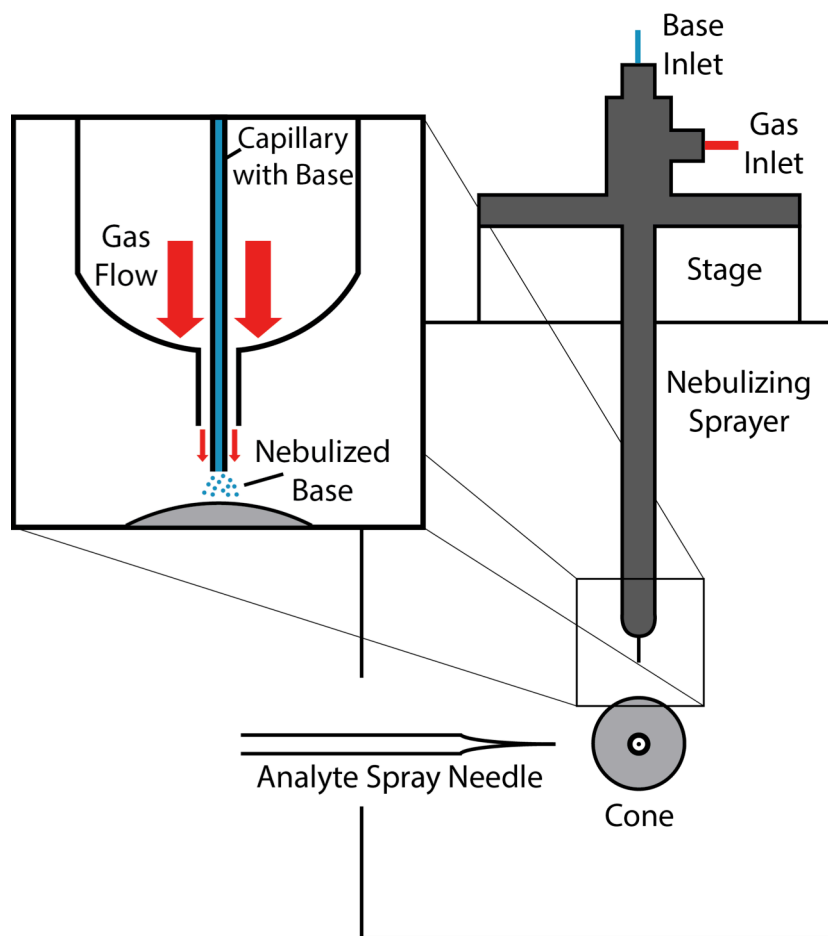


**Figure 2-1.** A schematic diagram of the modified nanoelectrospray ion source for the Synapt G2 instrument used in these studies. Nebulized base molecules are introduced into the source perpendicular to the analyte spray. Base solution flows through a stainless steel capillary, which is enclosed in a hollow chamber within the sprayer. Sheath gas flows through the hollow chamber and exits out the sprayer tip. The tip is designed to force sheath gas over the end of the capillary, causing the base to nebulize for interaction with electro sprayed protein complex ions.

mL/hr, with a gas pressure of 20 psi.

To generate protein complex ions, an aliquot of sample (~5  $\mu\text{L}$ ) was sprayed from the Nano-Lock Spray with the capillary voltage ranging from 1.8-2.0 kV, with the source operating in positive mode and the sample cone operated at 20 V. The trap travelling-wave ion guide was operated with an argon gas pressure of  $3.3 \times 10^{-2}$  mbar and a 50 V trap bias (as much as 150 V was used in solution phase charge reduction experiments). The travelling-wave ion mobility cell was operated with a nitrogen gas pressure of 3.5 mbar and employed a series of DC voltage waves (wave heights: 30-35 V, wave velocities: 500-600 m/s) to generate ion mobility separations. The ToF-MS was operated over an  $m/z$  range of 800-15000 with a pressure of  $1.6 \times 10^{-6}$  mbar. Collision cross-section (CCS) measurements were made using known CCS values of avidin, ADH, and PK, as well as cytochrome c, concanavalin A tetramer, and glutamine dehydrogenase (Sigma-Aldrich), as calibrants using the method described previously.<sup>8,28</sup> All mass spectra were calibrated externally using a solution of cesium iodide (100 mg/mL) and were processed on Masslynx 4.1 software (Waters). Charge reduction effectiveness was determined using:

$$Eff(\%) = \frac{q_{avg,Control} - q_{avg,CR}}{q_{avg,Control}} \quad (2.1)$$

where  $q_{avg,Control}$  and  $q_{avg,CR}$  are the average charge state distributions ( $q_{avg}$ ) for control and charge reduced (CR) protein ions, and are calculated using:

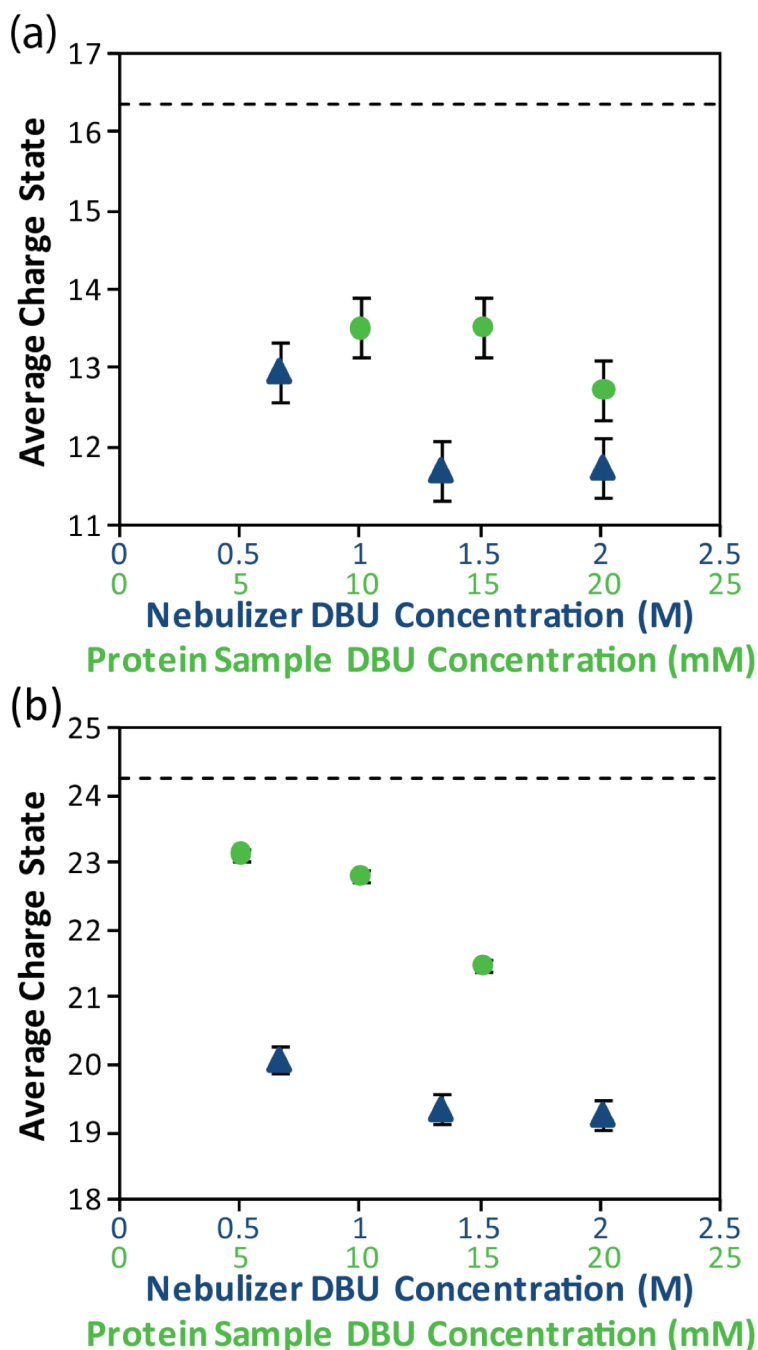
$$q_{avg} = \frac{\sum_i q_i \times w_i}{\sum_i w_i} \quad (2.2)$$

where  $q_i$  is the charge on the  $i^{th}$  charge state and  $w_i$  is the signal intensity for the  $i^{th}$  charge state.

## 2.3 Results and Discussion

Initial experiments in our laboratory were aimed at characterizing many different methods of charge reduction in terms of multiple figures of merit, some of which are unique to the IM-MS experiment. For example, in order to successfully build model structures of multiprotein complexes, collision cross-section measurements of proteins in their compact state are usually preferred over measurements of unfolded forms because compact states are more facilely-related to solution-phase architectures.<sup>48</sup> Although limited measurements have been performed to assess the influence of charge reducing ion-neutral chemistries on the structures of small monomeric proteins,<sup>38</sup> no data is currently available that rigorously assesses the influence of such chemistries on the gas-phase quaternary structure of proteins or in comparison with the solution-phase additive approaches for charge reducing ions produced by ESI. In addition to monitoring the gas-phase structure of the ions produced using various charge reduction protocols, we have evaluated charge reduction strategies in terms of two other figures of merit. We define charge reduction ‘*efficiency*’ as the amount of charge reduction agent required to observe a given level of charge reduction. Further, we define charge reduction ‘*effectiveness*’ as the ultimate extent of charge reduction observed, under a given set of experimental conditions, relative to control datasets (see *Experimental* section for details).





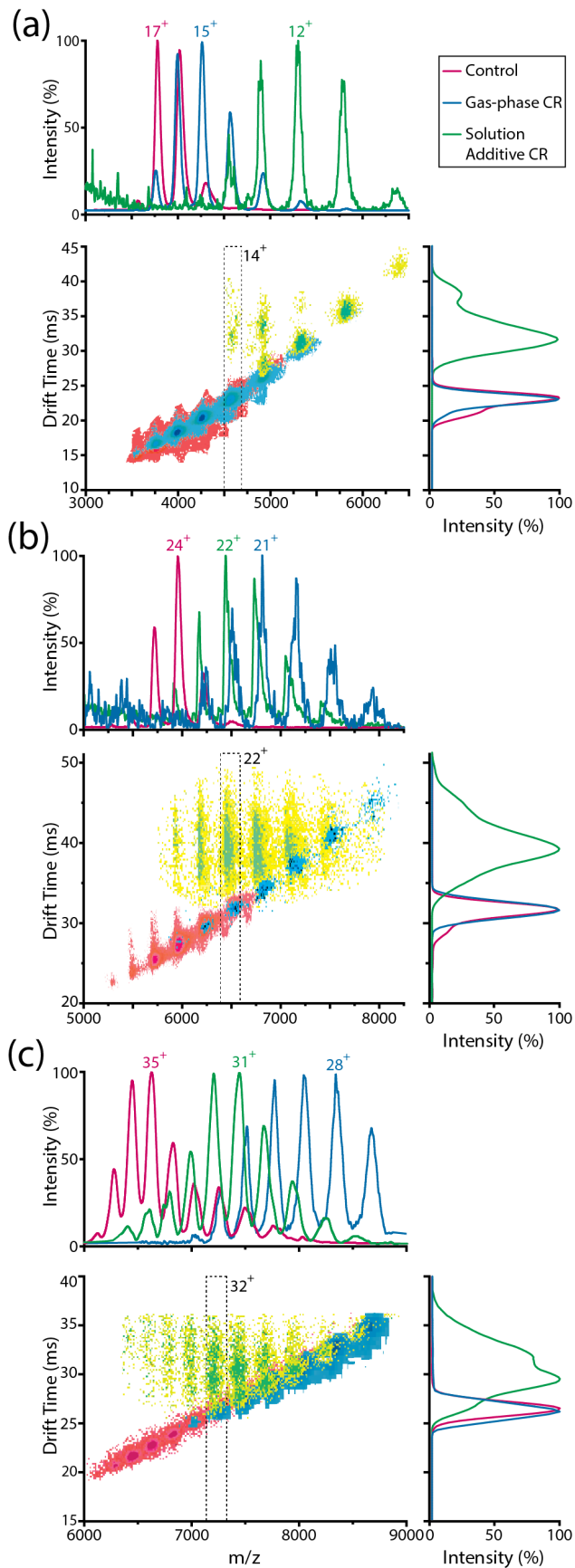
**Figure 2-2.** Plots of average avidin (a) and ADH (b) tetramer charge state against the concentration of DBU used in nebulized base solutions (▲) and as an additive in protein samples (●). Error bars shown for each measurements represent standard deviation calculations from average charge state measurements spanning at least three replicates. In all cases, solution-phase additives exhibit higher charge reduction efficiencies (charge reduction per-unit of base concentration) and the use of nebulized base exhibits greater charge reduction effectiveness (ultimate charge reduction amount achieved).

Figure 2-2a shows charge reduction *effectiveness* and *efficiency* data for the avidin tetramer (64 kDa) acquired using our two charge reduction conditions. The plots presented show trends in the average protein charge state distribution ( $q_{avg}$ ) recorded under optimum instrument conditions for charge reduction (i.e., optimized acceleration voltages, see *Experimental Methods*) versus DBU solution concentration for gas-phase ion-neutral charge reduction ranging from 0.7-2.0 M (blue) and DBU solution additive concentration ranging from 10-20 mM (green). The data shows that

the concentration of charge reducing agent, used either as a solution additive or nebulized into the source for ion-neutral

chemistry, is inversely correlated with the average protein charge state recorded for the avidin tetramer. In addition, while the solution additive approach exhibits substantially higher charge reduction efficiencies (charge reduction per-unit concentration of base utilized), ion-neutral charge reduction results in more effective charge reduction, evidenced by the lower average protein charge states achieved using this approach in Figure 2-2a. Higher base concentrations added to protein complex samples in solution result in signal suppression and protein complex disruption (data not shown). Similar trends are observed for the alcohol dehydrogenase tetramer (144 kDa), and are shown in Figure 2-2b over the concentration ranges 0.7-2.0 M and 5-15 mM for in source gas-phase charge reduction (blue) and solution additive charge reduction (green), respectively. Again, the solution additive approach is a substantially more efficient process with respect to the base utilized in the experiment, routinely producing significant charge reduction using 4 orders of magnitude less base than equivalent ion-neutral reaction chemistry approaches. Conversely, ultimate charge reduction effectiveness values for both avidin and ADH datasets respectively were calculated to be 22 and 11% for the solution additive protocol and 28 and 20% for the ion-neutral reaction chemistry approach. Similar trends are observed for protein complex charge reduction when other basic molecules are used (e.g., TEA and DBN, data not shown). Thus, while adding base molecules directly into protein complex samples is a more *efficient* means of charge reduction, nebulized base used for ion-neutral charge reduction following nESI is a more *effective* charge reduction method under the conditions used here.

The results recognize the metrics of charge reduction *efficiency* and *effectiveness* as critical measures that allow for the analytical comparison of charge reduction protocols in general. However, the influence of such approaches on the gas-phase structure and topology of protein complexes measured by IM-MS is arguably a more important criterion for assessing the



◀ **Figure 2-3.** Mass spectra (top) and drift time versus m/z contour plots (bottom) of (a) avidin, (b) alcohol dehydrogenase, and (c) pyruvate kinase. Red spectra and contour plots correspond to control conditions, blue spectra and contour plots correspond to gas-phase charge reduction conditions with DBU, and green spectra and contour plots correspond to solution additive charge reduction conditions with DBU. We have acquired similar datasets where DBU is replaced with either DBN or TEA bases. Increased IM drift times observed on the contour plots corresponding to solution-phase additive datasets indicate protein complex unfolding relative to control and ion-neutral charge reduction data.

applicability of such methods for applications in structural biology. Figure 2-3a shows data for the avidin tetramer (64 kDa) acquired using three experimental conditions. The red contour plot represents a control dataset, with no base added either in solution or in gas-phase. As the avidin tetramer is ionized and transferred into IM-MS with minimal gas-phase activation, charge states corresponding to avidin tetramer center around 17<sup>+</sup> with drift times that are consistent with compact native-like tetramers are observed by MS and IM respectively. In contrast, avidin tetramer ions produced from solutions with added

DBU (20 mM) exhibits extensive charge reduction (green in Figure 2-2a). As described in previous reports, DBU (and other similar bases) adheres to the surface of proteins complexes in solution and subsequent nESI generates clustered ion-neutral complexes. These ion-neutral clusters further desolvate such that the small basic molecules carry charge away from the protein complex ions, thus resulting in charge reduction.<sup>31</sup> In our experiments with DBU and similar bases, a small amount of accelerating voltage is necessary to reduce charges during desolvation, presumably by promoting the dissociation of basic molecules from the complex through energetic ion-neutral collisions. For the data shown in Figure 2-3a, the ions were accelerated at 150 V in the ion trap prior to the IM separation region of the instrument to produce maximum charge reduction, and similar results are achieved by applying activation voltage in the skimmer-cone region of the instrument. While the activation voltage used is insufficient to cause the protein complex to dissociate, IM data reveals that the protein complex ions generated by adding base in solution undergo substantial unfolding under these conditions. In contrast, if the same basic molecules are nebulized into the ion source region of the instrument, charge reduction is observed in the absence of energetic collisions and the ions remain compact (blue dataset, Figure 2-3a). Drift time spectra for each of the three ionization conditions are presented for the 14<sup>+</sup> ion of avidin tetramer. Control (red) and gas-phase charge reduced (blue) datasets correlate well, while solution additive charge reduction data (green) is shifted to longer drift times. Furthermore, drift time features are substantially broadened in solution additive data when compared with control datasets, and IM resolution is observed to decrease by approximately a factor of 2.

Similar results to these are observed for other multiprotein complex ions. Figure 2-3b shows data for ADH tetramer ions (144 kDa), where substantial unfolding is observed for the

more highly charged region of the charge state distribution produced from solutions with added DBU, and the ions exposed to nebulized DBU remain compact (drift time spectra shown for 22<sup>+</sup> ions). While the conclusions reached for this dataset are similar to those for avidin, some differences are apparent. For example, ADH tetramer ions charge reduced using solution additives exhibit a larger degree of gas-phase unfolding than observed in avidin datasets. In addition, the charge reduction effectiveness for ADH tetramer ions is observed to be substantially higher under the conditions used in Figure 2-3b than that observed for avidin datasets under similar conditions (27% for ADH versus 8% for avidin in Figure 2-3a). Similar observations are made in the case of PK (232 kDa) tetramer ions. The data shown in Figure 2-3c suggest that significant conformational changes occur for most of the PK tetramer charge states produced using the charge reduction method based on solution-additives (green). Similar to avidin and ADH, compact and ‘native-like’ PK IM data (drift time spectra show 29<sup>+</sup> ion) is observed for complexes exposed to nebulized base after ionization. In some cases, activating ions to produce charge reduction following the addition of base in solution produces ion populations that are compacted relative to both control (red) and gas-phase charge reduced (blue) datasets. Such compaction effects have been observed for other protein complexes upon activation,<sup>13,49</sup> and are consistent with collision-induced remodeling of the complex prior to gas-phase unfolding. We also observe a larger mass increase for ions having undergone charge reduction using the ion-neutral chemistry approach when compared to the solution-additive approach described here. This observation is consistent with the more gentle, less activating conditions that are possible when base is nebulized into the source rather than added in solution (see the *Experimental Methods* section above for notes on instrument conditions for the two experimental protocols used here).

Collision cross-section (CCS) measurements for the ions observed in Figure 2-3 are generated using calibration procedures that involve a set of known ions having a broad range of ion mobility and CCS values, and are plotted as a function of charge state in Figure 2-4.<sup>28</sup> Protein ions produced from gas-phase charge reduction generate CCS values similar to control in cases where charge states overlap (blue triangles and red diamonds respectively, Figure 2-4). A small exception to this general observation is apparent in our PK dataset, where CCS values for ions generated using gas-phase charge reduction are 1-3% smaller than equivalent ions generated from our control

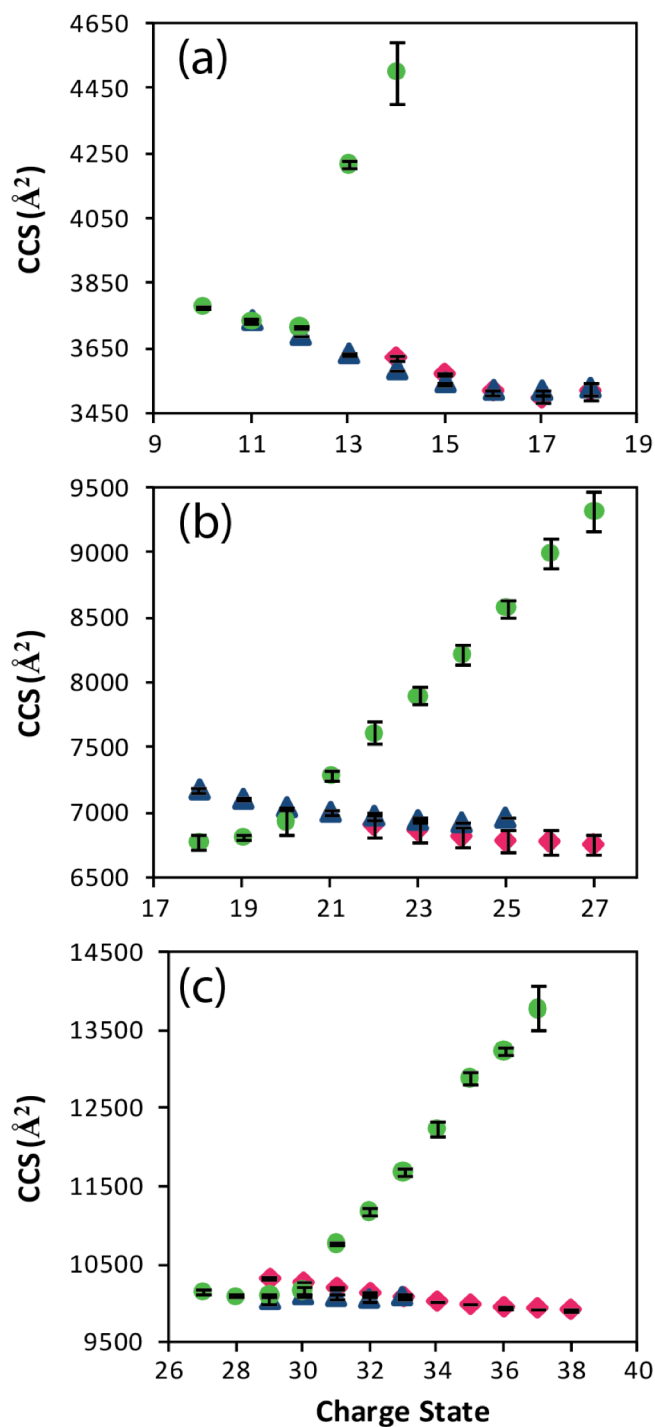


**Figure 2-4.** Collision cross-section (CCS) measurements versus charge state plots for (a) avidin, (b) alcohol dehydrogenase, and (c) pyruvate kinase, where (♦) indicate control conditions, (▲) indicate gas-phase charge reduction conditions with DBU, and (●) indicate solution additive charge reduction conditions with DBU. Significant increases in CCS are observed for solution additive datasets compared with both control and ion-neutral chemistry charge reduction data.

protocol. In contrast, for those ions produced by solution-phase additive approaches, large increases in CCS are observed in most cases when compared to ions produced using either the control or gas-phase charge reduction protocol (green circles). For example, the  $33^+$  charge state of PK, has a measured CCS from our control dataset of  $10084 \text{ \AA}^2$ . The same ion generated when DBU is nebulized into the ion source has a nearly identical CCS ( $10094 \text{ \AA}^2$ , 0.1% different), while the  $33^+$  ion measured after charge reduction from DBU added in solution is 16% larger than control ( $11684 \text{ \AA}^2$ ). This increase in CCS across most charge states further indicates protein unfolding upon activation, and confirms our analysis of the data shown in Figure 2-3. Decreases in CCS of ions following charge reduction via solution additives are also observed in our dataset. Figure 2-4b shows data for the ADH tetramer, in which CCS decreases  $\sim 6\%$  for the  $18^+$  ions produced with solution additives relative to their counterparts produced by gas-phase ion-neutral chemistry. Such decreases can also be a sign of collision induced remodeling of the protein complex topology.<sup>13,49</sup>

For all protein complex ions generated in control and gas-phase charge reduction datasets, the trend observed in CCS as a function of charge state is near-linear, having a negative slope. In addition, the observed slope is shallow, with the range of CCS values spanning less than 10% for all protein complexes produced by these two methodologies. As discussed above, the apparent compaction observed for protein complex ions as charge state is increased is similar to previous datasets,<sup>13,19,49</sup> and is likely due to the enhanced kinetic energies, and thus internal energies upon collisional activation, of the higher charge state ions observed. Other plausible explanations for the slight decrease in CCS observed as a function of center on the calibration function used to convert traveling-wave IM drift times to CCS values using ions of known CCS.<sup>48</sup> While the possibility of calibration errors cannot be completely eliminated from our analysis, our dataset

utilizes a recently developed database of calibrant values that span a large range of CCS and ion mobility values in order to minimize errors in the process<sup>28</sup> and makes significant errors in calibration unlikely.

Again, in contrast to datasets collected from ions produced from control samples or ion-neutral ion chemistry-based charge reduction, ions generated from solutions with basic additives result in significantly larger CCS values relative to control values and varying trends as a function of charge state. We have also collected data on concanavalin A tetramers (from *jack bean*, 103 kDa, data not shown), where the trends in CCS as a function of charge state are parabolic in nature, with the intermediate charge states exhibiting minimum CCS values. It is possible that trends in CCS for protein complex ions as a function of charge state could be used to recover structural information from the assembly or as a means of protein complex identification, and these areas are an active area of research in our laboratory. Note also that in some cases, the addition of base in solution acts as a disrupting agent similar to the addition of organic solvent or salts, resulting in the formation of protein dimers and monomers in solution. This is the case with concanavalin A tetramers where solution additives cause the dissociation of tetramer into dimers while gas-phase charge reduction approaches are able to retain the tetramer and reduce its charge. This further makes the case, in general, for gas-phase approaches to charge reduction, especially for more-fragile multiprotein complexes.

## **2.4 Conclusions**

In this report, we demonstrate that the addition of strong bases (TEA, DBN, DBU) in solution, while leading to charge reduced populations of electrosprayed protein complexes, can also result in unfolded protein conformers in the gas phase through the activation necessary to dissociate proton-bound base molecules from the surface of the complex. It is important to note that while



operative for the base molecules studied here, gas-phase unfolding has not been observed in other cases where small molecules have been added in solution in order to charge reduce multiprotein complexes. For example, imidazole has been used to reduce the charge state of the GroEL tetradecamer and IM-MS data indicate a compact configuration for the charge reduced species generated.<sup>14</sup> Similarly, crown ether compounds and triethylammonium acetate buffer have recently been used to alter the charge state of transthyretin tetramers in order to study their collision induced dissociation properties.<sup>21</sup> Here again, IM-MS data confirm compact conformations for the charge reduced tetramers prior to activation.

The critical differences associated with the base-protein complexes formed in our experiments likely relates to the stronger proton-bound interactions formed between highly-basic molecules and protein surfaces. These stronger interactions require increased energy to break, generated here in the form of activating collisions with inert neutrals. In addition to dissociating the protein-bound base molecules from the complex, the assembly unfolds in our experiments as well. This result is in stark contrast to those where the base is nebulized in the ion source and allowed to interact with the protein in the gas-phase through ion-neutral reaction chemistry. In these cases, base likely interacts with proteins in fewer numbers, and in a more discrete fashion, than the action of the same base molecules in solution. This would likely lead to fewer base molecules bound to the surface of the protein at any given time and, thus, the complexes created would require less thermal energy to dissociate and generate charge reduced species. Moreover, nebulization method is a more effective method since it produces ions that are more charge-reduced compared to method employing bases additives in solution. In summary, our results suggest that gas-phase ion-neutral chemistry approaches offer an alternative method to reduce charges for protein complexes that is accessible to a larger number of basic molecules than

equivalent approaches in solution, while having an enhanced ability to generate compact protein complex structures.

## 2.5 Acknowledgments

The authors thank the University of Michigan for support of this project through start-up funds (BTR).

## 2.6 References

- (1) Aebersold, R.; Goodlett, D. R. *Chem. Rev.* **2001**, *101*, 269.
- (2) Mann, M.; Hendrickson, R. C.; Pandey, A. *Annu. Rev. Biochem.* **2001**, *70*, 437.
- (3) Kaake, R. M.; Wang, X. R.; Huang, L. *Mol. Cell. Proteomics* **2010**, *9*, 1650.
- (4) Petrotchenko, E. V.; Borchers, C. H. *Mass Spectrom. Rev.* **2010**, *29*, 862.
- (5) Benesch, J. L. P.; Ruotolo, B. T.; Simmons, D. A.; Robinson, C. V. *Chem. Rev.* **2007**, *107*, 3544.
- (6) Heck, A. J. R. *Nat. Methods* **2008**, *5*, 927.
- (7) Robinson, C. V.; Sali, A.; Baumeister, W. *Nature* **2007**, *450*, 973.
- (8) Taverner, T.; Hernandez, H.; Sharon, M.; Ruotolo, B. T.; Matak-Vinkovic, D.; Devos, D.; Russell, R. B.; Robinson, C. V. *Accounts Chem. Res.* **2008**, *41*, 617.
- (9) Ruotolo, B. T.; Robinson, C. V. *Curr. Opin. Chem. Biol.* **2006**, *10*, 402.
- (10) Uetrecht, C.; Rose, R. J.; van Duijn, E.; Lorenzen, K.; Heck, A. J. R. *Chem. Soc. Rev.* **2010**, *39*, 1633.
- (11) Wyttenbach, T.; Bowers, M. T. *Annu. Rev. Phys. Chem.* **2007**, *58*, 511.
- (12) Loo, J. A.; Berhane, B.; Kaddis, C. S.; Wooding, K. M.; Xie, Y. M.; Kaufman, S. L.; Chernushevich, I. V. *J. Am. Soc. Mass Spectrom.* **2005**, *16*, 998.
- (13) Ruotolo, B. T.; Giles, K.; Campuzano, I.; Sandercock, A. M.; Bateman, R. H.; Robinson, C. V. *Science* **2005**, *310*, 1658.
- (14) van Duijn, E.; Barendregt, A.; Synowsky, S.; Versluis, C.; Heck, A. J. R. *J. Am. Chem. Soc.* **2009**, *131*, 1452.
- (15) Pukala, T. L.; Ruotolo, B. T.; Zhou, M.; Politis, A.; Stefanescu, R.; Leary, J. A.; Robinson, C. V. *Structure* **2009**, *17*, 1235.
- (16) Politis, A.; Park, A. Y.; Hyung, S. J.; Barsky, D.; Ruotolo, B. T.; Robinson, C. V. *PLoS One* **2010**, *5*.
- (17) Hyung, S. J.; Robinson, C. V.; Ruotolo, B. T. *Chem. Biol.* **2009**, *16*, 382.
- (18) Wang, S. C.; Politis, A.; Di Bartolo, N.; Bavro, V. N.; Tucker, S. J.; Booth, P. J.; Barrera, N. P.; Robinson, C. V. *J. Am. Chem. Soc.* **2010**, *132*, 15468.
- (19) Benesch, J. L. P. *J. Am. Soc. Mass Spectrom.* **2009**, *20*, 341.
- (20) Stengel, F.; Baldwin, A. J.; Painter, A. J.; Jaya, N.; Basha, E.; Kay, L. E.; Vierling, E.; Robinson, C. V.; Benesch, J. L. P. *Proc. Natl. Acad. Sci. U. S. A.* **2010**, *107*, 2007.

- (21) Pagel, K.; Hyung, S. J.; Ruotolo, B. T.; Robinson, C. V. *Anal. Chem.* **2010**, *82*, 5363.
- (22) Benesch, J. L. P.; Ruotolo, B. T.; Sobott, F.; Wildgoose, J.; Gilbert, A.; Bateman, R.; Robinson, C. V. *Anal. Chem.* **2009**, *81*, 1270.
- (23) Erba, E. B.; Ruotolo, B. T.; Barsky, D.; Robinson, C. V. *Anal. Chem.* **2010**, *82*, 9702.
- (24) Kitova, E. N.; Seo, M.; Roy, P.-N.; Klassen, J. S. *J. Am. Chem. Soc.* **2008**, *130*, 1214.
- (25) Valentine, S. J.; Anderson, J. G.; Ellington, A. D.; Clemmer, D. E. *J. Phys. Chem. B* **1997**, *101*, 3891.
- (26) Leary, J.; Schenauer, M.; Stefanescu, R.; Andaya, A.; Ruotolo, B.; Robinson, C.; Thalassinou, K.; Scrivens, J.; Sokabe, M.; Hershey, J. *J. Am. Soc. Mass Spectrom.* **2009**, *20*, 1699.
- (27) Scarff, C. A.; Thalassinou, K.; Hilton, G. R.; Scrivens, J. H. *Rapid Commun. Mass Spectrom.* **2008**, *22*, 3297.
- (28) Bush, M. F.; Hall, Z.; Giles, K.; Hoyes, J.; Robinson, C. V.; Ruotolo, B. T. *Anal. Chem.* **2010**, *82*, 9557.
- (29) Badman, E. R.; Hoaglund-Hyzer, C. S.; Clemmer, D. E. *Anal. Chem.* **2001**, *73*, 6000.
- (30) Bagal, D.; Zhang, H.; Schnier, P. D. *Anal. Chem.* **2008**, *80*, 2408.
- (31) Catalina, M. I.; van den Heuvel, R. H. H.; van Duijn, E.; Heck, A. J. R. *Chem.-Eur. J.* **2005**, *11*, 960.
- (32) Krusemark, C. J.; Frey, B. L.; Belshaw, P. J.; Smith, L. M. *J. Am. Soc. Mass Spectrom.* **2009**, *20*, 1617.
- (33) McLuckey, S. A.; Stephenson, J. L. *Mass Spectrom. Rev.* **1998**, *17*, 369.
- (34) Pitteri, S. J.; McLuckey, S. A. *Mass Spectrom. Rev.* **2005**, *24*, 931.
- (35) Scalf, M.; Westphall, M. S.; Krause, J.; Kaufman, S. L.; Smith, L. M. *Science* **1999**, *283*, 194.
- (36) Scalf, M.; Westphall, M. S.; Smith, L. M. *Anal. Chem.* **2000**, *72*, 52.
- (37) Smith, L. M. *J. Am. Soc. Mass Spectrom.* **2008**, *19*, 629.
- (38) Zhao, Q.; Schieffer, G. M.; Soyk, M. W.; Anderson, T. J.; Houk, R. S.; Badman, E. R. *J. Am. Soc. Mass Spectrom.* **2010**, *21*, 1208.
- (39) Zhao, Q.; Soyk, M. W.; Schieffer, G. M.; Fuhrer, K.; Gonin, M. M.; Houk, R. S.; Badman, E. R. *J. Am. Soc. Mass Spectrom.* **2009**, *20*, 1549.
- (40) Hernandez, H.; Robinson, C. V. *Nat. Protoc.* **2007**, *2*, 715.
- (41) Clemmer, D. E.; Jarrold, M. F. *J. Mass Spectrom.* **1997**, *32*, 577.
- (42) Valentine, S. J.; Counterman, A. E.; Clemmer, D. E. *J. Am. Soc. Mass Spectrom.* **1997**, *8*, 954.
- (43) Badman, E. R.; Myung, S.; Clemmer, D. E. *J. Am. Soc. Mass Spectrom.* **2005**, *16*, 1493.
- (44) Gross, D. S.; Schnier, P. D.; RodriguezCruz, S. E.; Fagerquist, C. K.; Williams, E. R. *Proc. Natl. Acad. Sci. U. S. A.* **1996**, *93*, 3143.
- (45) Schnier, P.; Gross, D.; Williams, E. *J. Am. Soc. Mass Spectrom.* **1995**, *6*, 1086.
- (46) Jarrold, M. F. *Annu. Rev. Phys. Chem.* **2000**, *51*, 179.
- (47) Ruotolo, B. T.; Hyung, S. J.; Robinson, P. M.; Giles, K.; Bateman, R. H.; Robinson, C. V. *Angew. Chem.-Int. Edit.* **2007**, *46*, 8001.

- (48) Ruotolo, B. T.; Benesch, J. L. P.; Sandercock, A. M.; Hyung, S. J.; Robinson, C. V. *Nat. Protoc.* **2008**, *3*, 1139.
- (49) Freeke, J.; Robinson, C. V.; Ruotolo, B. T. *Int. J. Mass Spectrom.* **2010**, *298*, 91.

## **Chapter 3. Ion Mobility-Mass Spectrometry Reveals Highly-Compact Intermediates in the Collision Induced Dissociation of Charge-reduced Protein Complexes**

**Russell E. Bornschein**, Shuai Niu, Joseph Eschweiler, Brandon T. Ruotolo, Prepared for submission to *Journal of The American Society for Mass Spectrometry* as Ion Mobility-Mass Spectrometry Reveals Highly-Compact Intermediates in the Collision Induced Dissociation of Charge-reduced Protein Complexes

### **3.1 Introduction**

Protein complexes are critically-important targets for structural biology, as such macromolecular complexes drive the majority of key cellular process and are, thus, highly sought drug targets.<sup>1</sup> In the post-genomic era, the rapid structural analysis of protein complexes, largely driven by advances in X-ray crystallography and nuclear magnetic resonance (NMR) spectroscopy, has catalyzed many breakthroughs in human health.<sup>2</sup> However, the limitations of such technologies for proteins that resist bacterial over-expression, are difficult to purify in large amounts, or are natively active within polydisperse ensembles necessitates the development of a broader suite of tools capable of protein complex structural analysis. Mass Spectrometry (MS) techniques readily offer rapid analysis of mixtures, and many techniques are available for probing the structures of protein complexes in solution.<sup>3</sup> Among these, ion mobility-mass spectrometry (IM-MS) has proved useful for determining the overall size and coarse-grained structure of intact protein complexes through measurements carried out in the gas-phase.<sup>4-8</sup>

Model structures of protein-protein complexes that rely upon IM-MS data are typically constructed by first measuring the intact assembly using MS.<sup>9</sup> This step is followed by various protocols aimed at disrupting the intact complex into subcomplexes, and eventually its

monomeric building blocks, as mass measurements of such species provides direct protein connectivity information.<sup>9</sup> For three-dimensional modeling, cross-section values from IM measurements for the intact assembly, as well as all observed subcomplexes, are input into a restraint-guided search of theoretical protein topologies that satisfy all experimental constraints. The accuracy of the IM-MS measurements, as well as the number of subcomplexes observed during data collection directly influences the confidence level and information content of the models generated.<sup>10-12</sup> Such IM-MS methods have recently been used to construct models of polydisperse heatshock proteins,<sup>13</sup> ATP Synthase,<sup>14</sup> the CRISPR-associated Cascade assembly,<sup>15</sup> amyloid-associated aggregates,<sup>16</sup> and replisome-related complexes.<sup>17</sup>

Of the information content typically required for IM-MS protein complex model generation, a comprehensive cross-section analysis of protein monomers that comprise the assembly is both an essential element and a bottleneck in current methodologies. For example, solution-phase disruption approaches for producing low charge state protein monomers for IM-MS measurements is currently the dominant approach to the problem; however, such data collection requires extensive screening of solution conditions to remove subunit proteins from the assembly without significant remodeling or unfolding.<sup>9,12,18-23</sup> An alternative method for generating IM information on compact protein subunits is through gas-phase dissociation. The most direct route to compact product ion formation in the gas phase is currently surface induced dissociation (SID), where ion-surface collisions of protein complex precursor ions induces activation on a short timescale in a shattering-type mechanism to produce compact subcomplex product ions.<sup>24,25</sup> For precursor ions having charge states produced under native MS conditions, collision induced dissociation (CID) produces highly charged, highly unfolded monomer ions along with stripped protein complexes at reduced charge states.<sup>26-28</sup> Such unfolded protein ions

are not readily relatable to protein structures in solution, and are thus not easily used in the context of protein complex model construction. CID of charge reduced protein complexes, on the other hand has been shown to eject compact subunits.<sup>29</sup> The primary example of this CID pathway comes from charge-reduced tetrameric transthyretin (TTR) ions, which have been observed to produce both compact monomers and peptide ions at higher energies and lower charge states.<sup>29</sup> Alternatively, charge amplification of stable boiling protein 1 (SP1) produces compact protein product ions following CID.<sup>30</sup> In both cases, the mechanism of ion formation is currently obscure, but it is clear that greater control and understanding of the processes involved would catalyze an enhanced capability to model multiprotein structures using IM-MS.

Methods for reducing analyte ion charge states range from simple solution manipulation approaches to more complex gas-phase ion-neutral and ion-ion reactions,<sup>31-39</sup> with advantages and disadvantages for each. Solution-phase manipulation approaches for charge reduction have the advantages simplicity and efficiency, however, such protocols also often sacrifice native protein-protein interactions, as well as the overall effectiveness of the charge reduction process.<sup>31-33</sup> Alternatively, gas-phase charge reduction approaches do not affect protein-protein interactions; however, require specialized instrument modifications and sacrifice molecular efficiency, in that charge reduction agents must typically be added in large excess to significantly reduce ion charge.<sup>33-39</sup>

Here we attempt to answer the underlying questions surrounding the formation of compact monomeric CID product ions from charge reduced protein complexes by studying avidin (64 kDa) and aldolase (157 kDa) tetramers. Using solution based charge reduction methods, we record collision induced unfolding (CIU) over a broad range of charge states to observe protein complex stabilities and unfolding patterns. Furthermore, we measure the

collision cross-sections (CCSs) of both parent and product ions produced by CID from each precursor charge state, as well as the charge state distribution (CSD) of the product ions formed. Current models of protein complex CID suggest that charge is equally distributed over all protein surface in the transition states accessed by the complex prior to dissociation, creating clear expectations for ratios of product ion/parent ion ratios of size and CSD. For both protein tetramers studied here, we observe ratios that do not align with such expectations without invoking intermediate states that are compacted, and constructed of compacted monomers. In the case of aldolase, such states are directly observed, however for avidin they are inferred from CSD and product ion data alone, possibly suggesting an unstable, transient intermediate species not captured on the timescale of our IM-MS measurements. We then use CCS data as physical constraints to build models describing the CID pathways observed for these two protein tetramers and discuss their significance.

## **3.2 Experimental**

### **3.2.1 Sample Preparation**

Avidin (chicken egg white) and aldolase (rabbit muscle) were prepared under native conditions in 200 mM ammonium acetate to a concentration of 10  $\mu$ M following buffer exchange using Bio-Rad spin columns with a 40 kDa low mass cutoff (Hercules, CA, USA). Charge reduced states were achieved under two different protocols; either by buffer exchanging and diluting protein samples into triethylammonium acetate (TEAA) or by addition of the charge reducing agent triethylamine (TEA), and in some cases TEAA, at various low concentrations to samples prepared in ammonium acetate.<sup>32</sup> All proteins, buffers, and charge reducing agents were purchased from Sigma-Aldrich (St. Louis, MO, USA).



### 3.2.2 Instrumentation and Data Analysis

IM-MS experiments were performed on a commercial quadrupole-traveling wave ion mobility-time-of-flight mass spectrometer (Q-TWIM-TOF MS) instrument purchased from Waters (Synapt G2 HDMS, Manchester, UK). IM-MS data was analyzed using MassLynx software and CCSs were measured using standard calibrants following a previously published protocol.<sup>13,40,41</sup> CIU and CID experiments were performed by increasing the collision energy in the “Trap T-Wave” region of the instrument, after quadrupole mass selection and prior to IM separation. Data were acquired at 5V intervals over a voltage range that allowed all charge states of a protein to be studied over the same laboratory-frame energy range (*i.e.*, tetramer charge state  $\times$  trap collision energy voltage).

Protein unfolding was assessed using CIU “fingerprints”, which are generated by plotting intensity normalized drift time chromatographs into 3D contour plots of CCS verse lab-frame collision energy. To record CIU threshold energies, the CCS of the most abundant peak was identified at each collision energy. From these CCSs the smallest CCS (at energy  $E_1$ ) was identified and all CCSs 2.5% greater than the smallest CCS were selected. From this list the CCS with the lowest energy (at energy  $E_2$ , where  $E_1 < E_2$ ) is chosen and is defined as the CIU energy threshold. Similarly, CID energy thresholds were measured from MS data, and are defined as the energy at which the greatest positive difference in relative product ion intensity between adjacent 5V steps is observed.

### 3.2.3 Molecular Modeling

Simulated monomer structures for avidin and aldolase were built starting from the known protein complex X-ray crystal structures (1AVE and 1ADO, respectively).<sup>42,43</sup> A single monomer subunit, extracted from the intact tetramer, was assigned charge evenly over its surface on the

most basic residues (Lys, Arg, His and N-terminus). All the molecular dynamics simulations were performed using the GROMACS[44] software package (ver. 4.5.5)<sup>44</sup>[B. Hess and C. Kutzner and D. van der Spoel and E. Lindahl] under a GROMOS96 53a6 force field.<sup>45</sup> The system was energy-minimized by the steepest decent method, and then went through an nvt and subsequently an npt simulation. The monomeric protein was then subjected to simulated annealing where the system temperature was varied from 300 K to 800 K then cooled back to 300 K in a periodic manner for 50,000 iterations over the course of a 20 ns simulation, in order to allow for escape from local minima and enhance equilibration. Every 5<sup>th</sup> 300 K structure was recorded (producing 10,000 total structures) throughout the simulation.<sup>46,47</sup> From these structures, the most compact model with the lowest potential energy, which also agreed with experimental CCS measurements (as computed using a scaled projection approximation in MOBCAL and IMoS),<sup>48,49</sup> was selected for further model building of tetramers with native-like geometries. To model tetramers with rearranged structures, spherical representations of compact monomers with CCSs equal to experimental measurements were docked to a trimer subunit (built from compact monomer spheres) of appropriate CCS and the conformational space was sampled with an exhaustive Monte Carlo search.<sup>10</sup> In the case of coarse-grained structures, CCS values were computed using a projection approximation, as described previously.<sup>10,11</sup> Final structures are selected based on agreement with experimental size (CCS) constraints and acceptable spherical overlap (15-45%).<sup>10</sup>

### **3.3 Results and Discussion**

The native charge states of aldolase (23<sup>+</sup>-27<sup>+</sup>), generated from ammonium acetate, and those produced via charge reduction (17<sup>+</sup>-22<sup>+</sup>) were measured over a collision energy range that included 540 eV-3600 eV (with the exception of 17<sup>+</sup>, for which our dataset has an upper limit of

3400 eV). Over this energy range, all protein charge states undergo structural transitions and dissociation. Figure 3-1A presents CIU fingerprints for 4 aldolase charge states (for all 11 CIU fingerprints see Appendix C Fig. C-1). Overlaid on these plots are dashed white lines, which represent the CID threshold measured for each ion. The CIU data recorded for the five charge states observed from unmodified ammonium acetate solutions are all very similar; each ion unfolds extensively prior to the onset of dissociation, with higher charge state ions adopting a greater number of meta-stable conformational states, but always trending towards a more

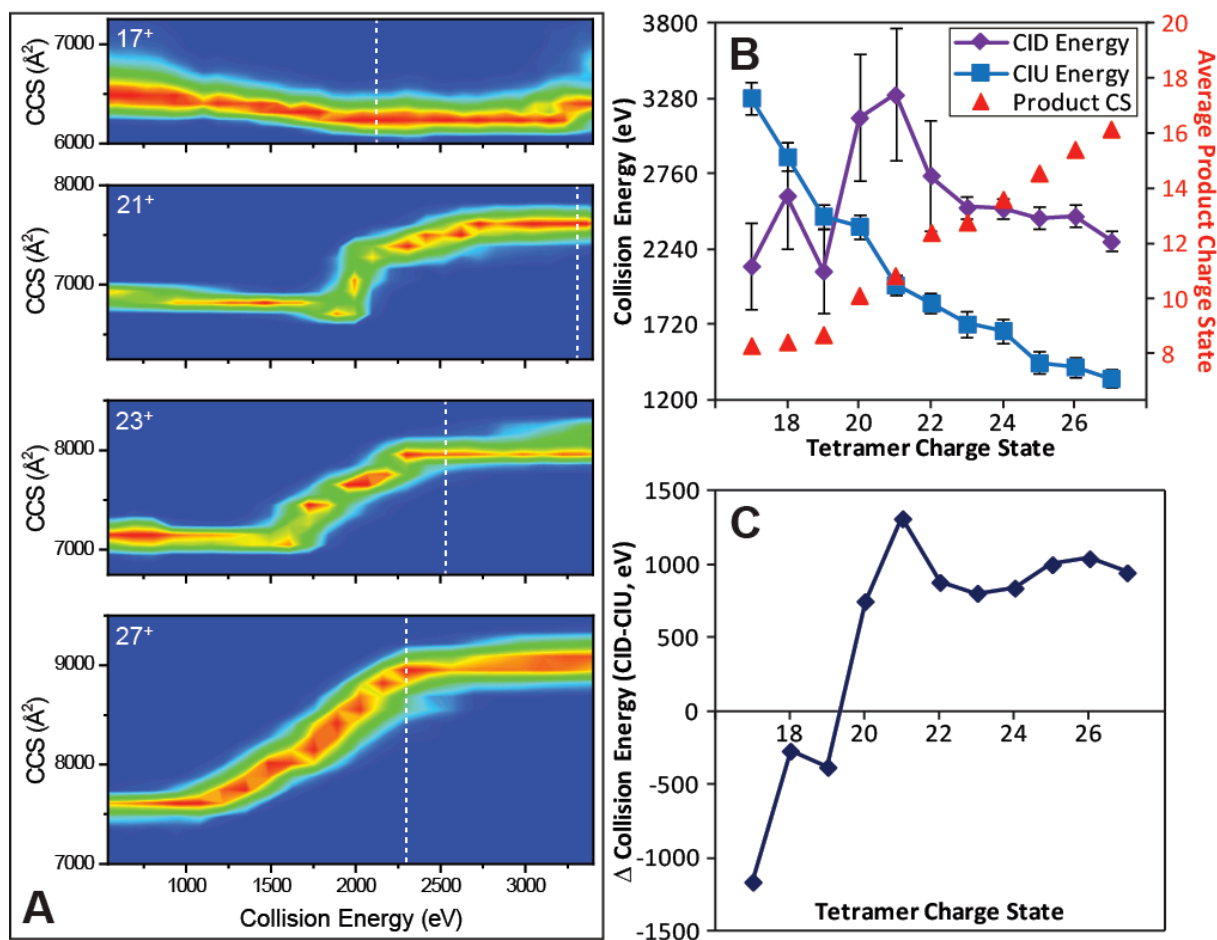


**Figure 3-1.** Representative CIU fingerprints (A) and comparison of CID and CIU threshold energies for aldolase. Dashed lines in CIU fingerprints represent CID energy thresholds. (B) CID (◆) and CIU (■) energy thresholds for measured tetramer charge states, along with the average monomer charge states (▲, right y-axis) produced during CID. (C) Laboratory-frame collision energy differences are plotted between the CID and CIU thresholds. A negative difference value indicates monomer dissociation prior to tetramer unfolding.

extended conformation. A transition in the protein's unfolding pathway becomes apparent beginning with the 21<sup>+</sup> ion, where a compacted conformational state is observed at lower energies compared to those that elicit monomer unfolding. This protein complex compaction is enhanced and observed over a broader range of energies as lower charge states are evaluated, mirroring previous work with cavity-bearing protein complexes.<sup>50</sup> Ultimately, the 17<sup>+</sup> produces an unfolded conformation with a CCS smaller (1.5%) than the low energy CCS of the intact complex due to extensive compaction at lower energies (4.1%).

Further evidence of a shift in dissociation pathway is indicated by the CID threshold energy for each aldolase precursor ion selected for CIU. As shown in Figure 3-1B, there is a general increase in the CID threshold energy value (purple) as the charge state decreases from 27<sup>+</sup> to 21<sup>+</sup>. However, this trend breaks down for lower charge states, where a significant decrease in the threshold energy is observed. It is important to note that this shift in threshold energy is isoenergetic with the tetramer compaction observed for the aldolase tetramer at lower charge states. As observed in Figure 3-1A, CIU threshold energy increases with decreasing tetramer charge state (Fig. 3-1B, blue). The expected asymmetric protein complex dissociation pathway is expected to exhibit significant unfolding prior to complex dissociation, and this is observed experimentally by plotting the difference between the CID and CIU thresholds observed as a function of tetramer charge state (Figure 3-1C). Higher charge states exhibit a positive difference supporting an asymmetric, protein-unfolding centric dissociation pathway. However, the energy difference for lower charge states (19<sup>+</sup>-17<sup>+</sup>) is negative, indicating that a significant population of product ions are likely produced from a compacted tetramer precursors, having undergone no significant unfolding.

Also plotted are the average monomer product ion charge states observed in our dataset (Fig. 3-1B, red). We record a decrease in product ion charge state with decreasing tetramer precursor charge state. However, we note that the average percentage of the total precursor ion charge transferred to the monomer product ions decreases only modestly over the range of ions studied here, ranging from 60% charge migration on average for the monomers from  $27^+$  tetramers to 46% charge migration on average for those monomers produced from  $19^+$  precursors, with similar values recorded for  $18^+$  and  $17^+$  tetramers as well. Taken together, the data in Figure 3-1 point to a shift in the dissociation pathway that likely occurs between the  $22^+$  and  $19^+$  charge states, characterized by a compacted tetramer transition state, and leads to a lower energy dissociation thresholds.

The native charge states of avidin ( $15^+$ - $17^+$ ), generated from protein prepared in ammonium acetate, as well as those produced via charge reduction ( $11^+$ - $16^+$ ), were measured over a laboratory-frame collision energy range of 540 eV-2400 eV (with the exception of the  $11^+$ , which has an upper limit of 2200 eV in our dataset). Over this energy range all charge states under go structural transitions and dissociation. Figure 3-2A shows CIU fingerprints for 4 avidin charge states (for all 7 CIU fingerprints see Appendix C Fig. C-2). Overlaid on these plots are dashed white lines, which represent the CID threshold characterized in the same manner as for the aldolase data described above. The three charge states observed for proteins generated from pure ammonium acetate solutions are very similar; each ion unfolds extensively prior to the onset of dissociation, with the transitions from compact, to intermediate, to extended state similar to both aldolase and previously reported data.<sup>29</sup> A transition in CIU is apparent at the  $14^+$  ion (see Appendix C Fig. C-2) indicated by a significant decrease in number of unfolded conformational states observed. This observation extends to all ions of lower charge. Unlike aldolase, the CIU

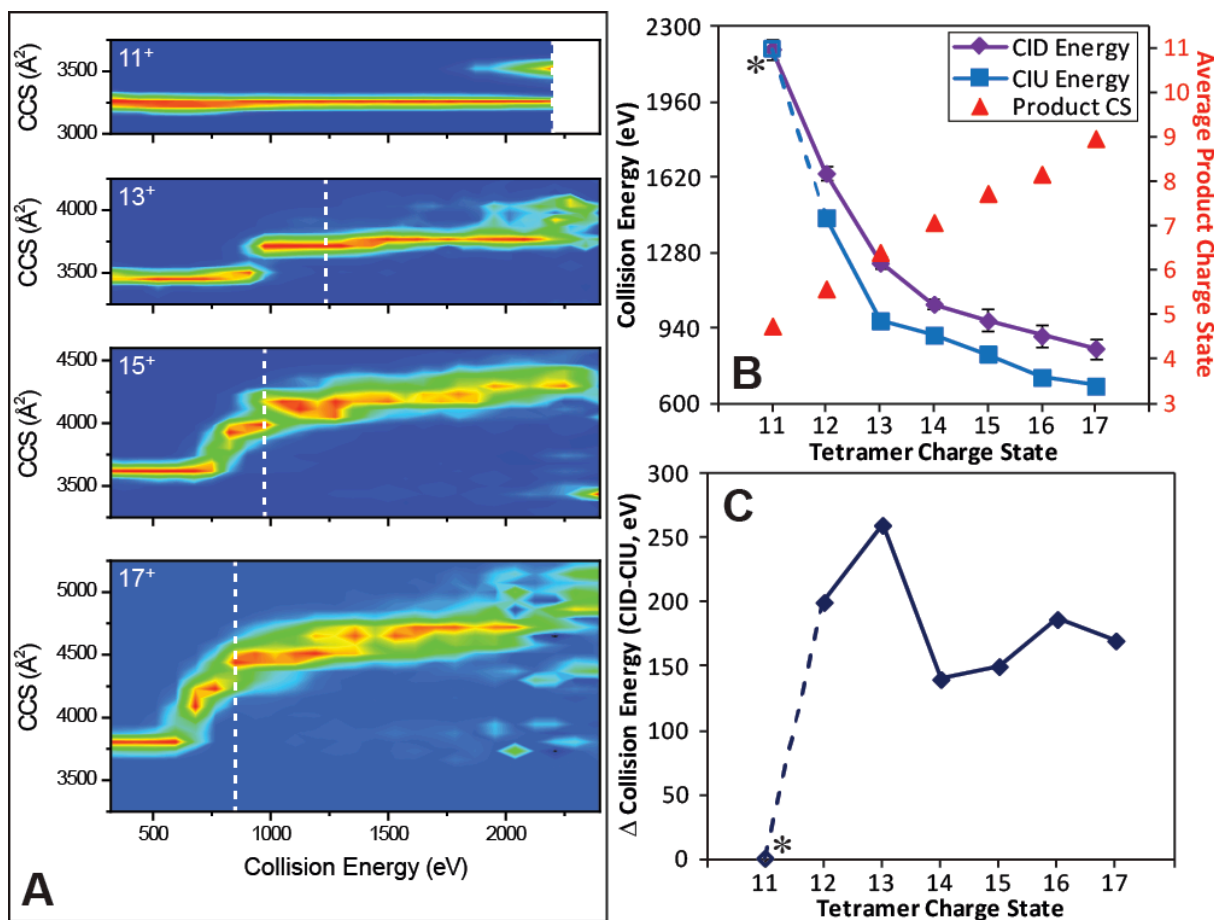


**Figure 3-2.** Representative CIU fingerprints (A) and comparison of CID and CIU threshold energies for avidin. Dashed lines in CIU fingerprints represent CID energy thresholds. (B) CID ( $\blacklozenge$ ) and CIU ( $\blacksquare$ ) energy thresholds for measured tetramer charge states, along with the average monomer charge states ( $\blacktriangle$ , right y-axis) produced during CID. (C) Collision energy differences are plotted between the CID and CIU thresholds. The CIU threshold for 11+ ( $*$ ) was not observed, and in its place we show a point at the highest attainable laboratory frame energy on our instrumentation for illustrative purposes.

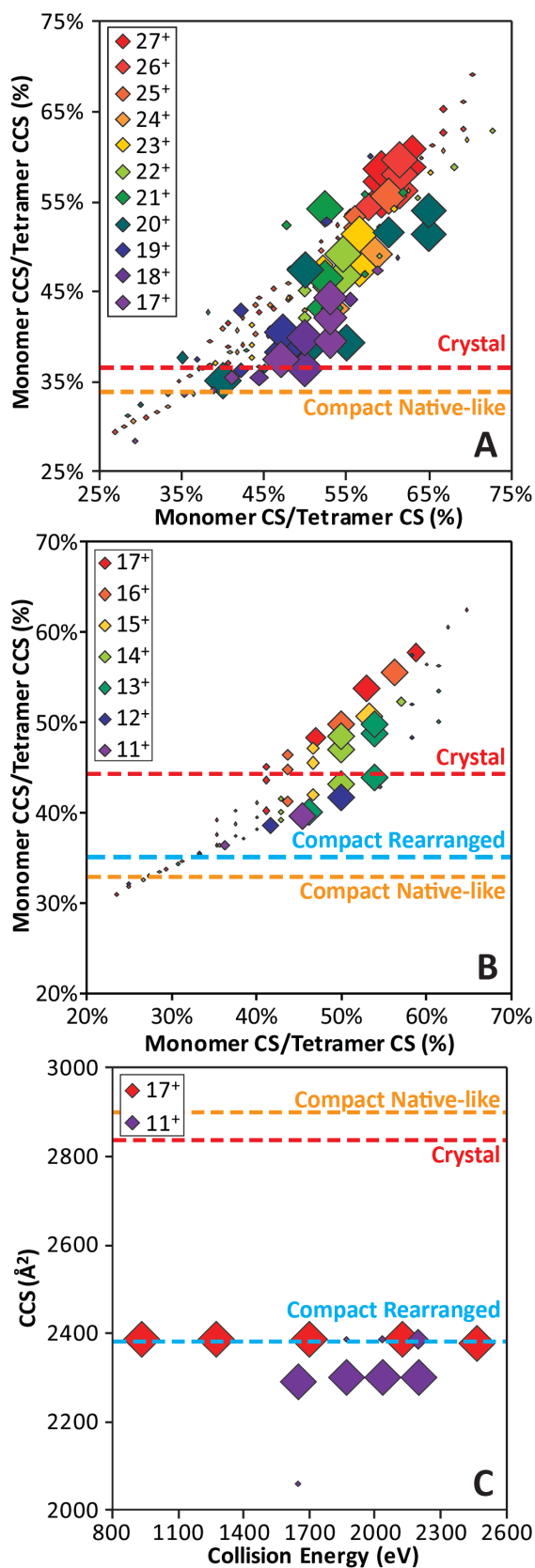
data for low charge states of avidin does not reveal any significant compaction within the intact tetramer.

In further contrast to our aldolase dataset, Figure 3-2B shows a much different general trend for CID and CIU threshold energies, where values decrease continuously in the case of avidin across the entire charge state range studied. In addition, the charge states acquired by monomer product ions are observed to decrease in a near-linear fashion as a function of decreasing precursor ion charge state, and the energy required for CIU does not exceed that for CID in our avidin dataset, both in contrast to the non-linear transitions and trends observed for

aldolase above. Both data are in good agreement with previous CIU/CID data for TTR, where a general mechanism absent of any precursor structure transitions was invoked to explain the IM-MS data collected as a function of charge state.<sup>29</sup>

Current models of the protein complex CID pathway, that describe how unfolded monomers as well as stripped, charge-reduced protein complexes are produced as product ions, require that charge is equally partitioned over the surface area of the unfolded transition states accessed by the assembly during activation.<sup>51</sup> This requirement produces several testable values that can be extracted from our aldolase and avidin datasets. The first, is the ratio of the monomer product ion size to the tetramer precursor ion size (monomer CCS/tetramer CCS, expressed as a % of tetramer CCS), and the second is a ratio of monomer and tetramer precursor charge state (CS). Figure 3-3 plots these two metrics against each other for data acquired for aldolase (Figure 3-3A) and avidin (Figure 3-3B), along with idealized ratios of CCS values, represented as horizontal dashed lines, derived from models described below. The relative number of ions that account for each point in the diagram is represented by the relative size of that point within the plot. In general, we observe a positive trend for both assemblies, in that protein charge asymmetry general increases with increasing size asymmetry (*e.g.*, from monomer unfolding). The differences we observe between the two datasets shown in Figure 3-3, however, far outweigh their similarity. For example, the aldolase data shown in Figure 3-3A can be approximated by a single, near linear trend line, whereas there is a clear discontinuity for the





◀ **Figure 3-3.** Plots of Monomer/tetramer CCS ratio versus monomer/tetramer charge state (CS) ratio for (A) aldolase and (B) avidin, and (C) plot of avidin trimer CCSs produced during CID. Data point sizes are scaled relative to observed product ion signal intensities. (C) Plot of measured 7<sup>+</sup> avidin trimer product ion CCSs versus laboratory frame collision energy for 17<sup>+</sup> and 11<sup>+</sup> tetramer parent ions. Dashed red lines on panels A and B represent monomer/tetramer size ratios from X-ray data and the trimer CCS computed from X-ray data for panel C. Dashed orange lines on panels A and B represent the monomer/tetramer size ratio computed from a compact, native-like model computed following relaxation of the structure in the gas-phase and on panel C, the trimer size computed similarly. Dashed blue lines represent the monomer/tetramer size ratio from a compact rearranged model (panel B) of avidin and the avidin trimer size from a compact rearranged model (panel C, see supporting information).

avidin in the data shown in Figure 3-3B. In addition, when compared with idealized CCS ratios between X-ray derived monomers and tetramers, which should function as a lower-limit to the size differences recorded provided X-ray structures are preserved in the gas-phase during activation, the majority of aldolase values are greater (83.1%), while 59.7% of avidin data points lie below such a threshold.

In order to develop models of avidin and aldolase that account for a larger proportion of the data acquired than those derived from

unmodified X-ray structures, we began by building putative models of intermediate tetramer structures based on the compacted portion of our CCS dataset. Such models, once generated, would act to alter the monomer/tetramer CCS ratios that we project on to the plots shown in Figure 3-3A and 3-3B. In the case of aldolase, data shown in Figure 3-1 clearly shows the evidence of tetramer compression, especially in cases where lower charge states are studied. To build representations of such a compacted aldolase tetramer, we subjected the crystal structure of an aldolase monomer to simulated annealing in the gas phase producing a compacted monomer structure in good agreement with experimental CCS measurements. We then constructed an aldolase tetramer using the compacted experimental CCS as a constraint, but keeping the symmetry and quaternary organization of the monomers similar to those found in the crystal structure. To build this model, it was necessary to minimize the number of contacts between adjacent monomers, thus likely weakening the interactions between individual aldolase units. The dashed orange line in Fig. 3-3A represents the size ratio found in this “Compact Native-like” structure, and projects a CCS ratio value lower than 91.2% of our experimental data.

Models for a compacted avidin tetramer are more problematic to conceptualize, as we collected no direct evidence of tetramer compaction in our CIU data shown in Figure 3-2A. To constrain a compacted tetramer model, we recorded CCS values for stripped trimer ions produced from CID (Figure 3-3C). We were able to observe such trimer product ions from multiple avidin precursors, and all ions observed possess a smaller CCS value than any X-ray derived trimer (red dashed line, Figure 3-3C). Due to the comparatively low CID efficiency observed for charge reduced aldolase tetramer ions, we are unable to record CCS values for aldolase trimer product ions in a similar manner. Using experimental measurements of compact avidin monomers, a coarse-grained symmetrical trimer geometry was generated, and found to

agree well with experimental trimer CCS values (2385 versus 2381 Å<sup>2</sup>). Following this optimization, an exhaustive Monte Carlo search was performed to develop a model of the avidin tetramer based on restraints derived from the compacted trimers and monomers observed as product ions, along with the ‘native-like’ tetramer size recorded for all low charge state ions in Figure 3-2A. Models that satisfy the monomer and trimer experimental CCS restraints and have sufficient spherical overlap between subunits to indicate physical interaction (>15%) have tetramer CCSs that are well below experimental CCS measurements (6% smaller for the model is closest agreement; see Appendix C Table C-1). Alternatively, models that satisfied experimental restraints for monomer, trimer, and tetramer CCS were found to be unphysical, showing spherical overlap of 2.6%, well below the threshold for biologically relevant contacts (15%). This result implies that a compacted avidin intermediate must be transient on the timescale of our IM measurement, leading to a form of the protein complex that produces monomer and trimer product ions that possess charge states and sizes that align with our data, but does not possess an intact CCS resembling the values recorded directly for the avidin tetramer. During this process, we also constructed an avidin tetramer model in a similar fashion to those we built for aldolase. Both of these models, when projected onto Figure 3-3B, account for a significantly larger portion of the data collected for avidin CID product ions when compared with those values extracted directly from unmodified X-ray coordinate files, with a simple compacted model (Figure 3-3B, dashed line in orange) accounting for a larger portion of the data (93.5) than a model that includes rearrangements that account for our avidin trimer size measurements (91.9%; Figure 3-3B, dashed line in blue).

### 3.4 Conclusions

Within the gas-phase, multiprotein complex ions retain native-like conformations and can be studied using IM-MS.<sup>5,6</sup> With additional subunit and subcomplex IM-MS size measurements, where the subunits and subcomplexes also retain a semblance of their native-like, intra-complex conformations, coarse-grained and hybridized models of the complex structure can be produced.<sup>10-12</sup> Traditional methods of disrupting complexes in solution are not universal, and require extensive screening to produce optimized solution conditions.<sup>9,23</sup> Gas-phase dissociation, having a more universal pathway, is desirable for its broad application; however, native-like monomer conformations are not retained in the gas-phase.<sup>26-28</sup> Under charge reducing conditions evidence of compact monomer dissociation, ideally suited from building model structure, has been demonstrated for the TTR tetramer.<sup>29</sup> Here, we show evidence for two additional proteins, aldolase and avidin, producing compact gas-phase monomers following collisional activation of charge reduced ions.

Collision induced dissociation and unfolding of charge reduced ions of aldolase and avidin confirms the ability to induce dissociation of proteins prior to unfolding, consistent with previous data. Data presented here shows aldolase undergoing tetramer compaction on the experimental timescale prior to dissociation of compacted monomers. Both of these compact gas-phase conformations are smaller than expected based on predicted values from crystal structures. Simulated annealing of the monomer generates compact monomers with sizes that agree with experimental measurements. The size of tetramers build from compact monomer, where a native-like geometry is maintained, also agrees with experimental measurements. Avidin tetramer, unlike aldolase, maintains a constant size until the onset of unfolding. However, like aldolase, dissociation produces compact monomers, in addition to compact trimmers, with

smaller sizes than predicted from crystal structures. Like aldolase, simulated annealing of the avidin monomer produced compact conformations with sizes in good agreement with experimental measurements. Tetramers build from compact monomers with a native-like geometry were also in good agreement with experimental measurements, but the trimer sizes was not. A coarse-grained trimer with a rearranged symmetric geometry was build to agree with experimental size measurements. A Monte Carlo search of potential monomer-trimer conformations generated tetramer conformations with minimal subunit interaction while still maintaining physical interactions; however; the size did not agree with experimental values. From these models we infer the existence of a compacted transient species conformation that is unobservable on the experimental timescale.

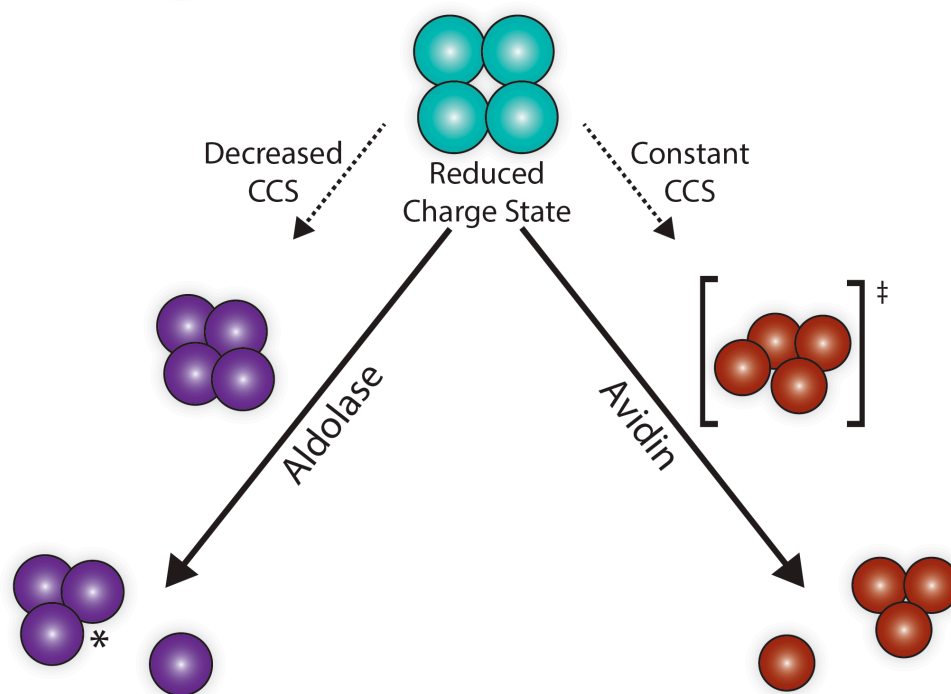


**Figure 4.** Proposed dissociation pathways for aldolase (purple) and avidin (red). Both systems produce compact product ions through compaction of the tetramer prior to dissociation. The key differences between the two systems are the lifetime of the compact species, and potential remodeling of the quaternary structure of avidin in the transient compact state. The lifetime of the compact avidin species is proposed to be so short that it cannot be observed on the timescale of our IM-MS experiment. Aldolase trimer ( $*$ ) was not measured due to low CID signal intensity for charge reduced precursor ions.

Figure 3-4 presents the two distinct pathways for unfolding and dissociation taken by aldolase and avidin. Under the purple pathway (left), aldolase undergoes tetramer compaction to produce gas-phase species with compact CCSs. Dissociation of this compact tetramer produces compact product ions (trimer, marked by  $*$ , was not observed due to low dissociation efficiency). Under the red pathway (right), avidin tetramer maintains a constant CCS up until the point of dissociation. Compact, rearranged transient species, not observed on the timescale of the experiment, exist as the immediate precursor to complex dissociation. Dissociation proceeds from the transient compact species to generate compact product ions. Explanations for differences between the two proteins are being explored to understand the observation of two distinct pathways. The compaction of aldolase observed during CIU strongly resembles

compaction of charge reduced multiprotein complexes with ring-like conformations.<sup>50</sup> However, aldolase does not exist in a ring-like conformation. Avidin is known to have particularly strong intermolecular interactions and falls in the ‘dimer of dimers’ class of tetramers.<sup>23</sup> The unfolding data for avidin strongly resembles TTR,<sup>29</sup> which is also a dimer of dimers.<sup>52</sup> We postulate that this dimer of dimers conformation is a driving factor in the observed dissociation pathway, and warrants further investigation.

### 3.5 Acknowledgements

Funding for this work was supplied by the National Science Foundation (BTR, CAREER Award, 1253384).

### 3.6 References

- (1) Jorgensen, W. L. *Science* **2004**, *303*, 1813.
- (2) Csermely, P.; Korcsmáros, T.; Kiss, H. J. M.; London, G.; Nussinov, R. *Pharmacology & Therapeutics* **2013**, *138*, 333.
- (3) Hyung, S.-J.; Ruotolo, B. T. *PROTEOMICS* **2012**, *12*, 1547.
- (4) Clemmer, D. E.; Hudgins, R. R.; Jarrold, M. F. *J. Am. Chem. Soc.* **1995**, *117*, 10141.
- (5) Ruotolo, B. T.; Giles, K.; Campuzano, I.; Sandercock, A. M.; Bateman, R. H.; Robinson, C. V. *Science* **2005**, *310*, 1658.
- (6) Ruotolo, B. T.; Robinson, C. V. *Curr. Opin. Chem. Biol.* **2006**, *10*, 402.
- (7) Uetrecht, C.; Versluis, C.; Watts, N. R.; Wingfield, P. T.; Steven, A. C.; Heck, A. J. R. *Angew. Chem. Int. Ed.* **2008**, *47*, 6247.
- (8) van Duijn, E.; Barendregt, A.; Synowsky, S.; Versluis, C.; Heck, A. J. R. *J. Am. Chem. Soc.* **2009**, *131*, 1452.
- (9) Zhong, Y.; Hyung, S.-J.; Ruotolo, B. T. *Expert Rev. Proteomics* **2012**, *9*, 47.
- (10) Hall, Z.; Politis, A.; Robinson, Carol V. *Structure* **2012**, *20*, 1596.
- (11) Politis, A.; Park, A. Y.; Hyung, S. J.; Barsky, D.; Ruotolo, B. T.; Robinson, C. V. *PLoS One* **2010**, *5*.
- (12) Pukala, T. L.; Ruotolo, B. T.; Zhou, M.; Politis, A.; Stefanescu, R.; Leary, J. A.; Robinson, C. V. *Structure* **2009**, *17*, 1235.
- (13) Ruotolo, B. T.; Benesch, J. L. P.; Sandercock, A. M.; Hyung, S. J.; Robinson, C. V. *Nat. Protoc.* **2008**, *3*, 1139.
- (14) Zhou, M.; Morgner, N.; Barrera, N. P.; Politis, A.; Isaacson, S. C.; Matak-Vinković, D.; Murata, T.; Bernal, R. A.; Stock, D.; Robinson, C. V. *Science* **2011**, *334*, 380.
- (15) van Duijn, E.; Barbu, I. M.; Barendregt, A.; Jore, M. M.; Wiedenheft, B.; Lundgren, M.; Westra, E. R.; Brouns, S. J. J.; Doudna, J. A.; van der Oost, J.; Heck, A. J. R. *Mol. Cell. Proteomics* **2012**, *11*, 1430.

- (16) Bernstein, S. L.; Dupuis, N. F.; Lazo, N. D.; Wyttenbach, T.; Condrón, M. M.; Bitan, G.; Teplow, D. B.; Shea, J.-E.; Ruotolo, B. T.; Robinson, C. V.; Bowers, M. T. *Nat Chem* **2009**, *1*, 326.
- (17) Politis, A.; Park, A. Y.; Hall, Z.; Ruotolo, B. T.; Robinson, C. V. *J. Mol. Bio.* **2013**, *425*, 4790.
- (18) Hernández, H.; Dziembowski, A.; Taverner, T.; Séraphin, B.; Robinson, C. V. *EMBO reports* **2006**, *7*, 605.
- (19) Sharon, M.; Taverner, T.; Ambroggio, X. I.; Deshaies, R. J.; Robinson, C. V. *PLoS Biol* **2006**, *4*, 1314.
- (20) Taverner, T.; Hernandez, H.; Sharon, M.; Ruotolo, B. T.; Matak-Vinkovic, D.; Devos, D.; Russell, R. B.; Robinson, C. V. *Accounts Chem. Res.* **2008**, *41*, 617.
- (21) Zhou, M.; Sandercock, A. M.; Fraser, C. S.; Ridlova, G.; Stephens, E.; Schenauer, M. R.; Yokoi-Fong, T.; Barsky, D.; Leary, J. A.; Hershey, J. W.; Doudna, J. A.; Robinson, C. V. *Proc. Natl. Acad. Sci. U. S. A.* **2008**, *105*, 18139.
- (22) Leary, J.; Schenauer, M.; Stefanescu, R.; Andaya, A.; Ruotolo, B.; Robinson, C.; Thalassinou, K.; Scrivens, J.; Sokabe, M.; Hershey, J. *J. Am. Soc. Mass Spectrom.* **2009**, *20*, 1699.
- (23) Zhong, Y.; Feng, J.; Ruotolo, B. T. *Anal. Chem.* **2013**, *85*, 11360.
- (24) Zhou, M.; Dagan, S.; Wysocki, V. H. *Analyst* **2013**, *138*, 1353.
- (25) Zhou, M.; Jones, C. M.; Wysocki, V. H. *Anal. Chem.* **2013**, *85*, 8262.
- (26) Jurchen, J. C.; Garcia, D. E.; Williams, E. R. *J. Am. Soc. Mass Spectrom.* **2004**, *15*, 1408.
- (27) Jurchen, J. C.; Williams, E. R. *J. Am. Chem. Soc.* **2003**, *125*, 2817.
- (28) Ruotolo, B. T.; Hyung, S.-J.; Robinson, P. M.; Giles, K.; Bateman, R. H.; Robinson, C. V. *Angew. Chem. Int. Ed.* **2007**, *46*, 8001.
- (29) Pagel, K.; Hyung, S. J.; Ruotolo, B. T.; Robinson, C. V. *Anal. Chem.* **2010**, *82*, 5363.
- (30) Erba, E. B.; Ruotolo, B. T.; Barsky, D.; Robinson, C. V. *Anal. Chem.* **2010**, *82*, 9702.
- (31) Verkerk, U. H.; Peschke, M.; Kebarle, P. *J. Mass Spectrom.* **2003**, *38*, 618.
- (32) Catalina, M. I.; van den Heuvel, R. H. H.; van Duijn, E.; Heck, A. J. R. *Chem.-Eur. J.* **2005**, *11*, 960.
- (33) Bornschein, R. E.; Hyung, S.-J.; Ruotolo, B. T. *J. Am. Soc. Mass Spectrom.* **2011**, *22*, 1690.
- (34) Kharlamova, A.; DeMuth, J.; McLuckey, S. *J. Am. Soc. Mass Spectrom.* **2012**, *23*, 88.
- (35) Ebeling, D. D.; Westphall, M. S.; Scalf, M.; Smith, L. M. *Anal Chem* **2000**, *72*, 5158.
- (36) Ebeling, D. D.; Westphall, M. S.; Scalf, M.; Smith, L. M. *Rapid Commun. Mass Spectrom.* **2001**, *15*, 401.
- (37) Frey, B. L.; Lin, Y.; Westphall, M. S.; Smith, L. M. *J. Am. Soc. Mass Spectrom.* **2005**, *16*, 1876.
- (38) Badman, E. R.; Chrisman, P. A.; McLuckey, S. A. *Anal. Chem.* **2002**, *74*, 6237.
- (39) Campuzano, I. G.; Schnier, P. *Int. J. Ion Mobil. Spec.* **2013**, *16*, 51.
- (40) Hernandez, H.; Robinson, C. V. *Nat. Protoc.* **2007**, *2*, 715.



- (41) Bush, M. F.; Hall, Z.; Giles, K.; Hoyes, J.; Robinson, C. V.; Ruotolo, B. T. *Anal. Chem.* **2010**, *82*, 9557.
- (42) Pugliese, L.; Coda, A.; Malcovati, M.; Bolognesi, M. *J. Mol. Bio.* **1993**, *231*, 698.
- (43) Blom, N.; Sygusch, J. *Nat Struct Mol Biol* **1997**, *4*, 36.
- (44) Hess, B.; Kutzner, C.; van der Spoel, D.; Lindahl, E. *J. Chem. Theory Comput.* **2008**, *4*, 435.
- (45) Oostenbrink, C.; Villa, A.; Mark, A. E.; Van Gunsteren, W. F. *Journal of Computational Chemistry* **2004**, *25*, 1656.
- (46) Lindahl, E.; Hess, B.; van der Spoel, D. *J Mol Model* **2001**, *7*, 306.
- (47) Soper, M. T.; DeToma, A. S.; Hyung, S.-J.; Lim, M. H.; Ruotolo, B. T. *Phys. Chem. Chem. Phys.* **2013**, *15*, 8952.
- (48) Benesch, J. L. P.; Ruotolo, B. T. *Current Opinion in Structural Biology* **2011**, *21*, 641.
- (49) Larriba, C.; Hogan, C. J. *J. Phys. Chem. A* **2013**, *117*, 3887.
- (50) Hall, Z.; Politis, A.; Bush, M. F.; Smith, L. J.; Robinson, C. V. *J. Am. Chem. Soc.* **2012**, *134*, 3429.
- (51) Wanasundara, S.; Thachuk, M. *J. Am. Soc. Mass Spectrom.* **2007**, *18*, 2242.
- (52) Blake, C. C. F.; Geisow, M. J.; Oatley, S. J.; Rérat, B.; Rérat, C. *J. Mol. Bio.* **1978**, *121*, 339.

## **Chapter 4. Ion Mobility-Mass Spectrometry Reveals General Trends in the Gas-phase Ejection of Compact Subunits from Intact Protein Complexes**

**Bornschein RE**, Ruotolo BT, Prepared for submission to *Analyst* as Ion Mobility-Mass Spectrometry Reveals General Trends in the Gas-phase Ejection of Compact Subunits from Intact Protein Complexes

### **4.1 Introduction**

Macromolecular protein complexes play a critical role in carrying out most of the key functions within the cell, from synthesis to cell death.<sup>1</sup> The quaternary structures of these multiprotein machines, therefore, are key targets for structural biology, in that such information can often lead to breakthroughs in human health and disease treatments.<sup>2,3</sup> High-resolution methods aimed at the direct collection of protein structure information, such as X-ray diffraction (XRD) and nuclear magnetic resonance (NMR) spectroscopy, are often limited by stringent sample requirements in terms of purity, amount, protein flexibility, and assembly polydispersity.<sup>4</sup> Multiple mass spectrometry (MS) techniques are poised to overcome many of these challenges to develop lower-resolution protein complex models across the proteome in a high-throughput fashion.<sup>5</sup> Approaches such as ion mobility (IM),<sup>6,7</sup> chemical cross-linking (CXL),<sup>8,9</sup> and hydrogen/deuterium exchange (HDX),<sup>10-12</sup> when coupled to MS, have the ability to probe protein secondary, tertiary, and quaternary structure in addition to primary structure, thus enabling the generation of models of protein architecture in cases where classical structural biology tools provide little information.

Ion mobility-mass spectrometry (IM-MS) is unique amongst the technologies listed above, in that protein structures are probed entirely in the gas-phase. Experimental evidence has demonstrated that native-like gas-phase conformations can be retained during nanoelectrospray ionization (nESI) when neutral pH, volatile aqueous buffers are used as solvents.<sup>6,13-15</sup> From IM-MS data, both stoichiometry and size (*via* measured collision cross-section; CCS) information can be determined and used to build low-resolution coarse-grain model structures of multiprotein assemblies.<sup>16-18</sup> However, in order to build these coarse-grain topology models, subunits and subcomplexes must be measured in the gas-phase, and these assemblies must possess native-like conformations that are strongly-correlated with solution structures. Disruption of multiprotein complexes can be initiated in solution, through the alteration of ionic strength, solvents composition, and pH.<sup>19,20</sup> While such approaches are currently the most reliable and broadly applied method for generating structurally-informative subcomplexes for protein complex model construction, broad application of solution-phase disruption IM-MS is currently hampered by an incomplete mechanistic understanding of subcomplex formation and protein-dependant responses to specific disruption agents.<sup>15,18,19,21-23</sup> Alternatively, gas-phase dissociation methods, such as collision induced dissociation (CID)<sup>24</sup> and surface induced dissociation (SID),<sup>25</sup> are a promising class of techniques that potentially enable the targeted, universal production of subcomplex information for protein complex modeling efforts. However, for the vast majority of protein complex ions, CID usually results in the generation of highly-unfolded monomeric product ions following an asymmetric charge partitioning mechanism, where the monomer carries a disproportionate amount of the parent ion charge relative to mass.<sup>26-28</sup> IM measurements for such ions are not typically useful for building protein structure models, and thus controlling

the conformation of product ions produced from intact protein assemblies is a challenge for gas-phase structural biology.<sup>28</sup>

Recently, CID of charge-reduced protein complexes was observed to produce compact, native-like monomer product ions.<sup>29</sup> Under such conditions, CID products can be used for building topology models.<sup>29</sup> Previous studies of this altered CID pathway have all been conducted using solution-phase charge state manipulation techniques, which ultimately limits the number of compact protein charge states screened, as well as covering a relatively limited set of protein complexes. To fully utilize such CID CCS information for high-throughput structural biology, the level of charge reduction necessary to alter the CID pathway toward the ejection of compact protein building blocks must be comprehensively characterized in order to generate predictive trends. Previously, we described a continuous gas-phase ion-neutral charge reduction source,<sup>30</sup> and observed compact charge reduced protein complexes formed by a process that was both more effective but less efficient than those generated by solution-phase and ion-ion approaches.

Here, we adapt a recently-described corona discharge probe (CDP)<sup>31</sup> to broadly and efficiently study the amount of charge reduction necessary to alter the CID pathways of protein-protein complexes. We find a positive correlation between the threshold charge required to generate compact product ions from CID and the intact molecular mass of the precursor ion selected, for a broad array of protein complexes. In addition, we discover that for the  $\beta$ -galactosidase and catalase tetramers, the energetic barriers associated with peptide bond dissociation become either lower or iso-energetic than those associated with compact protein ejection for charge-reduced protein complexes. We analyze and discuss these results in light of their general utility for protein complex structural analysis.

## 4.2 Experimental

### 4.2.1 Sample Preparation

Ammonium acetate and triethylammonium acetate (TEAA) were purchased from Sigma Aldrich (St. Louis, MO). Aldolase (rabbit muscle, tetramer 157 kDa), avidin (chicken egg white, tetramer 64 kDa),  $\beta$ -galactosidase ( $\beta$ -Gal; *E. coli*, tetramer 466 kDa),  $\beta$ -lactoglobulin ( $\beta$ -Lac; bovine, monomer 18.6 kDa and dimer 37 kDa), catalase (bovine, tetramer 233 kDa), concanavalin A (ConA; jack bean, tetramer 103 kDa), cytochrome c (CytC; equine, monomer 12.3 kDa), hemoglobin (Hgb; bovine, dimer 32.4 kDa and tetramer 64.8 kDa), serum amyloid P (SAP; human, pentamer 125 kDa), and triosephosphate isomerase (TPI; rabbit muscle, dimer 53.3 kDa) were all purchased (Sigma Aldrich) as lyophilized powder. Stock samples were prepared into ammonium acetate at various concentrations. CytC was prepared to a final concentration of 10  $\mu$ M in 49.5% water:49.5% methanol:1% trifluoroacetic acid (TFA). All other proteins were prepared to a final concentration of 10  $\mu$ M (with the exception of TPI which had a final concentration of 20  $\mu$ M) in 200mM ammonium acetate following buffer exchange using Bio-Rad spin columns (Hercules, CA, USA). Alcohol dehydrogenase (ADH; yeast, 153 kDa), glutamic dehydrogenase (GDH; bovine, 336 kDa) and pyruvate kinase (PK; rabbit, 237 kDa) were also prepared for collision cross-section (CCS) calibration.

### 4.2.2 Instrumentation and Data Analysis

Ion mobility-mass spectrometry (IM-MS) experiments were performed on a commercially available Waters Synapt G2 HDMS (Manchester, UK) platform with a modified nESI source for performing gas-phase ion-ion charge reduction (see below). IM-MS data was processed using MassLynx and Driftscope software (Waters) to measure unknown CCS values following an established protocol<sup>32</sup> using calibrants of known CCS values.<sup>33</sup>

Definitions of charge reduction efficiency and effectiveness used here are identical to those described previously.<sup>30</sup> Briefly, charge reduction efficiency refers to the amount of charge reduction agent required to reduce protein ion charge states by a fixed amount, whereas charge reduction effectiveness refers to the ultimate amount of charge reduction observed under any set of conditions tested. To determine CID thresholds, the relative parent ion and product ion intensities were evaluated at each collision energy. The CID threshold is defined by the energy at which the product ion intensity reaches 50% (or 50% of the steady state intensity). To determine collision induced unfolding (CIU) thresholds, the drift time of the most abundant peak is identified at each collision energy. The CIU threshold is defined by the energy at which the drift time of the most intense peak is 2.5% longer than the shortest observed drift time. CID and CIU threshold are screened simultaneously across analyte charge states to identify the charge state at which the CID and CIU thresholds converge to the same energy, or invert when the CID threshold occurs at a lower energy than the CIU threshold.

#### **4.2.3 Corona Discharge Charge Reduction**

A CDP for performing gas-phase ion-ion charge reduction was constructed based on a previously described design.<sup>31</sup> Briefly, a steel tube with a plastic cuvette attached to one end was mounted onto the nESI source housing in-line with the sampling cone, where the cuvette end is nearest the cone. Mounted to the open end of the cuvette is a grounded 0.5 mm thick stainless steel plate with a 1.5 mm aperture. Contained in the steel tube is a PTFE tube (0.030 inch i.d., 1/16 inch o.d.; Fisher Scientific) containing a 0.368 mm diameter platinum wire (Fisher) with one end ground to a fine point. The fine-point end of the platinum wire is positioned in a point-to-plane geometry with the stainless steel plate at a distance of 1.5-2.5 mm. The other end of the platinum wire is connected to a negative high-voltage power supply (Stanford Research Systems,

Sunnyvale, CA) through a 25 M $\Omega$  resistor (Newark Ohmite, Chicago, IL). Nitrogen gas is teed into the PTFE tubing through a PEEK tee (Fisher). The external surface of the stainless steel plate was positioned approximately 1.5 cm from the sampling cone. Gas pressure and applied voltages were varied between 60 to 90 psi and -6500 to -8500 V, respectively.

## **4.3 Results and Discussion**

### **4.3.1 CDP-nESI Source Optimization**

Samples containing denatured CytC were used to optimize CDP conditions for maximum charge reduction while maintaining signal intensity. Screened variables include CDP gas pressure, applied voltage, sampling cone voltage and source backing pressure. Representative, optimized MS data from these screens are shown in Figure 4-1. Higher CDP pressures (Figure 4-1a) and voltages (Figure 4-1b) resulted in greater shifts in charge state distributions (CSDs) to lower charge states but at a significant cost to signal intensity, while lower pressures and voltages produce less significant shifts in CSDs with little cost to signal intensity. To balance the shift in CSDs with ion transmission, the gas pressure and applied voltages were optimized to 70 psi and -7250 V, respectively. Lower charge states are characterized by broad MS peaks with higher mass shifts, likely to due to anion attachment from the CDP. To promote collisional cleaning, mild in-source activation was applied by raising the sampling cone voltage and lowering the backing pressure. Higher sampling cone voltages had little effect on signal intensity, and was therefore optimized to the maximum value of 200 V to aid in adduct reduction. Backing pressure (Figure 4-1c) proved to have a significant effect on both the CSD and the level of adduction. For studying intact protein complexes, lower backing pressures had a significant effect on signal intensity, and therefore pressure was optimized at approximately 7 mbar for such larger ions.

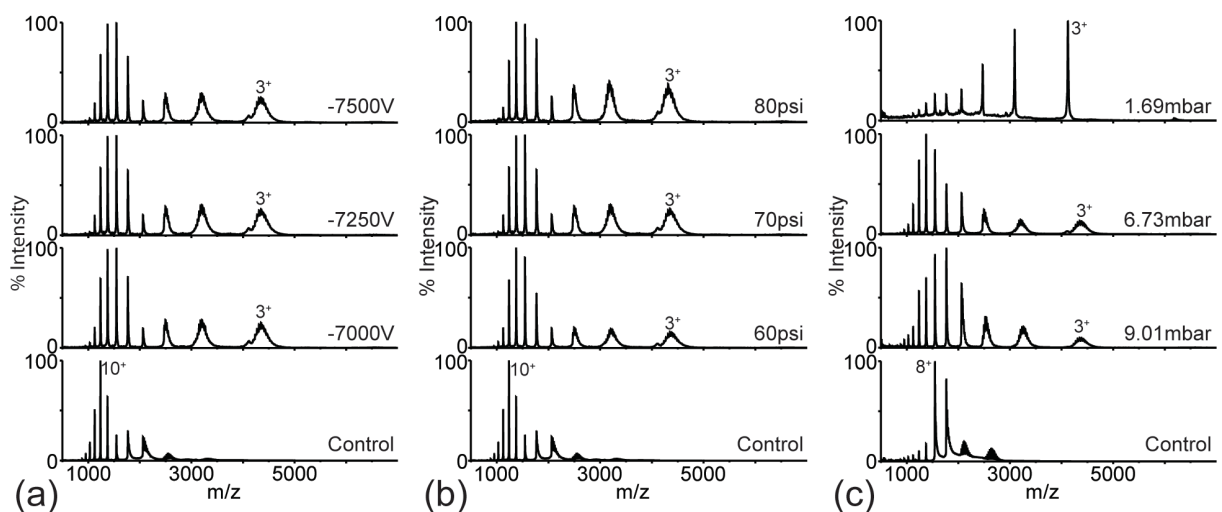


**Figure 4-1.** Mass spectra for denatured cytochrome C under various charge reduction conditions. In order to find the optimal conditions, under various (a) probe voltages with probe pressure held at 70 psi, (b) probe pressures with voltage held at -7250 V, and (c) source backing pressures with the probe voltage and pressure held at -7250 V and 70 psi, respectively. At higher probe voltages and pressures, greater levels of charge reduction are observed with decreased signal intensity. A compromise between charge reduction effectiveness and signal loss is made using the optimized conditions of -7250 V and 70 psi. At lower source backing pressures with sampling cone voltage at 200 V, in-source activation aids in stripping neutral and charge adductions, producing spectra with higher intensity peaks at lower charge states at higher resolution. To reduce structural effects due to in-source activation, the source backing pressure is raised to approximately 7 mbar for all intact protein complex, while maintain a sampling cone voltage of 200V.

Under the conditions described above, the extent of charge reduction for intact protein complexes was assessed. Figure 4-2 presents optimized data from these screens (for additional proteins see Appendix D Figures D-1 to D-6). Under control nESI conditions,  $\beta$ -Lac (Figure 4-2a) the most intense peaks for the monomeric and dimeric form of the protein correspond to the  $7^+$  and  $12^+$  charge states, respectively. Using the optimized charge reduction conditions described above, the most intense peaks for  $\beta$ -Lac shift to the  $5^+$  and  $9^+$  charge states for monomer and dimer, respectively, with the lowest observed charge states being  $4^+$  for both monomer and dimer. In the case of the TPI dimer (Figure 4-2b), the lowest charge state shifts from  $13^+$  to  $8^+$  upon activation of the CDP, while the most intense peak remains constant at the  $15^+$  charge state. Similarly, for the SAP pentamer (Figure 4-2c), while the most intense peak remains the  $24^+$



under both conditions, the lowest observed charge state shifts from  $22^+$  to  $11^+$  when the CDP is activated. Interestingly, we observe a minor increase in the most intense charge state for  $\beta$ -Gal tetramer (Figure 4-2d), which shifts from  $47^+$  to  $49^+$  upon CDP activation, however, the lowest observed charge state decreases as expected, from  $44^+$  to  $36^+$ . While these data demonstrate some differences in the CSD shifts observed, all protein show significant charge reduction with respect to their lowest charge states using the CDP. Structural effects from in-source activation used to aid in charge stripping were monitored through comparison of CCS measurements to traditional native MS conditions (see Appendix D Table D-1). While high charge states did display evidence of unfolding, the low charge state ions of interest did maintained compact conformations throughout the ionization process. Furthermore, our optimized conditions appear effective for different complexes, across a broad range of masses (18.6 to 466 kDa) and assembly stoichiometries (monomers to pentamers).

While TEAA addition in solution was, overall a more effective method of charge reduction when compared with the CDP source used in these studies, we observed two examples where CDP was the more effective approach. For example, we observe the  $11^+$  charge state of the avidin tetramer using TEAA in solution (see Chapter 3), while  $8^+$  ions were generated using the CDP source (see Appendix D Fig. D-1). Similarly, using TEAA to charge reduce aldolase generated  $17^+$  ions (see Chapter 3) but using the CDP generated  $14^+$  ions (see Appendix D Fig. D-2). Despite minor limitation, therefore, we find the CDP approach to be a generally flexible and effective approach toward protein complex charge reduction, which provides a universal approach capable of reducing the charge state of a broad range of assemblies, independent of their stabilities in solution.

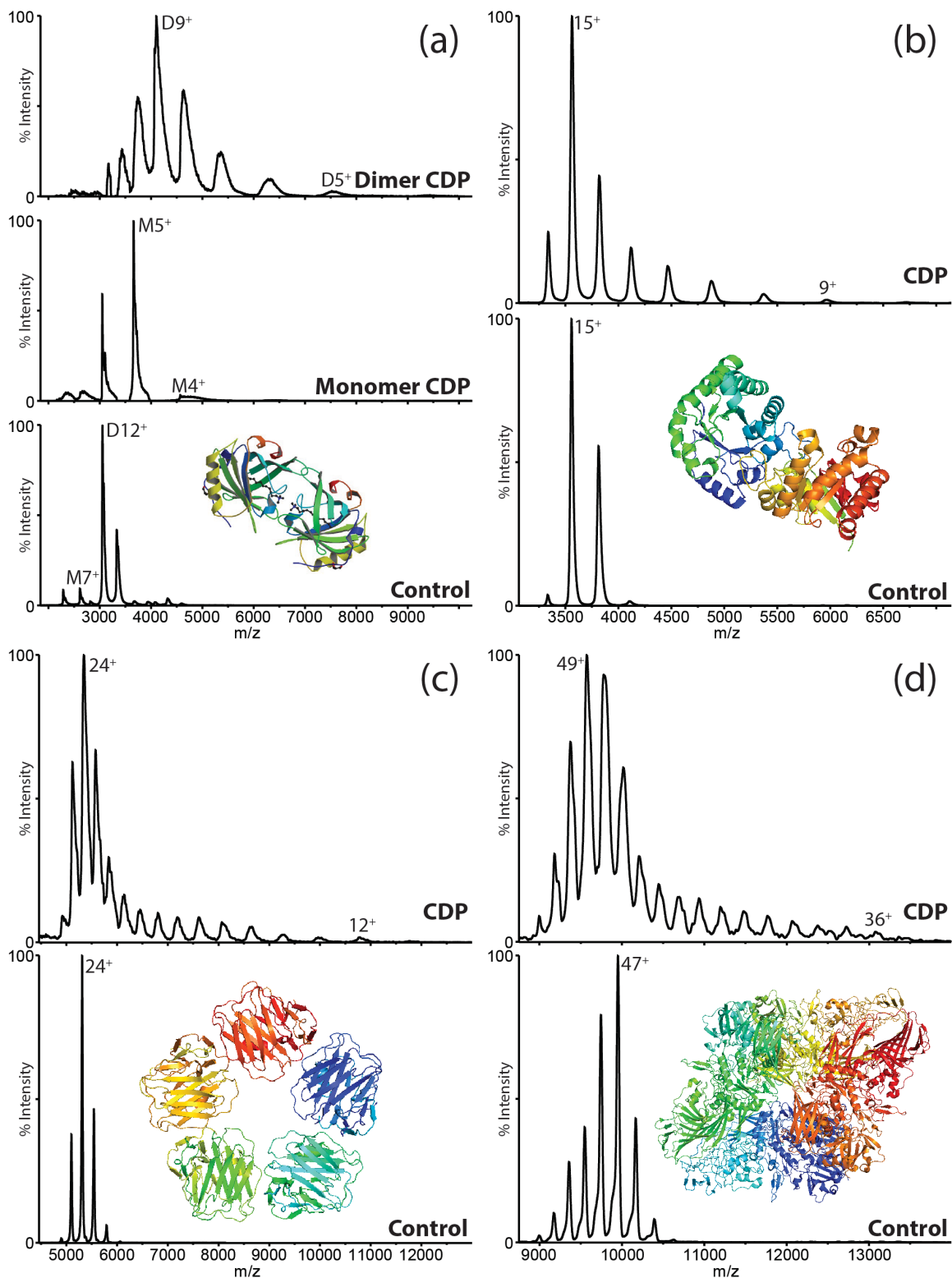


**Figure 4-2.** Mass spectra from (a)  $\beta$ -lactaglobulin, (b) triosephosphate isomerase, (c) serum amyloid P, and (d)  $\beta$ -galactosidase with (top) and without (bottom) corona discharge probe turned on. The corona discharge probe has little effect on the charge state of the most abundant peaks across all complexes. The lowest charge states shift dramatically due to charge reduction, and in the case of SAP, the lowest charge state decreases by ten charges.

### 4.3.2 Detecting the Dissociation of Compact Subunits

We used the optimized CDP conditions described above to screen the CID and CIU responses for a range of protein complexes in order to determine the charge states at which the CID threshold precedes the threshold for CIU. By definition, ions that undergo CID from states that do not unfold must eject product ions that are similarly compact. During the course of our experiments, we assessed the relative stability of ions produced by charge reduction in solution using TEAA against those produced by CDP. In general, we found them to be equivalent, as shown for the 12+ charge state of the avidin tetramer (see Appendix D Fig. D-7).

To rapidly screen the CID and CIU energy landscape for protein complexes as a function of charge state, IM drift time data was monitored to determine the minimum collision energy at which CIU is observed. Based on previous studies, the CIU energy threshold is defined as that energy at which a 2.5% increase in drift time/CCS relative to the smallest recorded value is observed (see Chapter 3). Figure 4-3a shows CCS values extracted from IM drift time data for 7<sup>+</sup>  $\beta$ -Lac dimer ions over an acceleration voltage range of 20 to 200V. We observe protein complex compaction with no observable unfolding over the energy range attainable. From this same data, protein complex CID can be monitored, and is shown in Figure 4-3b. As accelerating voltage used to activate the ions is increased, we observe the relative intensity of the 7<sup>+</sup> dimer ion decrease while signals corresponding to the 3<sup>+</sup> and 4<sup>+</sup> monomer ions increase. At an accelerating voltage of 200 V, where we observe no precursor ion CIU, monomers account for more than 50% of the total ion intensity, indicating the CID threshold energy has been surpassed. Similar data was acquired for a range of protein complexes, including:  $\beta$ -Gal tetramer,  $\beta$ -Lac dimer, ConA tetramer, Hgb dimer and tetramer, SAP pentamer, and TPI dimer.

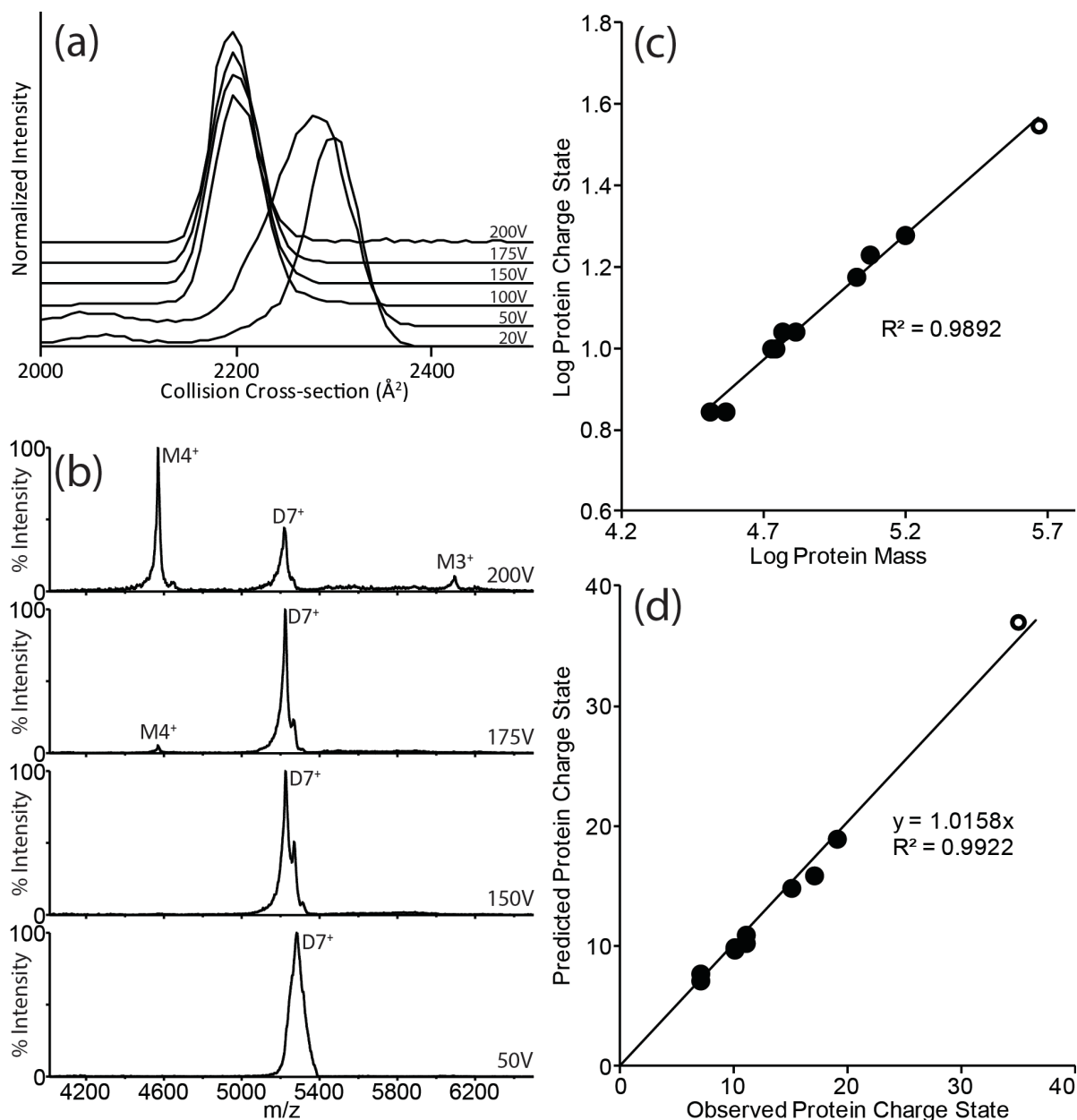


**Figure 4-3.** Representative data for  $\beta$ -lactaglobulin used to determine the charge state where CID and CIU threshold energies converge, and plots of all identified charge states from CID-CIU convergence screen. For  $7^+$   $\beta$ -lactaglobulin the (a) CCS data show compaction consistent with other studies and no unfolding over the full energy range of the instrument, while (b) mass spectra for different collision energies show the onset of monomer dissociation approximately 175 V. At 200 V, the monomer ion intensity accounts for more than 50% of the total ion intensity, indicating that the collision energy has exceeded the CID threshold energy. (c) Plot of *log* Protein Charge State versus *log* Protein Mass showing the linearity of the data for over mass range of 429 kDa ( $\beta$ -Lac (37 kDa) to  $\beta$ -Gal (466 kDa)). (d) Plot of Predicted Protein Charge States generated from equation found in (c) versus Observed Protein Charge States. This plot also shows good linearity between theoretical charge states and measured charge states in a near one-to-one relationship.  $\beta$ -galactosidase data (open circle in c and d) is highlighted since at the CID threshold generated product ions associated with monomer backbone cleavage of up to 300 residues.

These data were combined with the threshold energies previously determined for avidin and aldolase tetramers (Chapter 3) and for tetrameric transthyretin (TTR).<sup>29</sup> The identified charge states required for compact monomer ejection were then plotted as the  $\log(\text{protein charge state})$  against the intact mass of the precursor ion, plotted as  $\log(\text{protein mass})$ , from the expected oligomer mass taken from the protein data bank (PDB), and the resultant plot is shown in Figure 4-3c. This plot is highly linear, with an  $R^2$  of 0.9892. From these data, the charge state required for compact protein monomer ejection from its precursor assembly in the gas phase can be predicted using the following equation:

$$CS = 0.012M^{0.62} \quad (1)$$

where  $M$  is the expected sequence mass of the protein complex. In Figure 4-3d, we use this equation to predict the charge state required for onset of the compact monomer CID pathway, and compare these predicted charge states to those determined experimentally. A one-to-one relationship is observed, exhibiting good agreement to a linear fit ( $R^2 = 0.9922$ ), further supporting the predictive strength of Equation 1.

In order to evaluate the structure-relevant information content of the CID products generated via the compact monomer ejection pathway, we recorded CCS data for monomer product ions generated from the protein complex precursor charge states reported in Figure 4-3c and d. The analysis of this data is shown in Figure 4-4 for the following precursor ions:  $7^+$   $\beta$ -Lac dimer (a),  $10^+$  TPI (b),  $7^+$  Hgb dimer (c – Hgb A and d – Hgb B, open circles),  $11^+$  Hgb tetramer (c and d, closed circles),  $11^+$  avidin (e),  $15^+$  ConA (f),  $17^+$  SAP (g), and  $19^+$  aldolase (h). Dashed lines on each plot indicated the theoretical CCS value predicted from the monomer extracted from the X-ray structure, as described previously.<sup>34</sup> In cases where more symmetric charge partitioning is observed, measured CCS values are smaller than those predicted (see Fig. 4-4a, c,

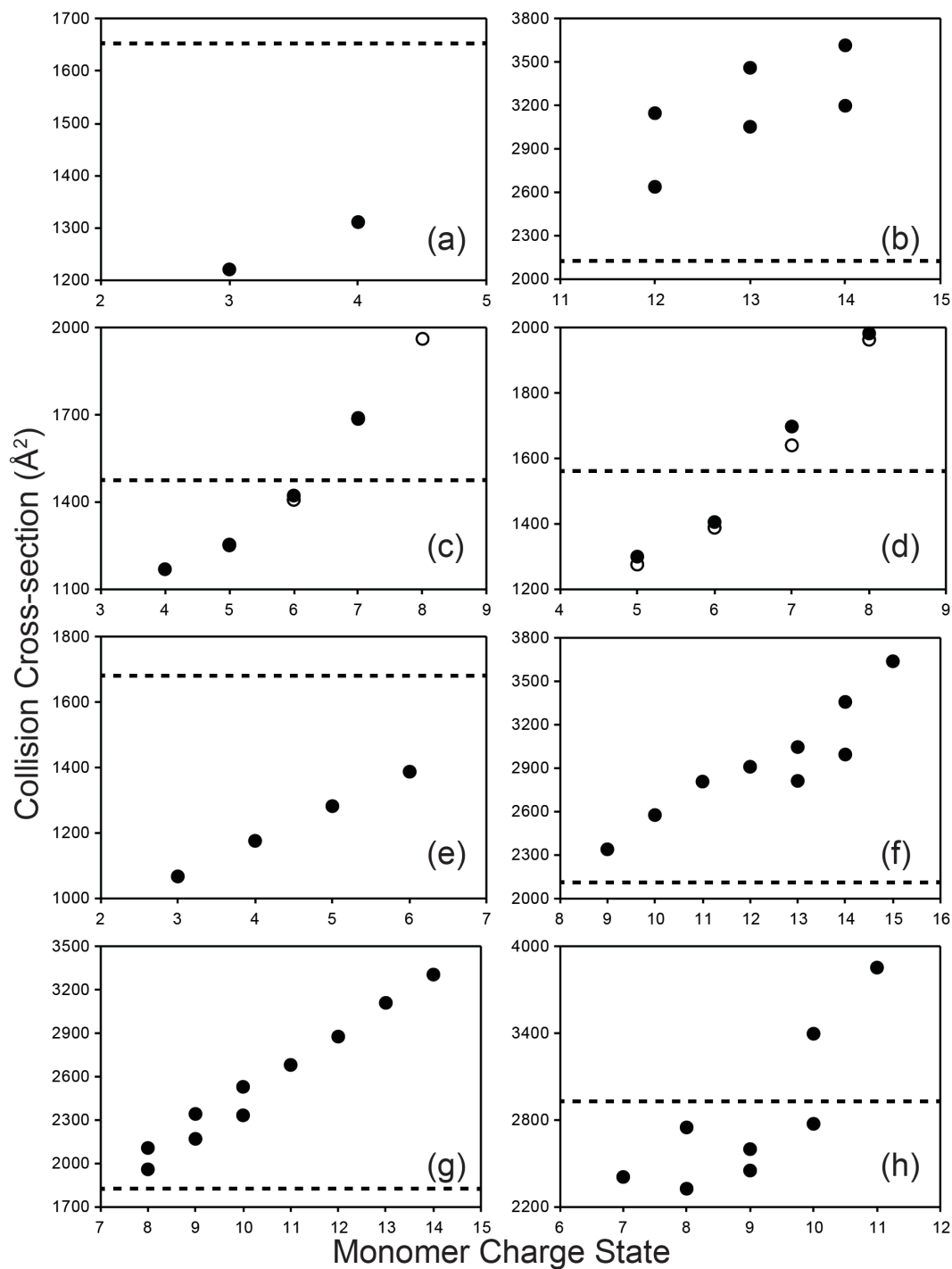


**Figure 4-4.** Monomer collision cross-sections for (a)  $\beta$ -lactaglobulin, (b) triosephosphate isomerase, (c) hemoglobin A, (d) hemoglobin B, (e) avidin, (f) concanavalin A, (g) serum amyloid P, and (h) aldolase. For hemoglobin, monomers were generated from dimers (open circles) and tetramers (closed circles). Dashed lines correspond to predicted CCS values from known oligomer crystal structures. In cases where measured CCS values correlate well with or are much lower than predicted values (a, c, d, e, h), dissociation proceeds via a symmetric charge partitioning pathways. While in cases where measured CCS values are larger than predicted values (b, c, d, f, g), dissociation proceeds via an asymmetric charge partitioning pathways

d, e, and h), however in cases where charge partitioning with highly asymmetric, the measured CCS values are greater than those predicted (see Fig. 4-4b, c, d, f, and g), with the lowest charge state ions usually producing CCS measurements in closest agreement with theory. It is worth noting that, in cases where asymmetric charge partitioning-type CID was observed, the highest product ion charge state often exceeds the parent ion charge, supporting a charge reduction mechanism that includes direct anion attachment to the precursor ion, thus facilitating facile charge stripping following collisional activation.<sup>35</sup>

### 4.3.3 Alternative Dissociation Pathways

Data for  $\beta$ -Gal is highlighted in Figure 4-3c (open circle), as dissociation from compact states did not produce monomer ions. CID of low charge state precursor ions generate product ions that are related to covalent bond fragmentation and peptide product ions.<sup>29</sup> As shown in Figure 4-5a, CID of the  $35^+$  charge state produces product ions with a measured mass of  $34800 \pm 80$  Da that is identified as a species produced from monomer backbone dissociation. Based on mass, we believe this product ion is likely a result of monomer backbone cleavage of around 300 residues (1021 total residues per monomer). In comparison to the dissociation products from  $47^+$   $\beta$ -Gal, shown in Figure 4-5b, we see that higher charge states also follow an alternative dissociation pathway, which has not been previously reported. This native charge state dissociation pathway is characterized by a bimodal product ion distribution where the two species have measured masses of  $32870 \pm 30$  Da (similar to low charge state dissociation) and  $47450 \pm 30$  Da. Relative to the intact monomer mass of  $\beta$ -Gal (117 kDa), we believe these two species to be monomer backbone cleavage products of approximately 300 and 400 residues, respectively. While dissociation of  $\beta$ -Gal does not follow the traditional pathway, the observed low charge state dissociation is consistent with native charge states. This data shows that low-charge state

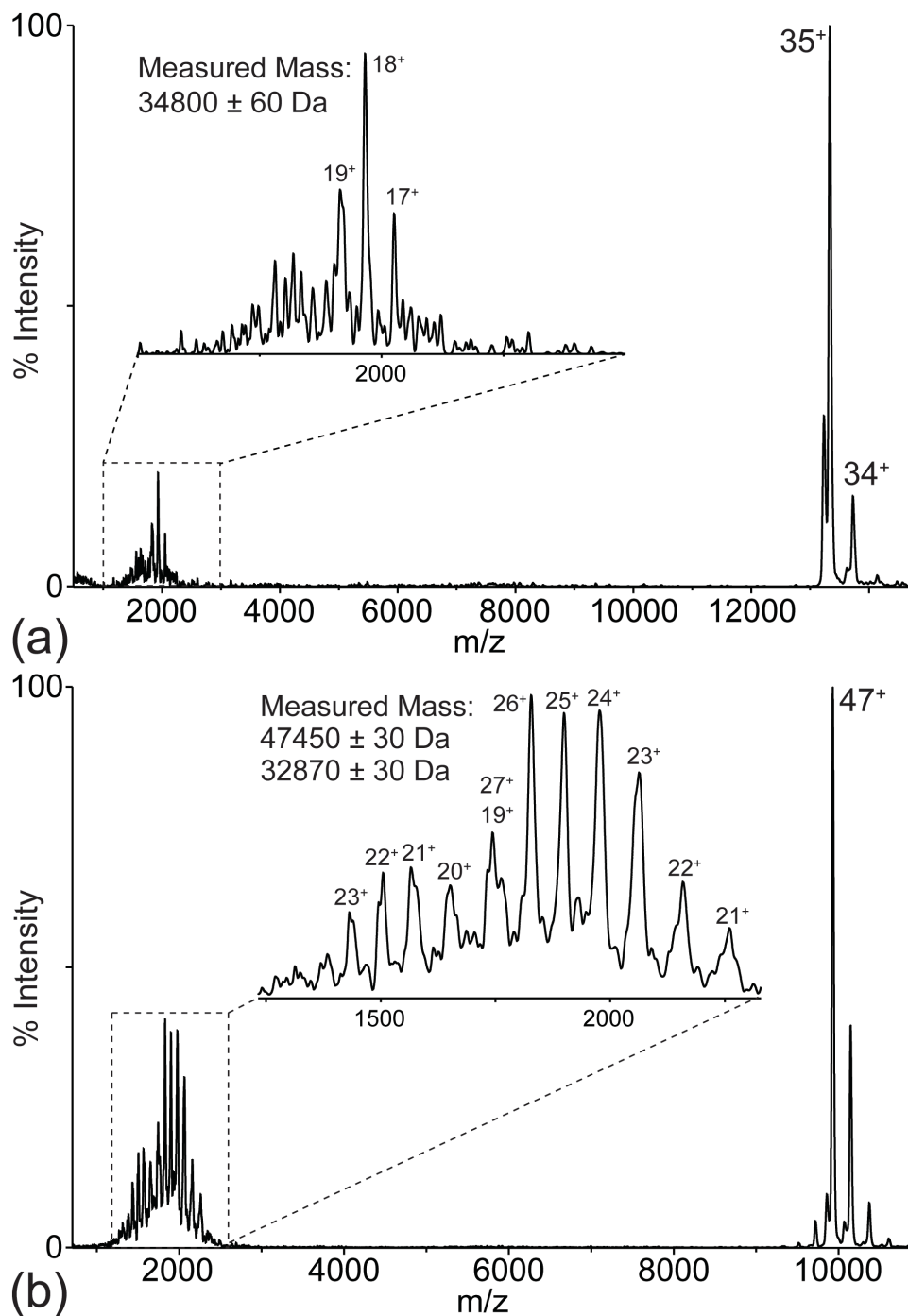


**Figure 4-5.** Mass spectra produced from dissociation of (a)  $35^+$  and (b)  $47^+$   $\beta$ -galactosidase. Insets show blown up regions of product species produced from dissociation. For  $35^+$   $\beta$ -Gal, dissociation produces a single species with a  $17^+$  to  $19^+$  charge distribution which has a measured mass of  $34800 \pm 60$  Da which is identified as product ions associated with monomer backbone cleavage of around 300 residues. Similarly, for  $47^+$   $\beta$ -Gal, dissociation produces a two species with  $19^+$  to  $24^+$  and  $21^+$  to  $27^+$  charge distributions which have measured masses of  $32870 \pm 30$  Da and  $47450 \pm 30$  Da which are identified as product ions associated with monomer backbone cleavage of around 300 and 400 residues, respectively.

dissociation from compact species can still be predicted from Equation 1, even if the pathway is



non-traditional.

However, we did not observe catalase precursor ions of any charge state to release compact monomers. Instead, relatively low charge state precursor ions produced both unfolded monomer ions and heme-related product ions, as shown in the data for the 24<sup>+</sup> tetramer (Figure 4-6a). Similarly produced heme ions generated during CID of Hgb aid in identification of the 616.2 m/z species as the traditional singly charged heme co-factor. However, rather than observe the traditional heme-oxygen peak at 632 m/z, 619.2 m/z and 635.2 m/z peaks corresponding to a 3 Da shift of the heme and heme-O peaks are present. An additional peak, 648.2 m/z, is identified as heme-O<sub>2</sub>. The source of the 3 Da shift remains unknown, but is believed to be due to a relatively high abundance of an unidentified isotope. When compared to 33<sup>+</sup> tetramer (Figure 4-6b), dissociation also produces low-intensity monomer peaks and the same four heme-related peaks. Additionally, a high-intensity distribution of low-mass peaks was observed with a mass of approximately 19.5 kDa, which can be identified as monomer backbone cleavage of approximately one-third the intact monomer mass. A fourth low-intensity, high-mass distribution is also observed with a measured mass of approximately 214 kDa, identified as trimer bound to approximately two-thirds of the monomer. This is direct evidence of backbone cleavage occurring from the intact, unfolded tetramer, not a secondary dissociation event. It is worth noting that catalase and  $\beta$ -Gal are the two largest protein complexes included in this study. As such, caution should be taken when attempting to extrapolate the trends observed here toward large protein systems, especially when such systems contain co-factors and non-protein binding partners.

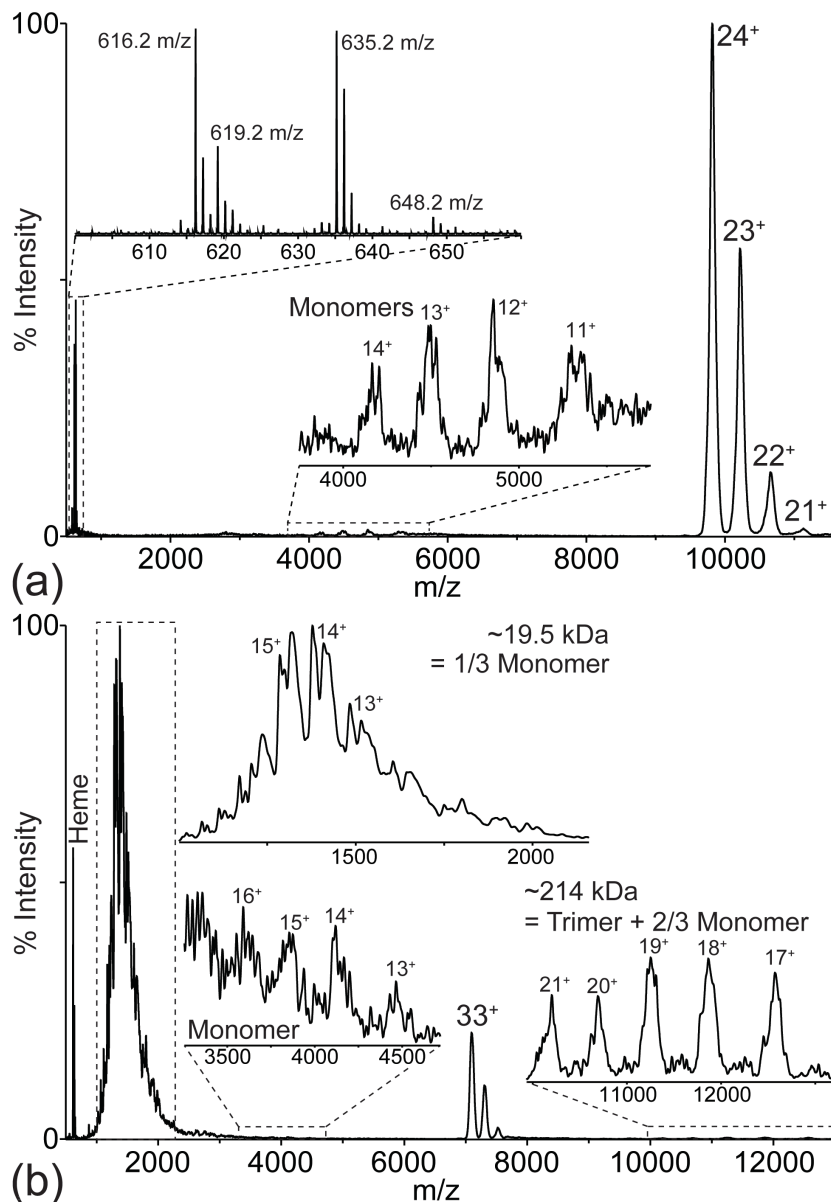


**Figure 6-6.** Mass spectra produced from dissociation of (a) 24<sup>+</sup> and (b) 33<sup>+</sup> catalase. Insets show blown up regions of product species produced from dissociation. For 24<sup>+</sup> catalase, dissociation produces two types of species. Monomers are produced with a charge state distribution ranging from 11<sup>+</sup> to 14<sup>+</sup>. A second set of peaks in the low mass-to-charge region is observed with m/z values of 616.2 m/z, 619.2 m/z, 635.2 m/z, and 648.2 m/z. The 616.2 m/z species is identified as the singly charged heme co-factor. 619.2 m/z and 635.2 m/z peaks correspond to a 3 Da shift of traditional heme and heme-O peaks, while the 648.2 m/z peak can be identified as heme-O<sub>2</sub>. The source of the 3 Da shift remains unknown. For 33<sup>+</sup> catalase, in addition to the same heme-associated peaks and low-intensity monomer peaks (with a charge state distribution ranging from 13<sup>+</sup> to 16<sup>+</sup>), there are two additional distributions with charge distributions ranging from 13<sup>+</sup> to 15<sup>+</sup> and 17<sup>+</sup> to 21<sup>+</sup>, which have measured masses of approximately 19.5 kDa and 214 kDa, respectively. The former distribution is identified as product ions associated with backbone cleavage of approximately one-third of the monomer while the latter distribution is identified as the complementary product ions, trimer bound to two-thirds of the monomer.

## 4.4 Conclusions

Here, we have evaluated a CDP device as an effective method for generating lower charge states across a broad range of intact protein complexes under equivalent conditions. Following a detailed evaluation of the operation of the CDP device, we then utilized its ability to quickly produce large numbers of charge reduced protein ion signals to study the consequences of such charge reduced states on the CID pathway of intact protein complex ions. The low charge states produced were screened to identify those charge states for which the dissociation and unfolding threshold energies converge to the same value or invert to produce product ions before the onset of unfolding. The identified charge states show that CID-CIU convergence can be predicted to a high degree of accuracy based on precursor mass alone over a mass range of approximately 429 kDa. The product ions were largely compact, but also included minor products in the forms of unfolded monomers, large peptide fragment ions, and protein co-factor release as a charged product. All of these product ions have been reported previously in the literature from protein complex precursor ions,<sup>29,36</sup> however, the preferential appearance of large protein ions produced from backbone cleavage from both low and native charge state precursor ions of  $\beta$ -Gal and catalase has not, and may pose a limitation for charge reduction protocols that seek compact protein product ions exclusively if other such dissociation pathways are observed. We also observe enhanced charge stripping following the collisional activation of charge reduced protein complex ions produced using the CDP source, which clearly points to a direct anion attachment mechanism for CDP protein charge reduction.

The work presented here builds substantially on previous data for charge reduced protein complex ions and their CID product ions. The predictive relationship presented in Equation 1 represents a potentially useful framework for high-throughput structural biology protocols,

where monomer size information is often difficult to recover from solution disruption experiments alone. The size information recorded for these monomers suggests a range of values for each monomer ejection, whereas both the average and the lowest CCS values for each dataset may, in many cases, provide a good starting point from which to evaluate the data in the structural biology content for protein complex topology modeling efforts. Future work will be focused on broadening the available dataset of charge reduced protein CID data to include a greater number of large protein complexes that contain non-protein binding components and post-translational modifications, in order to more completely evaluate the breadth of the correlations provided in this report.

#### 4.5 Acknowledgements

Funding for this work was supplied by the National Science Foundation (BTR, CAREER Award, 1253384).

#### 4.6 References

- (1) Jorgensen, W. L. *Science* **2004**, *303*, 1813.
- (2) Csermely, P.; Korcsmáros, T.; Kiss, H. J. M.; London, G.; Nussinov, R. *Pharmacology & Therapeutics* **2013**, *138*, 333.
- (3) Loo, J. A. *Mass Spectrom. Rev.* **1997**, *16*, 1.
- (4) Hyung, S.-J.; Ruotolo, B. T. *PROTEOMICS* **2012**, *12*, 1547.
- (5) Ruotolo, B. T.; Giles, K.; Campuzano, I.; Sandercock, A. M.; Bateman, R. H.; Robinson, C. V. *Science* **2005**, *310*, 1658.
- (6) Kanu, A. B.; Dwivedi, P.; Tam, M.; Matz, L.; Hill, H. H. *J. Mass Spectrom.* **2008**, *43*, 1.
- (7) Jin Lee, Y. *Molecular BioSystems* **2008**, *4*, 816.
- (8) Leitner, A.; Walzthoeni, T.; Kahraman, A.; Herzog, F.; Rinner, O.; Beck, M.; Aebersold, R. *Mol. Cell. Proteomics* **2010**, *9*, 1634.
- (9) Englander, S. W. *J. Am. Soc. Mass Spectrom.* **2006**, *17*, 1481.
- (10) Engen, J. R. *Anal. Chem.* **2009**, *81*, 7870.
- (11) Kaltashov, I. A.; Bobst, C. E.; Abzalimov, R. R. *Anal. Chem.* **2009**, *81*, 7892.
- (12) Wilm, M.; Mann, M. *Anal. Chem.* **1996**, *68*, 1.
- (13) Ruotolo, B. T.; Robinson, C. V. *Curr. Opin. Chem. Biol.* **2006**, *10*, 402.
- (14) Leary, J.; Schenauer, M.; Stefanescu, R.; Andaya, A.; Ruotolo, B.; Robinson, C.; Thalassinou, K.; Scrivens, J.; Sokabe, M.; Hershey, J. *J. Am. Soc. Mass Spectrom.* **2009**, *20*, 1699.

- (15) Hall, Z.; Politis, A.; Robinson, Carol V. *Structure* **2012**, *20*, 1596.
- (16) Politis, A.; Park, A. Y.; Hyung, S. J.; Barsky, D.; Ruotolo, B. T.; Robinson, C. V. *PLoS One* **2010**, *5*.
- (17) Pukala, T. L.; Ruotolo, B. T.; Zhou, M.; Politis, A.; Stefanescu, R.; Leary, J. A.; Robinson, C. V. *Structure* **2009**, *17*, 1235.
- (18) Zhong, Y.; Feng, J.; Ruotolo, B. T. *Anal. Chem.* **2013**, *85*, 11360.
- (19) Zhong, Y.; Hyung, S.-J.; Ruotolo, B. T. *Expert Rev. Proteomics* **2012**, *9*, 47.
- (20) Hernández, H.; Dziembowski, A.; Taverner, T.; Séraphin, B.; Robinson, C. V. *EMBO reports* **2006**, *7*, 605.
- (21) Levy, E. D.; Erba, E. B.; Robinson, C. V.; Teichmann, S. A. *Nature* **2008**, *453*, 1262.
- (22) Zhou, M.; Sandercock, A. M.; Fraser, C. S.; Ridlova, G.; Stephens, E.; Schenauer, M. R.; Yokoi-Fong, T.; Barsky, D.; Leary, J. A.; Hershey, J. W.; Doudna, J. A.; Robinson, C. V. *Proc. Natl. Acad. Sci. U. S. A.* **2008**, *105*, 18139.
- (23) Aquilina, J. A. *Proteins: Structure, Function, and Bioinformatics* **2009**, *75*, 478.
- (24) Zhou, M.; Dagan, S.; Wysocki, V. H. *Angew. Chem. Int. Ed.* **2012**, *51*, 4336.
- (25) Jurchen, J. C.; Garcia, D. E.; Williams, E. R. *J. Am. Soc. Mass Spectrom.* **2004**, *15*, 1408.
- (26) Jurchen, J. C.; Williams, E. R. *J. Am. Chem. Soc.* **2003**, *125*, 2817.
- (27) Ruotolo, B. T.; Hyung, S.-J.; Robinson, P. M.; Giles, K.; Bateman, R. H.; Robinson, C. V. *Angew. Chem. Int. Ed.* **2007**, *46*, 8001.
- (28) Pagel, K.; Hyung, S. J.; Ruotolo, B. T.; Robinson, C. V. *Anal. Chem.* **2010**, *82*, 5363.
- (29) Bornschein, R. E.; Hyung, S.-J.; Ruotolo, B. T. *J. Am. Soc. Mass Spectrom.* **2011**, *22*, 1690.
- (30) Campuzano, I. G.; Schnier, P. *Int. J. Ion Mobil. Spec.* **2013**, *16*, 51.
- (31) Ruotolo, B. T.; Benesch, J. L. P.; Sandercock, A. M.; Hyung, S. J.; Robinson, C. V. *Nat. Protoc.* **2008**, *3*, 1139.
- (32) Bush, M. F.; Hall, Z.; Giles, K.; Hoyes, J.; Robinson, C. V.; Ruotolo, B. T. *Anal. Chem.* **2010**, *82*, 9557.
- (33) Benesch, J. L. P.; Ruotolo, B. T. *Current Opinion in Structural Biology* **2011**, *21*, 641.
- (34) McLuckey, S. A.; Stephenson, J. L. *Mass Spectrom. Rev.* **1998**, *17*, 369.
- (35) Versluis, C.; Heck, A. J. R. *Int. J. Mass Spectrom.* **2001**, *210–211*, 637.

## **Chapter 5. Conclusions and Future Directions**

### **5.1 Conclusions**

IM-MS as a structural biology tool has proven its usefulness for assessing multiprotein complex topologies, and when incorporated with complementary datasets and modeling has the potential to generate model structures at the atomic level.<sup>1-5</sup> However, in order to fully utilize IM-MS, complexes, subcomplexes, and individual subunits must be measured with retained native-like conformations in the gas phase, with the greatest challenge being the study of subunits and subcomplexes. Current methods for generating subunits and subcomplexes in solution require extensive screening of various solvent conditions in order to disrupt the complex while retaining substructural information.<sup>6</sup> Alternatively, gas-phase dissociation using CID of charge reduced protein complexes has demonstrated that compact subunit conformations can be retained,<sup>7</sup> however, altering solution conditions runs the risk of altering complex structure before entering the gas phase, and the mechanism for compact dissociation is not fully understood.

Here we have demonstrated that using gas-phase ion-neutral chemistry compact native-like conformations can be retained in the gas phase (Chapter 2). Furthermore, this method has demonstrated the ability to charge reduce species that would otherwise be too fragile to charge reduce using even the gentlest solution based charge reduction conditions (Appendix A). Therefore, gas-phase charge reduction approaches have demonstrated an ability to preserve gas-phase structures by minimizing analyte interactions with charge reducing agents and maintaining optimal solution conditions for native MS.

By studying the CID pathway of charge reduced states of aldolase and avidin using altered buffer conditions, we have discovered both species undergo structural rearrangements in the gas phase (Chapter 3). Aldolase undergoes a compaction of the tetramer before dissociation, consistent with other charge reduced species.<sup>8</sup> While avidin also undergo compaction, it is not observed by IM-MS but through compacted product monomers, with collision cross-sections much smaller than the theoretical monomer size calculated from the crystal structure. These latter observations demonstrate evidence of structural rearrangement during dissociation since monomer CCS values decrease while the tetramer CCS remains constant. Additional evidence of a structural rearrangement is found in the avidin product trimer CCS values, which are also much smaller than the theoretical size from a scaled projection approximation.

A corona discharge probe similar to the one built by Campuzano and Schnier<sup>9</sup> was used to probe charge states across a range of proteins to identify the charge state at which the CID threshold energy is lower than the CIU threshold energy (Chapter 4). The ion-ion gas-phase charge reduction approach here proved to be advantageous since broad CSDs were observed with high levels of charge reduction all under the same charge reduction conditions. It was discovered that the charge state can be predicted by analyte mass through a simple exponential relationship, similar to the relationship of mass to expected charge state from native MS conditions discovered by de la Mora.<sup>10</sup> This relationship is consistent for oligomer protein complexes covering more than a decade of mass space. The ability to predict when dissociation will occur prior to unfolding is essential for using this charge reduced CID pathway as a tool for producing and measuring subunits and subcomplexes from an uncharacterized multiprotein complex in the gas phase for purposes of building model structures; however, using this method as a tool must be done with caution, as experimental evidence has shown both cases where

product monomer ions are much larger and much smaller than predicted crystal structure monomers sizes. We have demonstrated the ability to generate the necessary charge states via two gas-phase charge reduction approaches and we have shown predictability in the charge state at which dissociation and unfolding energies converge, but there is still the question of the methods effect on gas-phase structure. We have observed two distinct pathways in the dissociation of low charge state multiprotein complexes and have been able to model these new gas-phase structures. What we do not understand is why these two proteins behave so differently, the effect is likely due to differences in inter-protein interactions as other variables have been screened (mass, stoichiometry, secondary and tertiary structure). Furthermore, the absence of compaction is the exception, not the rule. Understanding what makes these proteins behave differently is essential for using this method as a tool for structural biology.

## **5.2 Future Directions**

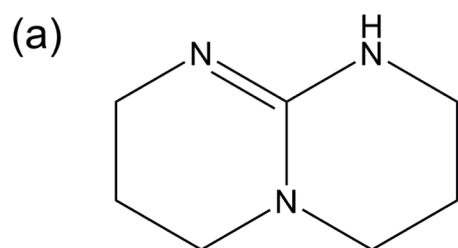
Understanding why some protein complexes behave differently during dissociation than others at low charge states will be a valuable analytical tool, since we will be able to categorize a particular protein based on a single metric. Furthermore, once we can accurately correct for gas-phase compaction of subunits and subcomplexes during dissociation, this technique will be essential for screening the unknown structure of key biological targets. This broadly applicable technique has proven its ability to measure subunit sizes, and in some cases subcomplexes. Additionally, we are not limited to only studying complete multiprotein complex assemblies; the gas-phase charge reduction techniques presented here can easily be applied to studying subcomplexes generated through solution disruption conditions. Essentially, it will act as a complementary technique to other more traditional methods of subunit generation by extending the range of measurable subunits when traditional solution methodologies disrupt native conformations. In



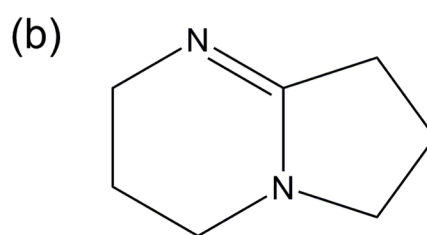
the short-term, some key questions remain in order to optimize charge reduction conditions and correlate experiments to theoretical structures, but the long-term implication of the technique in the field of structural biology is promising. IM-MS is a quickly developing structural biology tool, and with this added technique its range of applications is even greater.

### 5.2.1 Alternative Charge Reducing Agents

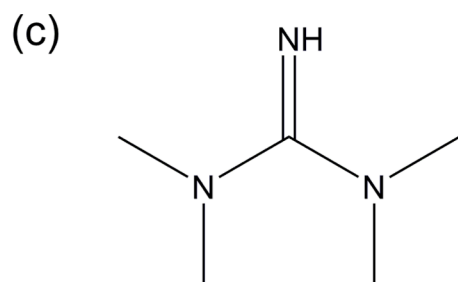
The gas-phase ion-neutral charge reduction presented here has been focused on charge reduction using the charge reducing agent 1,8-diazabicyclo[5.4.0]undec-7-ene (DBU).<sup>11</sup> However, many different charge reducing agents exist that have not been studied in the gas phase.<sup>12,13</sup> The structures and gas-phase basicities of four charge reducing agents are shown in Figure 5-1. While some of these reagents have been tested in the gas phase via introduction from the nebulizing



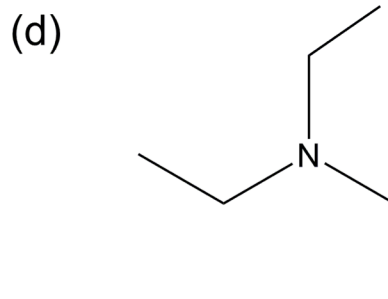
HPP - 1,5,7-triazabicyclo[5.5.0]dec-5-ene  
GB = 1022 kJ/mol



DBN - 1,5-diazabicyclo[4.3.0]non-5-ene  
GB = 1006 kJ/mol



TMG - 1,1,3,3 tetramethyl guanidine  
GB = 982.6 kJ/mol



TEA - triethylamine  
GB = 951 kJ/mol

**Figure 5-1.** Structures and gas-phase basicities for (a) 1,5,7-triazabicyclo[4.4.0]dec-5-ene, (b) 1,5-diazabicyclo[4.3.0]non-5-ene, (c) 1,1,3,3-tetramethyl guanidine, and (d) triethylamine. All four of these basic species have been used, and proven effective, as solution additives for charge reduction, and should be extensively tested as gas-phase ion-neutral charge reduction reagents.

sprayer (DBN and TEA), they have not been screened for structural retention/effects in the gas phase. Of additional interest for introduction via nebulizer spray are various neutral buffers known to cause charge reduction as an alternative solvent,<sup>12,14</sup> as well as strong bases, such as piperidine, which have been shown to be effective gas-phase charge reducing agents when seeded in gases.<sup>15</sup>

### **5.2.2 Redesigned Corona Discharge Probe**

The current design of the corona discharge probe utilizes gas flow parallel to the point-to-plane geometry in order to push generated anions out through an aperture in the plate.<sup>9</sup> A cross-section of a redesigned probe with the point-to-plane geometry perpendicular to the gas-flow is shown in Figure 5-2. This design improves upon the previous design in that the gas flow path is more open allowing for better disbursement of anions. Additionally, the new position of the point-to-plane geometry allows for better control of the point-to-plane distance and allows for the implementation of a Faraday cage, as was used in the earliest experiments with corona discharge charge reduction, to remove electric field effects within the source region.<sup>16,17</sup> Other experiments utilizing corona discharge charge reduction contained within source regions have demonstrated the reduced adduction by seeding the nitrogen gas with methanol.<sup>18</sup> Testing the effect of methanol, and other volatile organic solvents, with both the current CDP design and this new design could be advantageous as extensive adduction was observed throughout these current studies. Using alternative gases may also change the observed charge reduction as different anions may interact differently in the gas phase than current anions generated from nitrogen.<sup>19</sup>

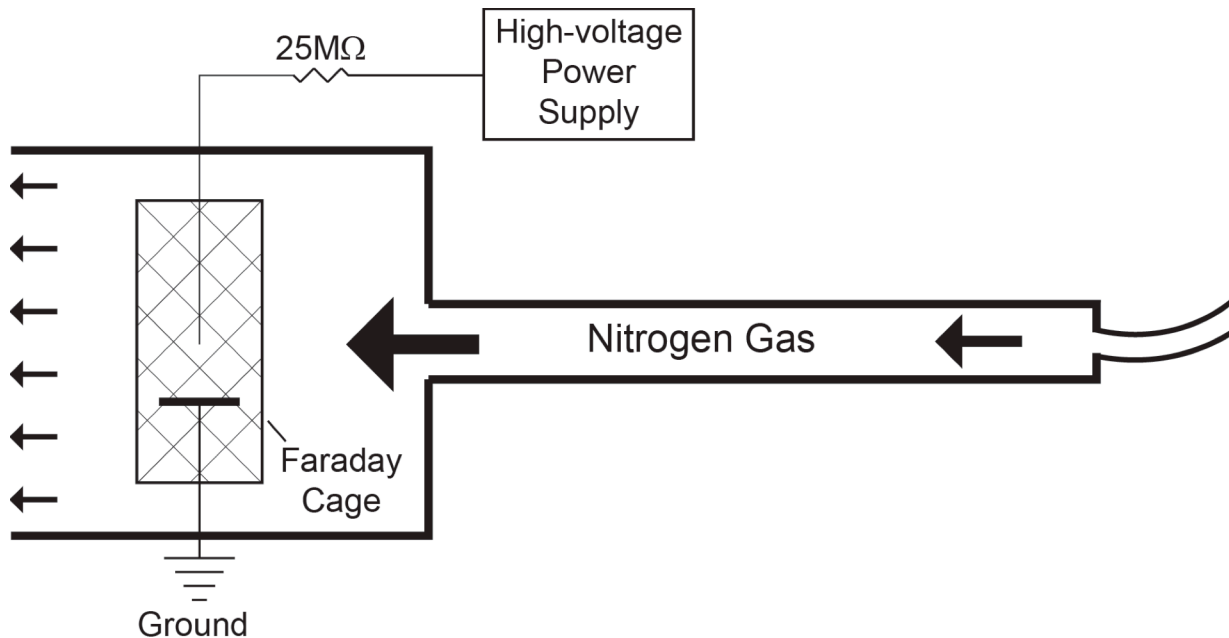


**Figure 5-2.** Cross-section of redesigned corona discharge probe with added Faraday cage and point-to-plane geometry positioned perpendicular to gas flow. Gas carrying anions exit through a larger opening, which will potentially allow for better disbursement of anions. The Faraday cage is employed to remove electric field effects in the source, in order to improve analyte ion transmission. The reorientated point-to-plane geometry also allows for better visual control over the point-to-plane distance.

### 5.2.3 Gas-Phase Supercharging

Ion-neutral charge reduction was performed here to preserve native-like gas-phase conformation.<sup>11</sup> Use of supercharging agents in solution has demonstrated that multiprotein complex structures are disrupted in solution due to these supercharging agents.<sup>20,21</sup> Recently, a gas-phase ion-neutral supercharging approach has been demonstrated by seeding curtain gas with acid vapor.<sup>22</sup> Conventional supercharging agents, such as sulfolane and *m*-nitrobenzyl alcohol (*m*-NBA), can be implemented for gas-phase supercharging through use of the nebulizing sprayer to preserve native-like conformations at high charge states.<sup>23,24</sup> Additionally, the sprayer could be used to introduce low concentration acids from volatile solvents. The desire for generating higher charge states of multiprotein complexes is motivated by the fact that higher

charge states have been observed to produce peptide fragments similar to top-down techniques following the traditional unfolding and dissociation.<sup>25</sup>

### 5.3 References

- (1) Taverner, T.; Hernandez, H.; Sharon, M.; Ruotolo, B. T.; Matak-Vinkovic, D.; Devos, D.; Russell, R. B.; Robinson, C. V. *Accounts Chem. Res.* **2008**, *41*, 617.
- (2) Pukala, T. L.; Ruotolo, B. T.; Zhou, M.; Politis, A.; Stefanescu, R.; Leary, J. A.; Robinson, C. V. *Structure* **2009**, *17*, 1235.
- (3) Politis, A.; Park, A. Y.; Hyung, S. J.; Barsky, D.; Ruotolo, B. T.; Robinson, C. V. *PLoS One* **2010**, *5*.
- (4) Hall, Z.; Politis, A.; Robinson, Carol V. *Structure* **2012**, *20*, 1596.
- (5) Hyung, S.-J.; Ruotolo, B. T. *PROTEOMICS* **2012**, *12*, 1547.
- (6) Zhong, Y.; Feng, J.; Ruotolo, B. T. *Anal. Chem.* **2013**, *85*, 11360.
- (7) Pagel, K.; Hyung, S. J.; Ruotolo, B. T.; Robinson, C. V. *Anal. Chem.* **2010**, *82*, 5363.
- (8) Hall, Z.; Politis, A.; Bush, M. F.; Smith, L. J.; Robinson, C. V. *J. Am. Chem. Soc.* **2012**, *134*, 3429.
- (9) Campuzano, I. G.; Schnier, P. *Int. J. Ion Mobil. Spec.* **2013**, *16*, 51.
- (10) de la Mora, J. F. *Analytica Chimica Acta* **2000**, *406*, 93.
- (11) Bornschein, R. E.; Hyung, S.-J.; Ruotolo, B. T. *J. Am. Soc. Mass Spectrom.* **2011**, *22*, 1690.
- (12) Catalina, M. I.; van den Heuvel, R. H. H.; van Duijn, E.; Heck, A. J. R. *Chem.-Eur. J.* **2005**, *11*, 960.
- (13) Bagal, D.; Zhang, H.; Schnier, P. D. *Anal. Chem.* **2008**, *80*, 2408.
- (14) Zhou, M.; Jones, C. M.; Wysocki, V. H. *Anal. Chem.* **2013**, *85*, 8262.
- (15) Kharlamova, A.; DeMuth, J.; McLuckey, S. *J. Am. Soc. Mass Spectrom.* **2012**, *23*, 88.
- (16) Ebeling, D. D.; Westphall, M. S.; Scalf, M.; Smith, L. M. *Anal Chem* **2000**, *72*, 5158.
- (17) Ebeling, D. D.; Westphall, M. S.; Scalf, M.; Smith, L. M. *Rapid Commun. Mass Spectrom.* **2001**, *15*, 401.
- (18) Frey, B. L.; Lin, Y.; Westphall, M. S.; Smith, L. M. *J. Am. Soc. Mass Spectrom.* **2005**, *16*, 1876.
- (19) Skalny, J. D.; Mikoviny, T.; Matejcik, S.; Mason, N. J. *Int. J. Mass Spectrom.* **2004**, *233*, 317.
- (20) Hogan, C. J., Jr.; Ogorzalek Loo, R. R.; Loo, J. A.; Mora, J. F. d. l. *Phys. Chem. Chem. Phys.* **2010**, *12*, 13476.
- (21) Sterling, H.; Kintzer, A.; Feld, G.; Cassou, C.; Krantz, B.; Williams, E. *J. Am. Soc. Mass Spectrom.* **2012**, *23*, 191.
- (22) Kharlamova, A.; Prentice, B. M.; Huang, T. Y.; McLuckey, S. A. *Anal. Chem.* **2010**, *82*, 7422.
- (23) Iavarone, A. T.; Jurchen, J. C.; Williams, E. R. *Anal. Chem.* **2001**, *73*, 1455.
- (24) Lomeli, S.; Peng, I.; Yin, S.; Ogorzalek Loo, R.; Loo, J. *J. Am. Soc. Mass Spectrom.* **2010**, *21*, 127.

(25) Benesch, J. L. P.; Sobott, F.; Robinson, C. V. *Anal. Chem.* **2003**, *75*, 2208.

## Appendix A: Chapter 2 Supporting Information

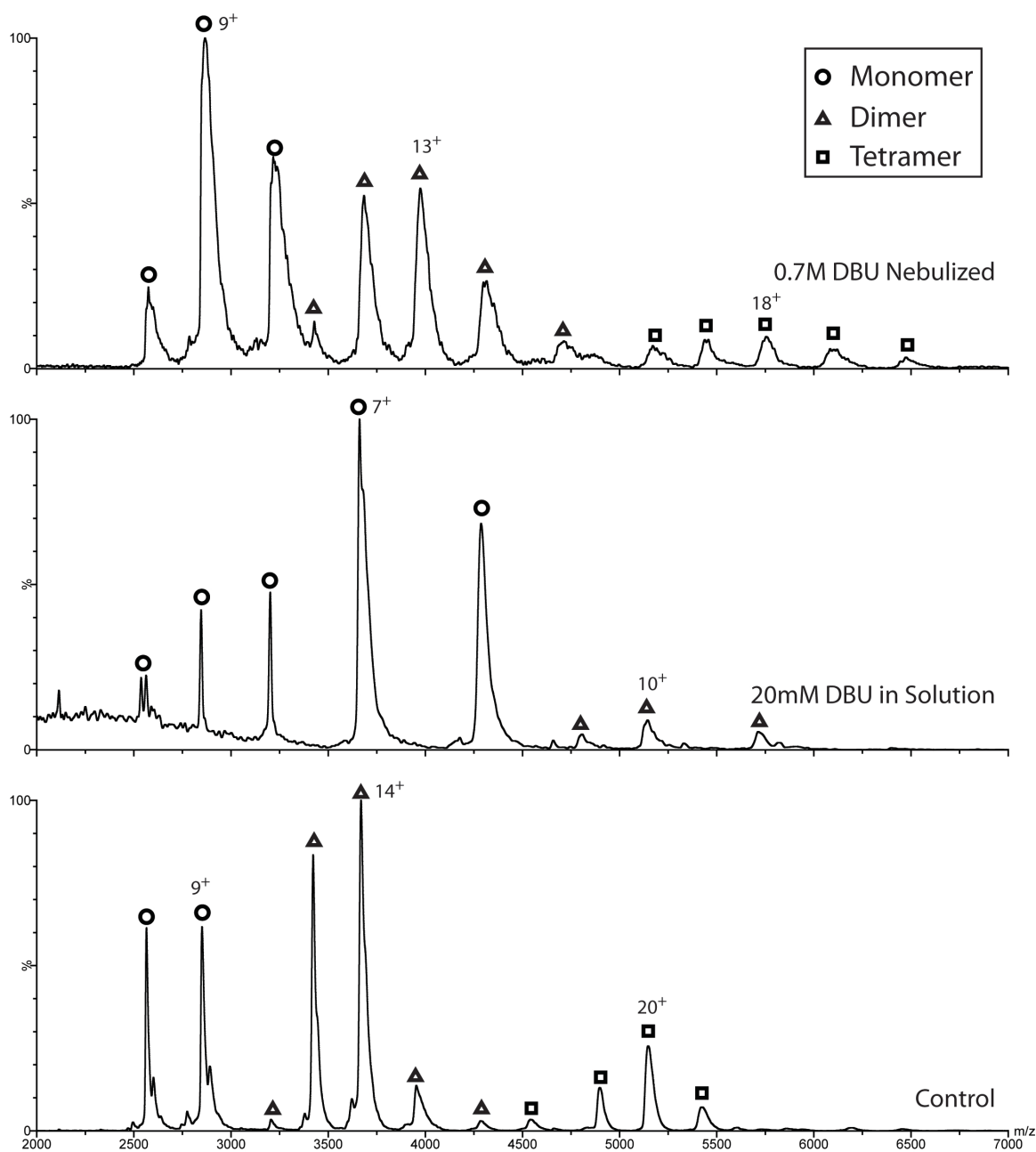


**Figure A-1.** Mass spectra for concanavalin A under control conditions (bottom), under solution additive charge reduction conditions with DBU (middle), and under gas-phase charge reduction conditions with DBU (top). Concanavalin A exits in equilibrium as tetramer ( $\square$ ), dimer ( $\blacktriangle$ ), and monomer ( $\circ$ ). In

solution additive charge reduction, dissociation of the tetramer into dimer and monomer is observed, while with gas-phase charge reduction approaches the tetramer structure is retained.

## **Appendix B: Protocol for Nebulizing Sprayer Operation**

The following section contains detailed information for operation of the nebulizing sprayer for charge reduction.

### **Preparation**

1. Make base solution to desired concentration. From trial and error, a 10% base solution is a good starting concentration as it induces charge reduction, but is not so high where signal will be completely neutralized. Experimental evidence shows that base concentration will determine the level of charge reduction.
2. Base flow rate will be high and droplets will accumulate in the source. Be sure to line bottom of source housing with disposable absorbent material such as paper towel or pigmat.
3. Nebulizer can be positioned orthogonal to source cone, as shown in Figure 2-1, or positioned in-line with source cone, similar to CDP orientation (see Chapter 4). It is important that base is not sprayed directly into the cone. In in-line orientation, sprayer should be aligned off-axis; directing the sprayer down and to the left of the cone orifice has proven effect, to prevent effecting other elements in the source cover as much of the cone and surrounding source block as possible with parafilm. In the orthogonal orientation, the sprayer is mounted on an adjustable stage, ensure position of stage does not allow spray to directly enter the cone.



4. Attach gas line to sprayer. Load 10 mL syringe with prepared base solution. Ensure syringe pump is setup for 10 mL syringe, load syringe, and attach tubing via syringe connector, ensure connector is snug.
5. Begin syringe pump with gas turned off at the flow rate to be used for charge reduction. This is done to load the capillary with base solution, higher flow rates cannot be used since backing pressure at high flow rates will cause syringe to disconnect from tubing.

### **Operation**

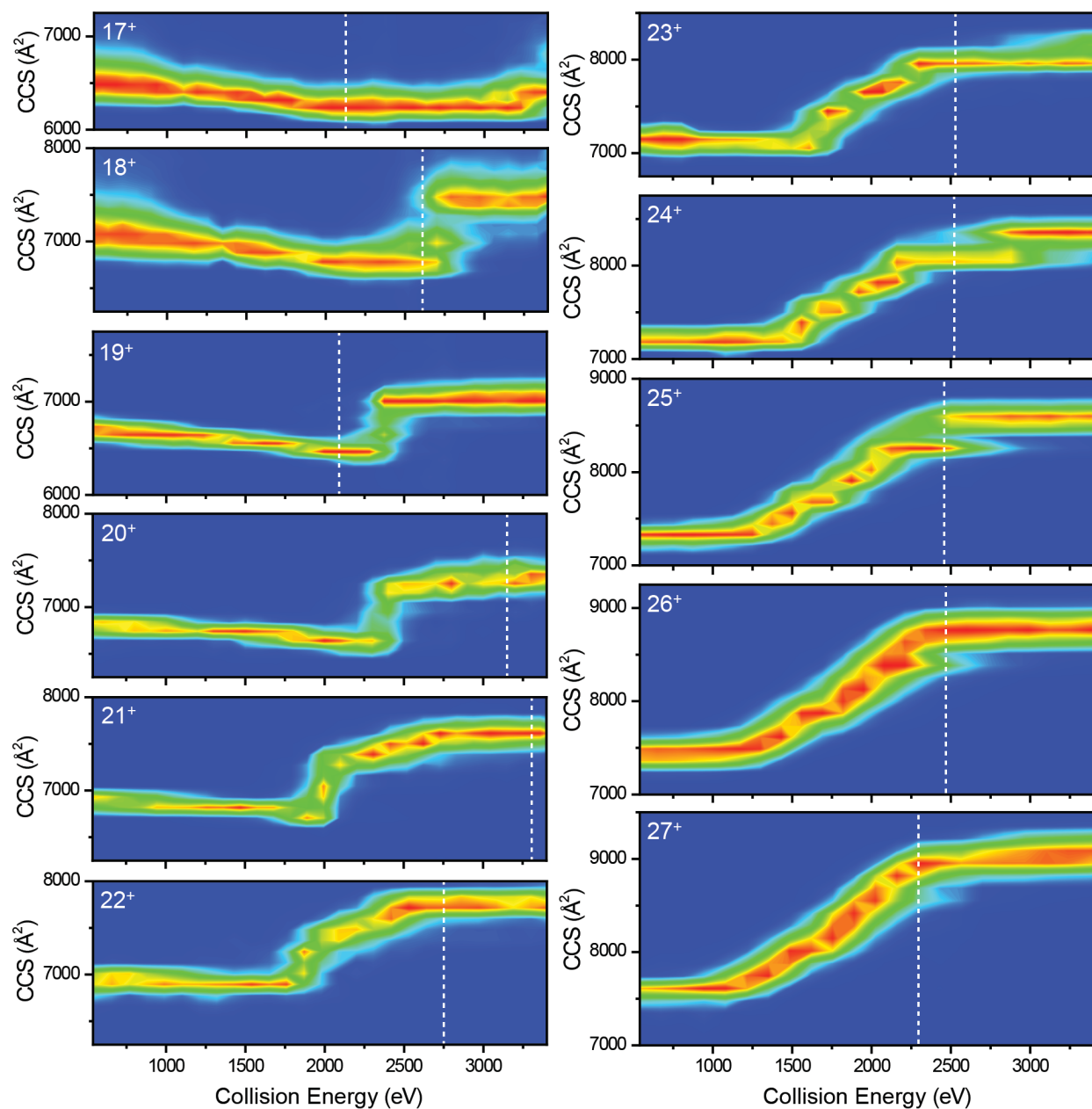
1. Ensure good MS signal before turning on nebulizer.
2. Begin syringe pump and gas flow, typical base flow rates range from 5-25 mL/hr, with 10 mL/hr utilized most often. Gas flow is operated at a pressure ranging from 20-35 psi, with 10 psi utilized when a 10 mL/hr flow rate is used. The gas pressure must be adjusted to ensure nebulization at the selecting flow rate. At higher flow rates, higher gas pressure must be used. This can be determined visually, if gas pressure is too low droplets will form at the end of the capillary.
3. Adjust nebulizer position to ensure nebulized droplets interact with the electrospray plume. If this is not done, base droplets do not interact with charged electrospray droplets and charge reduction is not observed.

### **Clean-up**

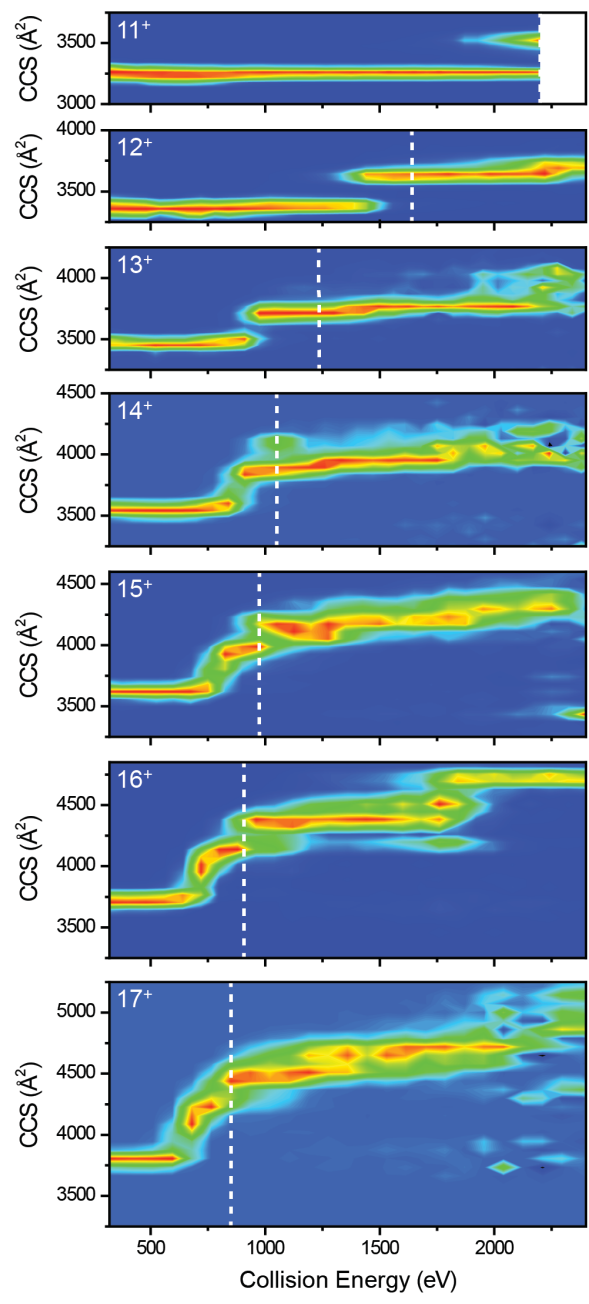
1. Flush syringe and tubing with a 50:50 methanol:water solution by running syringe pump and standard flow rates, again due to high backing pressure at high flow rates. This is critical since the water in the base solution will evaporate leaving concentrated base that will clog the tubing and capillary.

2. The source region must be thoroughly cleaned as any residual base with cause mild charge reduction. Clean the cone following standard protocol using 10% acetic acid, followed by methanol wash. Wipe down any surfaces that may have come into contact with base using methanol:water solution.
3. Dispose of any base contaminated paper towel or pigmats appropriately.

## Appendix C: Chapter 3 Supporting Information

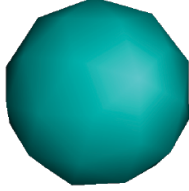
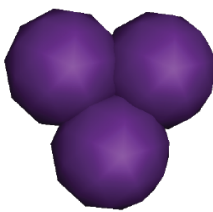
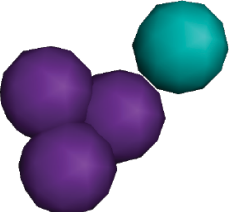
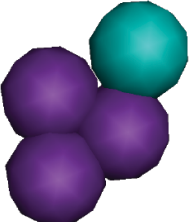


**Figure C-1.** Aldolase collision induced unfolding fingerprints for measured native and charge reduced charge states.



**Figure C-2.** Avidin collision induced unfolding fingerprints for measured native and charge reduced charge states.

**Table C-1.** Coarse grain avidin model structures generated during Monte Carlo search. Measured experimental CCS, calculated model CCS, and calculated spherical overlap are given for each model. A minimum 15% overlap indicates good subunit interaction. Tetramer models shown are the model in best agreement with CCS data and the model with a 15% minimum spherical overlap with a CCS closest to the experimental value.

Structure	Experimental CCS ( $\text{\AA}^2$ )	Model CCS ( $\text{\AA}^2$ )	Spherical Overlap
	1067	1068	---
	2385	2381	22.5%
	3240	3240	2.6%
	3240	3044	19%

## **Appendix D: Chapter 4 Supporting Information**

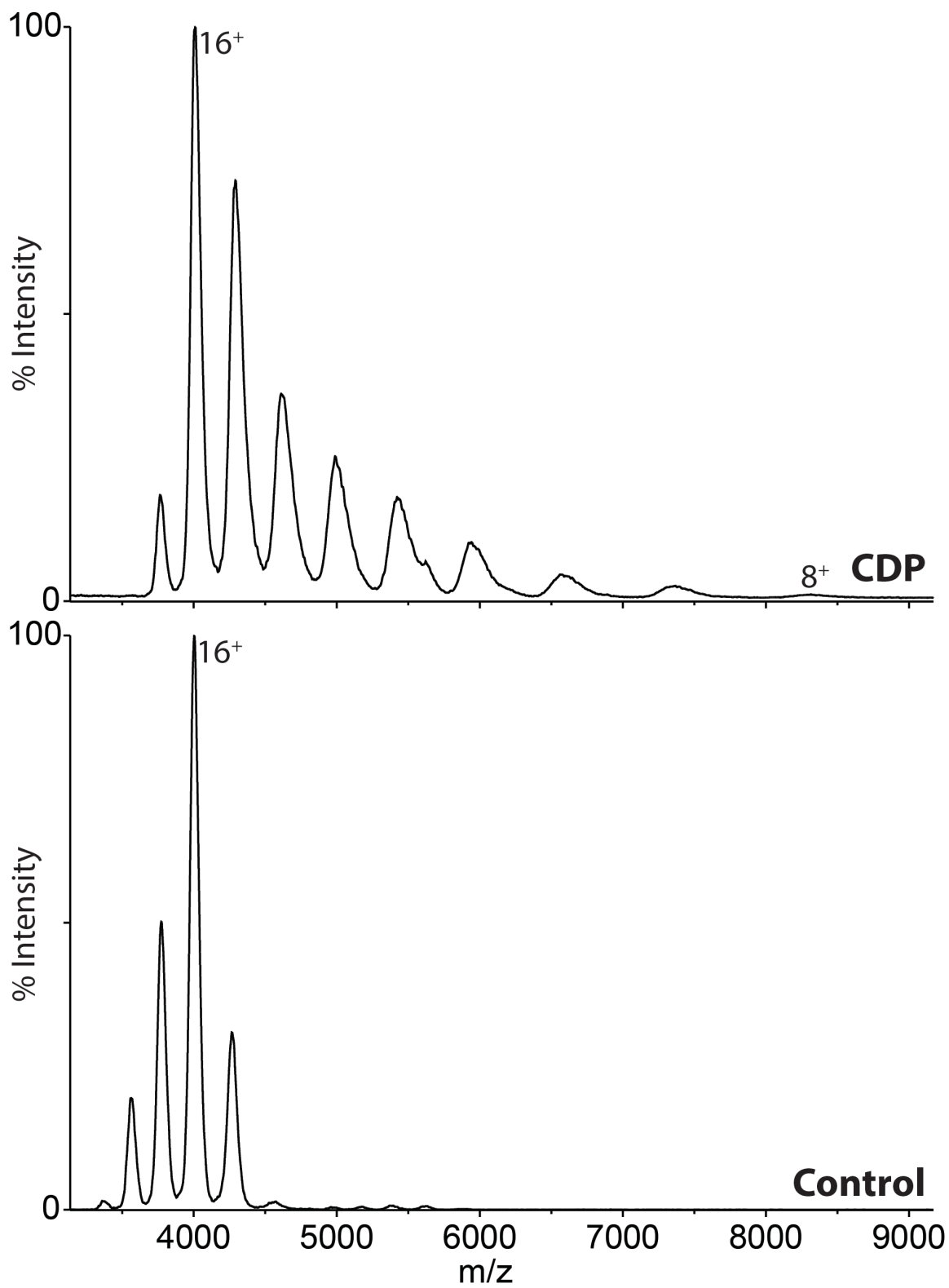


**Figure D-1.** Avidin mass spectra with and without corona discharge charge reduction.

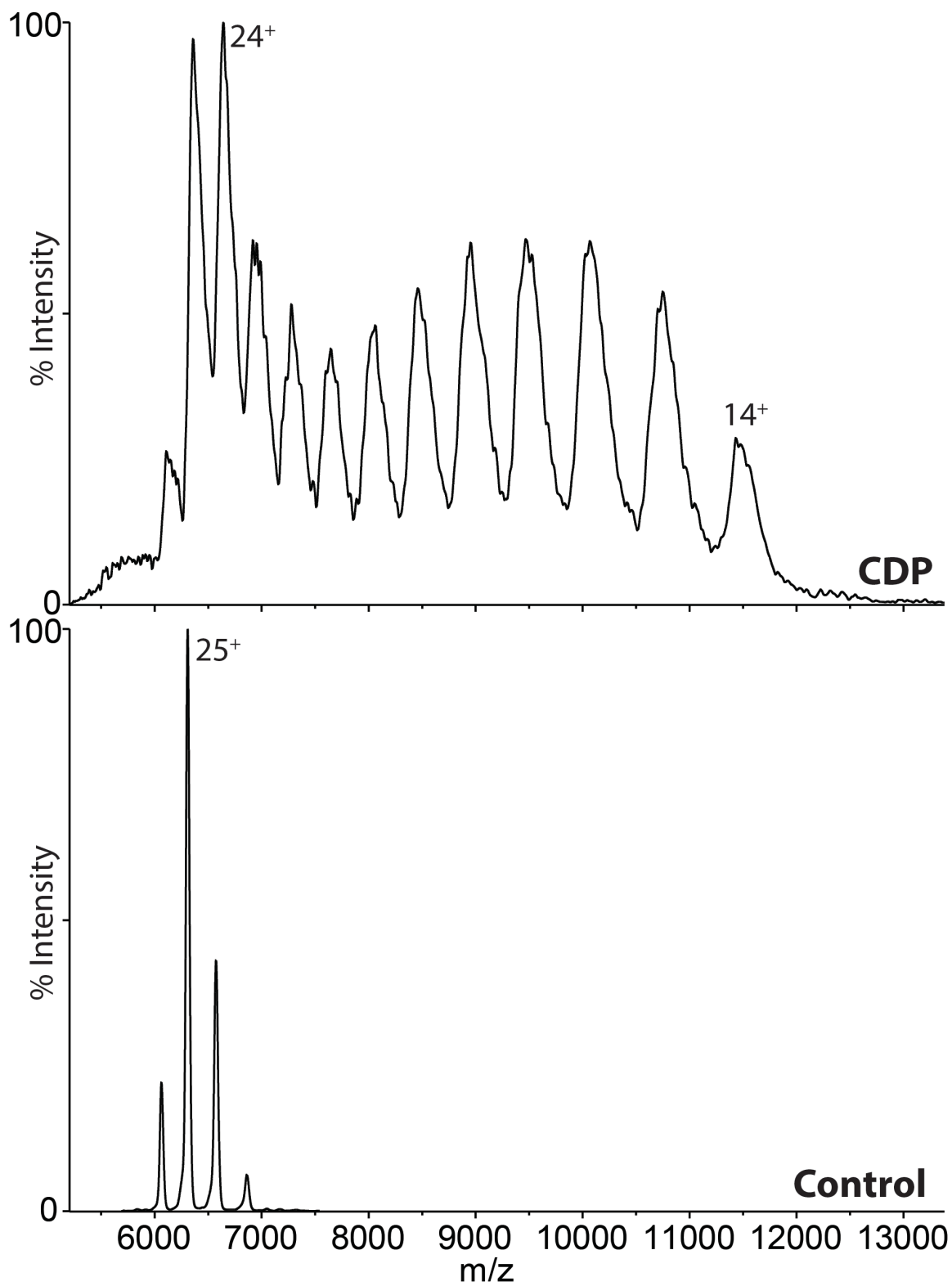


**Figure D-2.** Aldolase mass spectra with and without corona discharge charge reduction.



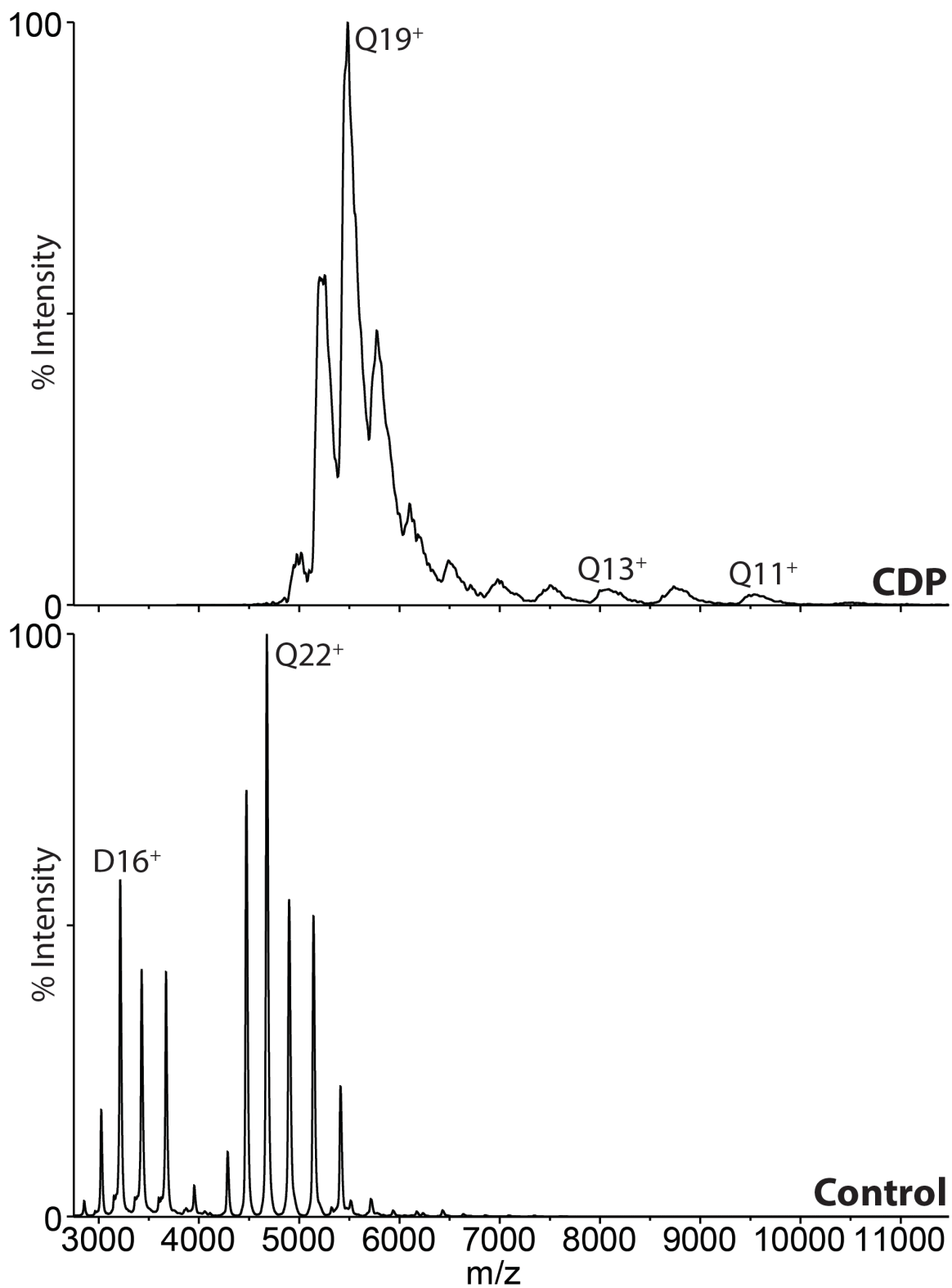


**Figure D-3.** Concanavalin A mass spectra with and without corona discharge charge reduction.

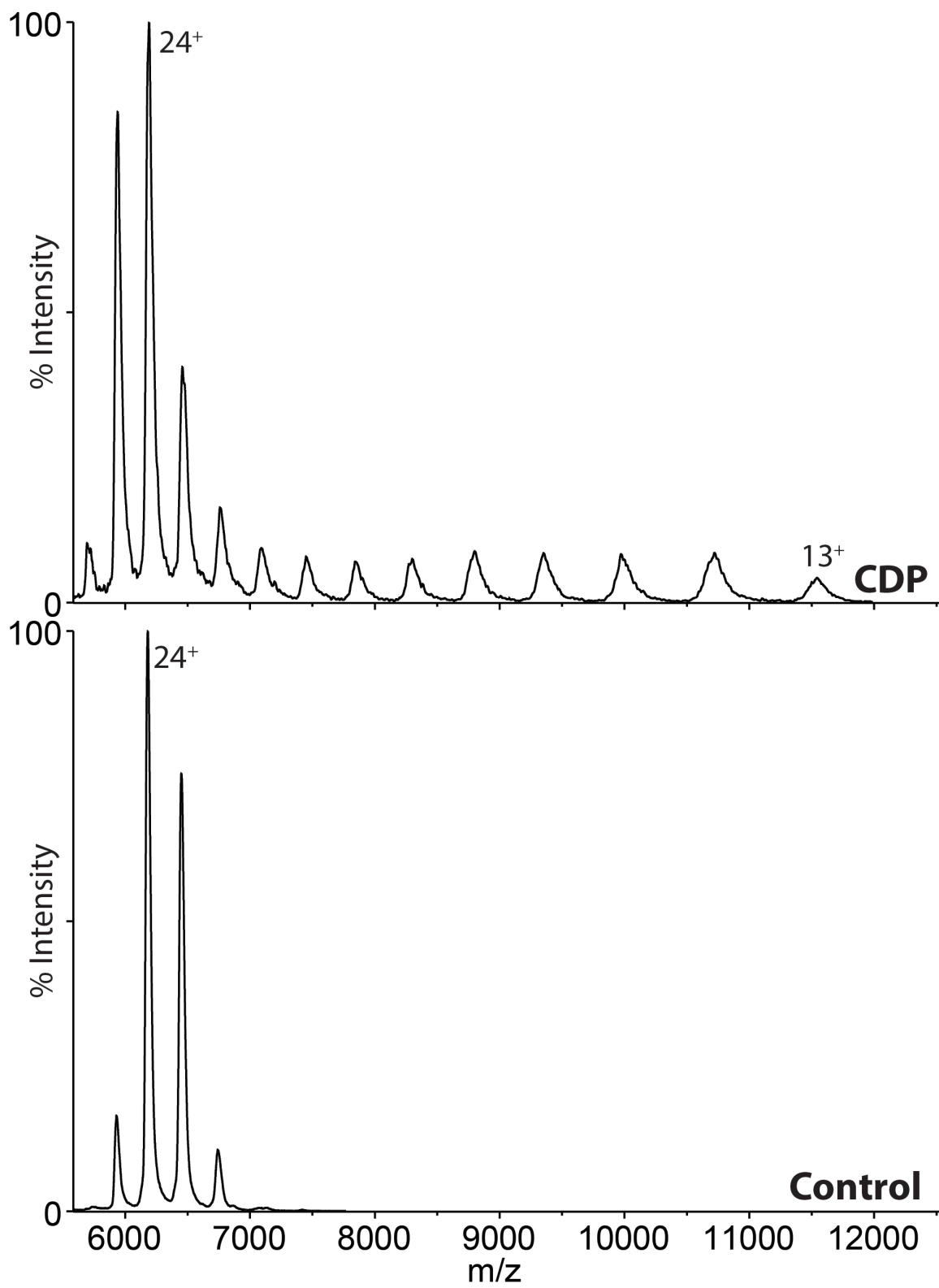


**Figure D-4.** Alcohol dehydrogenase mass spectra with and without corona discharge charge reduction.

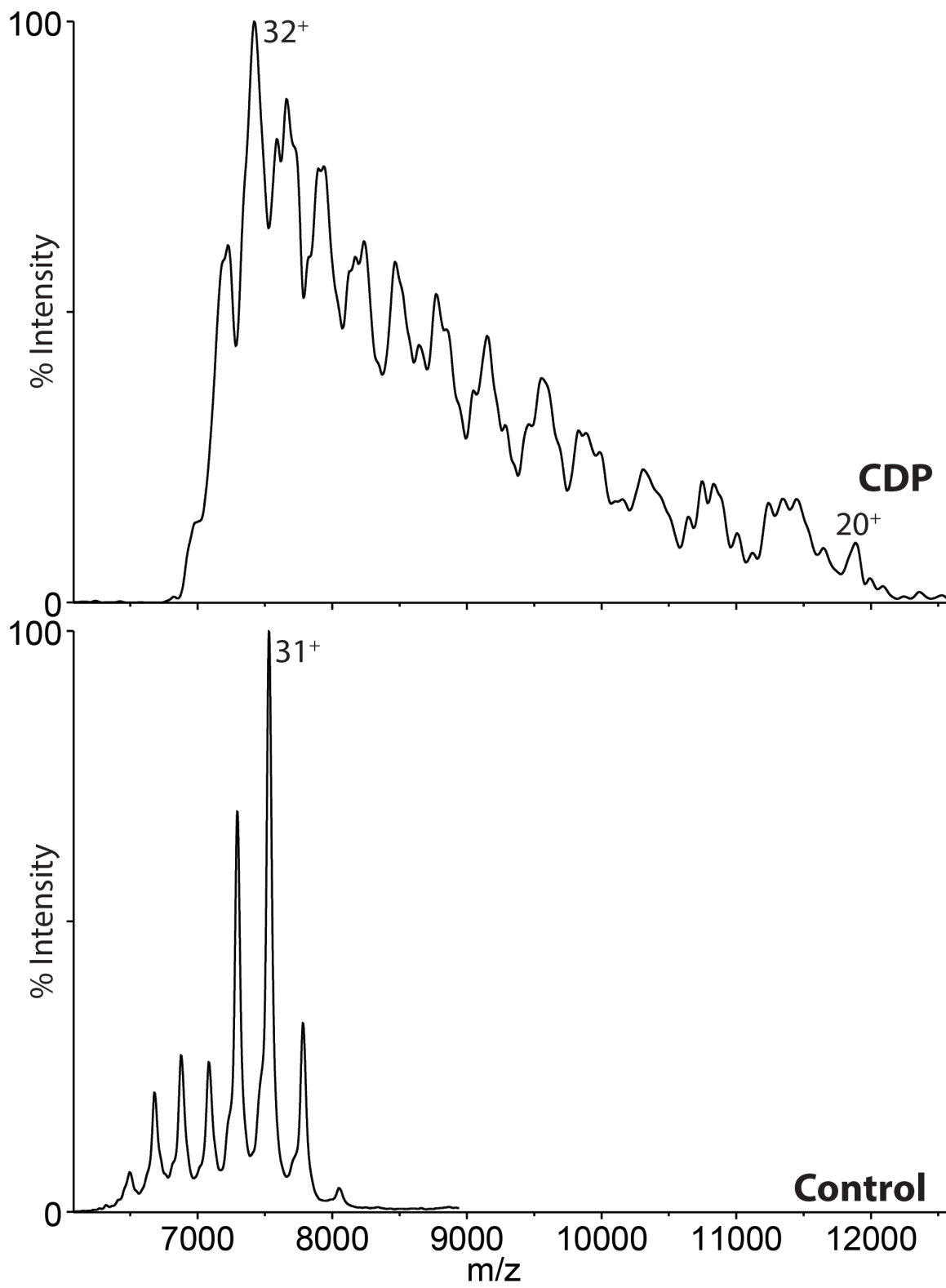


**Figure D-5.** Pyruvate kinase mass spectra with and without corona discharge charge reduction.

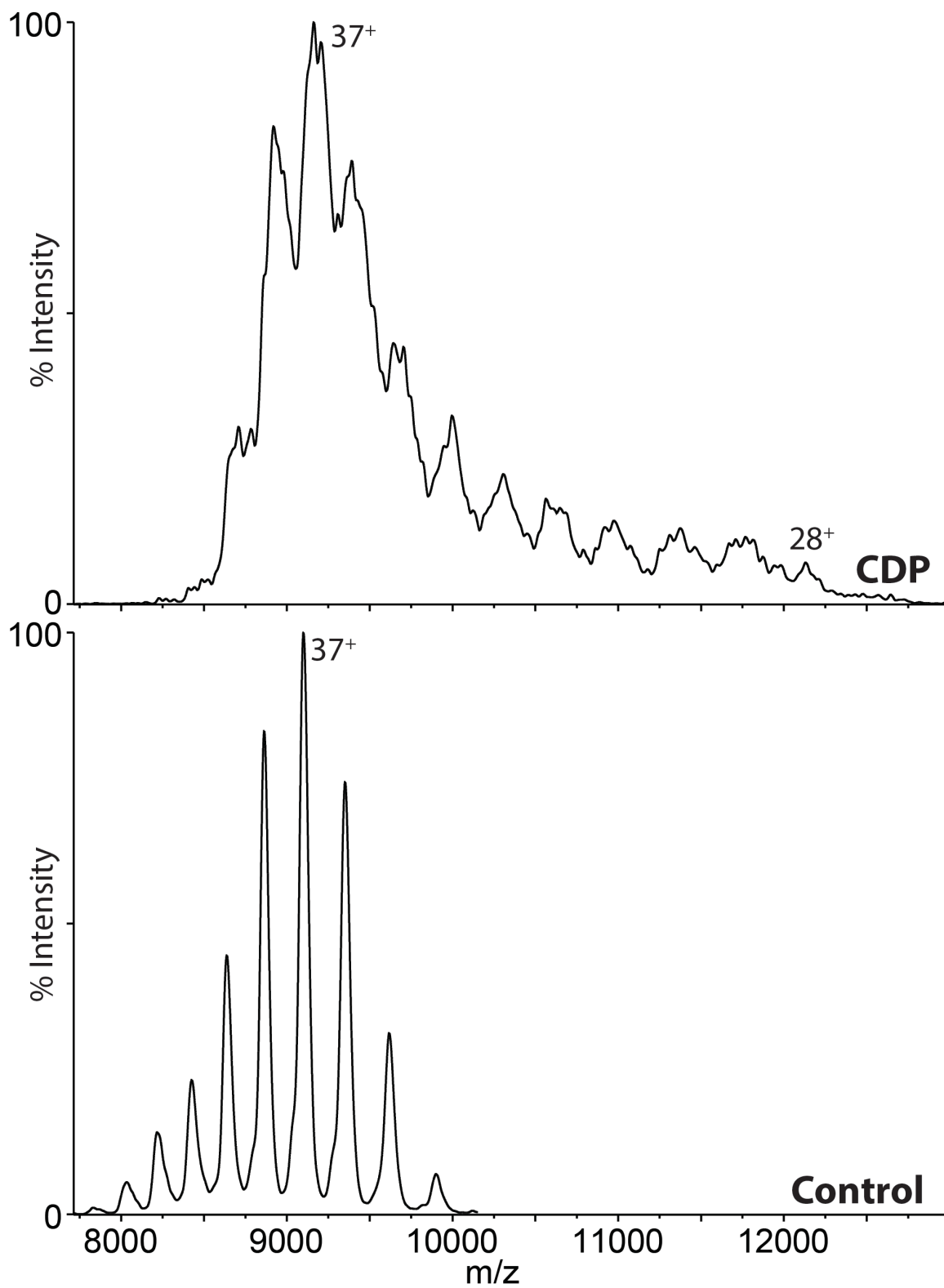


**Figure D-6.** Glutamate dehydrogenase mass spectra with and without corona discharge charge reduction.

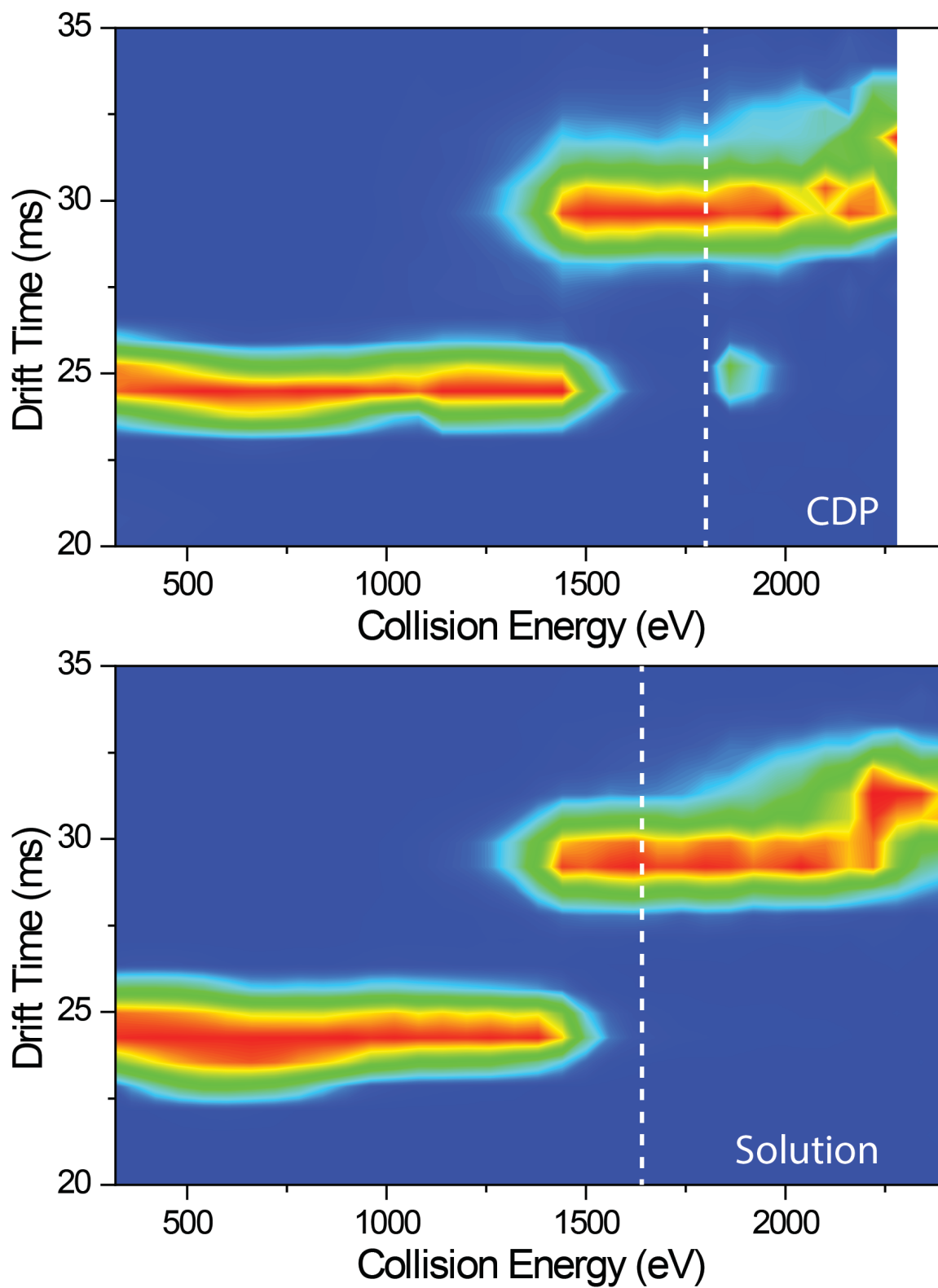


**Figure D-7.** Avidin CIU fingerprints generated from the 12+ ion with solution based charge reduction and corona discharge charge reduction.

**Table D-1.** Measured CCS values for each observed charge state of  $\beta$ -Lac dimer, TPI, SAP, and  $\beta$ -Gal under control and CDP charge reduction. Charge states denoted with a star (\*) were observed in the mass spectrum but has low drift time intensity, preventing CCS measurement.

		Measured CCS ( $\text{\AA}^2$ )							
		b-Lac dimer		TPI		SAP		b-Gal	
		Control	CDP	Control	CDP	Control	CDP	Control	CDP
<b>Oligomer Charge State</b>	4 <sup>+</sup>		*						
	5 <sup>+</sup>		*						
	6 <sup>+</sup>		2223						
	7 <sup>+</sup>		2301						
	8 <sup>+</sup>		2376		2801				
	9 <sup>+</sup>		2385		2896				
	10 <sup>+</sup>		2551		2986				
	11 <sup>+</sup>	2625	2623		3074		*		
	12 <sup>+</sup>	2723	2731		3159		*		
	13 <sup>+</sup>	2848		3236	3244		5821		
	14 <sup>+</sup>			3316	3328		5859		
	15 <sup>+</sup>			3382	3422		5906		
	16 <sup>+</sup>			3496	3542		5998		
	17 <sup>+</sup>						6088		
	18 <sup>+</sup>						6155		
	19 <sup>+</sup>						6244		
	20 <sup>+</sup>						6290		
	21 <sup>+</sup>						6380		
	22 <sup>+</sup>					6496	6437		
	23 <sup>+</sup>					6580	6568		
	24 <sup>+</sup>					6600	6620		
25 <sup>+</sup>					6658	6704			
26 <sup>+</sup>					6687	6765			
27 <sup>+</sup>					6774				
28 <sup>+</sup>					6887				
29 <sup>+</sup>									
30 <sup>+</sup>									
31 <sup>+</sup>									

32 <sup>+</sup>								
33 <sup>+</sup>								
34 <sup>+</sup>								
35 <sup>+</sup>								
36 <sup>+</sup>								*
37 <sup>+</sup>								17306
38 <sup>+</sup>								17368
39 <sup>+</sup>								17580
40 <sup>+</sup>								17471
41 <sup>+</sup>								17435
42 <sup>+</sup>								17494
43 <sup>+</sup>								17621
44 <sup>+</sup>							*	17726
45 <sup>+</sup>							17810	17646
46 <sup>+</sup>							17981	17637
47 <sup>+</sup>							17565	17780
48 <sup>+</sup>							17520	17779
49 <sup>+</sup>							17544	17681
50 <sup>+</sup>							17543	17688
51 <sup>+</sup>							17591	17668
52 <sup>+</sup>							17620	17699

## **Appendix E: Protocol for Corona Discharge Probe Operation**

The following section contains detailed information for operation of the corona discharge probe for charge reduction.

### **Preparation**

1. Clean stainless steel plate by washing in sonicator for 30 minutes in 10% acetic acid, followed by a 20 minute wash in water, followed by a final 20 minute wash in methanol. It is essential that the plate be clean, longer washings have shown improved performance.
2. The platinum wire needs to be ground to a fine point. This is best done fresh each day by first using a Dremel Rotary Tool to clean the wire and create a rough point. Next using fine grit sandpaper, the rough point should be smoothed to a clean point under a microscope.
3. Assemble probe (see Chapter 4). Point-to-plane distance should be 1.5-2.5 mm, with 2 mm most commonly used. FOR SAFETY: ensure stainless steel plate is grounded. If it is not grounded, discharge will occur with the steel tube. This will put a high voltage current through the source housing.
4. Turn on power supply and look for corona discharge, visible as a faint purple light. If point-to-plane distance is too small, current will be too high and circuit breaker will trip. If distance is too large, no corona discharge will be observed, or discharge will occur with stainless steel tube.
5. Position probe with plate approximately 1.5 cm from sample cone orifice, with plate aperture directed to the right of the cone. Positioning probe directly in-line with orifice or



to left of orifice (toward ESI emitter) prevents ions from traversing the 'Z' orientation of the source due to high ion velocities produced by the high gas flow rate.

### **Operation**

1. Before charge reducing analyte, optimize probe and ESI emitter positions using denatured CytC. Ensure good signal intensity before turning on CDP.
2. Increase sampling cone voltage to 200 V. For intact protein complexes, decrease backing pressure to ~7 mbar.
3. Turn on nitrogen gas flow. Gas pressure can range from 60-100 psi, with 70 psi most commonly used.
4. Turn on power supply. Voltages can range from 6500-8500 V, with 7250 V most commonly used.
5. Using CytC, adjust CDP position and ESI emitter position for optimized charge reduction. Ensure 3<sup>+</sup>, and low level 2<sup>+</sup>, charge states are observed.
6. Using same CDP and ESI emitter positions from CytC, charge reduce analyte. Slight adjustment to ESI emitter position may be necessary to ensure good signal intensity.
7. For performing unfolding experiments on intact protein complexes, it is necessary to increase the trap gas flow rate. Flow rate is typically operated at 7 mL/min, up from 5 mL/min.